AN EXPERIMENTAL INVESTIGATION OF VORTEX TUBE PERFORMANCE CHARACTERISTICS

by
Yakub Tüfekci

Submitted to the Institute of Graduate Studies in
Science and Engineering in partial fulfillment of
the requirements for the degree of
Master of Science
in
Mechanical Engineering

Yeditepe University
2009

AN EXPERIMENTAL INVESTIGATION OF VORTEX TUBE PERFORMANCE CHARACTERISTICS

APPROVED BY:

Asst. Prof. Namık Çıblak (Thesis Supervisor))	…….
Asst. Prof. Mustafa Polat	…….
Prof. Dr. Mehmet Akgün	…….

DATE OF APPROVAL: 10/12/2009

ACKNOWLEDGMENTS

Vortex tube is a heat pump with no moving parts. It generates cold and hot gases from pressurized inlet gas. The physics behind the temperature separation process inside the vortex tube is not explained yet. I would like to thank Asst. Prof. Namık ÇIBLAK who conceived the project idea and provided substantial direction and support throughout.

Special gratitude goes to my friends in DALGAKIRAN KOMPRESOR Research and Development Department and Kaan KOCAGÖNCÜ for their help and Mr. Adnan DALGAKIRAN, General Manager of the company, for his support during the project.

Considerable appreciation goes to The Scientific and Technological Research Council of Turkey (TÜBİTAK) who provided the scholarship with 2210 Program (National Scholarship Program for MSc Students).

This project is dedicated to my mother Fatma Zehra ÜLGÜR and family for their patience, tolerance and support. They have been always with me and without them, none of this would have been possible.

ABSTRACT

The primary aims of this project are to obtain a fundamental understanding of the temperature separation process of the Ranque - Hilsch Vortex Tube (RHVT) and to find an improved design by applying experimental methods.

The physics behind the temperature separation process inside the vortex tube is not explained yet. There are many theories while each of these theories may capture certain aspects of the device but none of these mechanisms completely explains the Ranque-Hilsch effect. For about 70 years, many investigators have been trying to find a theory which explains the whole vortex phenomena. The theoretical, experimental and computational methods helped to improve the understanding of vortex tubes, their performance, and capacity. However, most of the past work efforts based on theoretical and analytical studies have been unsuccessful to explain the energy separation phenomenon in the tube. Also, a few attempts of applying numerical analysis to the vortex tube have failed to predict the flow and temperature fields due to the complexity of the flow inside the tube. The failure of those calculations of vortex-tube flows was due to the choice of oversimplified models to describe the flow and because of that vortex tube models are non-linear and very complex. Also, related equations are difficult to solve theoretically. Thus, applying experimental method is selected for this study.

In this study, counter-flow vortex tube is investigated to find relationship between inlet and geometrical parameters and device performance. Vortex tube prototypes are designed by using a CAD software, manufactured by CNC machining centers, and finally, tested at several different conditions for improvement of performance characteristics of the device.

Current experimental study to investigate vortex phenomenon and improve its performance characteristics are presented in Chapter 5. Results that obtained from numerous different experiments are shown and evaluated to improve the device performance. Additional experiments are performed to examine the performance of the vortex tube under high inlet gas pressures up to 15.5 Bar (g), a first in literature. As a result

of this effort, two mathematical relations are found. By these equations, the actual temperature reduction and maximum isentropic efficiency of the prototype vortex tube can be calculated at any given inlet pressure and temperature.

ÖZET

Bu projenin temel hedefleri: Ranque - Hilsch Vorteks Tüpündeki (RHVT) sıcaklık ayrışması prosesini anlamak ve deneysel methodlar kullanarak daha gelişmiş bir vorteks tüp tasarımı yapabilmektir.

Vorteks tüpü içerisinde meydana gelen sıcaklık ayrışması olayı fiziksel olarak henüz açıklanmammıştır. Bulunan birçok teori olmasına karşın, bunlardan hiçbiri olayın tamamını açıklayamamaktadır. Literatürdeki teorik, deneysel ve analitik çalışmalar, cihazın daha iyi anlaşılmasını ve performans ile kapasitesinin arttırılmasını sağlamıştır. Fakat geçmişteki teorik ve analitik çalışmaların çoğu enerji ayrışmasını açıklamakta başarısızdır. Ayrıca cihaz içindeki akışın kompleksiği yüzünden, akış profilini tahmin etmekte başarısız olmuştur. Bunun nedeni, fazlasıyla basitleştirilmiş modellerin kullanımı ve vorteks tüpü modellerinin lineer olmayışıdır. Dahası ilgili matematiksel denklemlerin çözümü de oldukça zordur. Dolayısı ile, bu çalışmada deneysel methodun kullanımı tercih edilmiştir.

Bu çalışmada vorteks tüpünün performansı ile giriş parametreleri ve geömetrinin etkisini bulmak için karşıt akışlı vorteks tüpü incelenmiştir. Prototipler bilgisayar destekli tasarım programı kullanılarak tasarlanmış ve CNC makinalar ile imal edilmesinin ardından birçok farklı koşulda test edilmiştir.

Vorteks tüpünü inceleme ve geliştirme amaçlı yapılan bu çalışmanın sonuçları 5. bölümde sergilenmektedir. Cihazın performansını artıırabilmek için, birçok farklı koşulda deneyler yapılmıştır. Ayrıca, cihazın giriş basıncı literatürde ilk defa 15,5 bar seviyesine kadar arttırılmıştır. Bu sayede, iki matematiksel formül bulunmuştur. Bu formülleri kullanarak, giriş basıncına göre, vorteks tüpünün maksimum izantropik verimliliği ve gerçek sıcaklık düşürümü hesaplanabilmektedir.

TABLE OF CONTENTS

ACKNOWLEDGEMENTS iii
ABSTRACT iv
ÖZET vi
TABLE OF CONTENTS vii
LIST OF FIGURES ix
LIST OF TABLES xiv
LIST OF SYMBOLS/ABBREVIATIONS xvi
1. INTRODUCTION 1
1.1. Vortex Tubes 1
1.2. History of Vortex Tubes 4
1.3. Classification of Vortex Tubes 4
1.3.1. Classification by Design Characteristics 5
1.3.2. Classification by Flow Characteristics 5
1.3.2.1. Parallel Flow (Uni-Flow) Vortex Tubes 5
1.3.2.2. Counter Flow Vortex Tubes 5
1.4. Fundamentals of the Ranque – Hilsch Vortex Tube 7
1.4.1. Thermodynamics of the Ranque – Hilsch Vortex Tube 7
1.4.2. Fluid Dynamics of the Ranque – Hilsch Vortex Tube 10
1.5. Preview of Thesis 12
2. LITERATURE SURVEY 13
2.1. Previous Experimental Studies 14
2.2. Previous Computational Studies 25
2.3. Previous Theoretical Studies 30
3. PHYSICS OF VORTEX TUBES 33
3.1. Efficiency of Vortex Tubes 35
4. APPLICATIONS OF VORTEX TUBES 37
4.1. Simple Heating and Cooling Applications 37
4.2. Gas Liquefaction Applications 37
4.3. Mixture Separation Applications 39
5. CURRENT EXPERIMENTAL RESEARCH 40
5.1. Goals of This Study 40
5.2. Design of the Experimental Prototype 40
5.3. Experimental Apparatus 43

5.4. Experimental Results 46
5.4.1. Effect of the Number of Inlet Nozzles in Vortex Generator 48
5.4.2. Effect of the Length of the Hot Tube 51
5.4.3. Effect of the Vortex Cone Angles 54
5.4.4. Insulation Effect 58
5.4.5. Material Of the Hot Tube 60
5.4.6. Cold Orifice Ratio 63
5.4.7. Inlet Pressure 67
5.5. Optimum Vortex Tube Design 72
6. CONCLUSION AND FUTURE WORKS 75
REFERENCES 78
APPENDIX A: EXPERIMENTAL DATA AND CALCULATIONS OF SECTION 5.4.1 “Effect of the Number of Inlet Nozzles in Vortex Generators” 88
APPENDIX B: EXPERIMENTAL DATA AND CALCULATIONS OF SECTION 5.4.2 “Effect of the Length of the Hot Tube” 92
APPENDIX C: EXPERIMENTAL DATA AND CALCULATIONS OF SECTION 5.4.3 “Effect of the Vortex Cone Angles” 100
APPENDIX D: EXPERIMENTAL DATA AND CALCULATIONS OF SECTION 5.4.4 “Insulation Effect” 104
APPENDIX E: EXPERIMENTAL DATA AND CALCULATIONS OF SECTION 5.4.5 “Material of the Hot Tube” 106
APPENDIX F: EXPERIMENTAL DATA AND CALCULATIONS OF SECTION 5.4.6 “Cold Orifice Ratio”. 108
APPENDIX G: EXPERIMENTAL DATA AND CALCULATIONS OF SECTION 5.4.7 “Inlet Pressure” 111

LIST OF FIGURES

Figure 1.1. A vortex tube and flow inside it 1

Figure 1.2. Rotational motions of hot and cold beams inside the vortex tube 2

Figure 1.3. Examples of commercial vortex tubes 3

Figure 1.4. A vortex tube used for cooling of a camera lens 3

Figure 1.5. A parallel flow vortex tube 5

Figure 1.6. Counter flow vortex tube 6

Figure 1.7. Schematic illustration of industrial counter flow vortex tube 6

Figure 1.8. System Boundary applied to RHVT..... 8

Figure 1.9. Variation of $\Delta T_{o,c}$ with μ_c for typical RHVT 10

Figure 1.10. Axial velocity streamline plot and graphs of tangential and axial velocity and their distribution along the central axis of the RHVT 11

Figure 2.1. The first page of G. J. Ranque`s US patent received in 1934 13

Figure 2.2. Relative lengths of hot and cold tubes of Hilsch device 15

Figure 2.3. Cutaway view of Hilsch tube showing relation of spiral chamber to central pipe-coupling. Detail of spiral is at lower right 15

Figure 2.4. Graph of performance for three vortex tubes made by Rudolph Hilsch 16

Figure 2.5. Performance graph of Hilsch tube showing effect of hot tube stopcock adjustment for various inlet pressure adjustments 16

Figure 2.6. Effect of the cold orifice diameters on temperature reduction in the insulated vortex tube, Ti =29°C and P_i=3.5 bar 21

Figure 2.7. Effect of the number of inlet nozzles on temperature reduction in the insulated vortex tube, Ti=29°C and Pi =3.5 bar 22

Figure 2.8. Effect of the insulated and non-insulated tubes on temperature variation in (a) cold tube and (b) hot tube, for T_i =29°C and P_i= 3.5 bar 23

Figure 2.9. Velocity profiles of CFX calculation 27

Figure 2.10. Axial and radial flow patterns of the flow inside the vortex tube by CFX calculation 28

Figure 2.11. (a) Three-dimensional model of vortex tube in sector, (b) the hot end and cold end of vortex tube in sector provided with refinement in mesh..... 29

Figure 2.12. Temperature distribution of vortex tube in axial direction 29

Figure 4.1: Cooling of electrical control cabinets by using commercial vortex tubes (a) and (b). In (c), spot cooling of a cutting tool in milling operation and vortex tube as a personal air-conditioner (d) 38

Figure 4.2. Linde-type gas liquefaction process incorporating a vortex tube 39

Figure 5.1. Design pictures of the prototype: general view (a) and cross-sectional view of the vortex tube (b). Inlet and hot outlet collectors are shown in (c) and its cross-sectional view in (d)..... 41

Figure 5.2. (a), (b): Design pictures of generators with 3 and 4 inlet nozzles, and

its detailed view in tube assembly (c). One of vortex cone pictures (d) and its detailed, cross-sectional view in hot side of the tube (e). 42

Figure 5.3. Experimental apparatus used in all experiments except high pressure case 43

Figure 5.4. Experimental apparatus used in high pressure case. 44

Figure 5.5. Simple representation of the vortex tube including main parts and dimensions 44

Figure 5.6. Main parts used in experiments: Vortex Tube Prototype (a), VT with installed collectors and measurement devices (b), Rotary-Screw Compressor (c), Reciprocating 'Booster' Compressor (d), pressure regulator (e) and general parts used in (f). 45

Figure 5.7. Vortex generators with inlet nozzle numbers from 1 to 4. Other geometrical parameters of the generators are all the same. 49

Figure 5.8. Results of the experiments of vortex generators with inlet nozzle numbers from 1 to 4. Temperature increment vs. cold mass fraction shown in (a), while temperature reduction vs. cold mass fraction presented in (b). In (c): the maximum isentropic efficiencies obtained by generators and average mass flow rate during the experiments are shown. 50

Figure 5.9. Length of the hot tubes were changed from 15D to 50D. The seamless aluminum pipes had constant diameter of 19 mm during this group of experiments. 51

Figure 5.10. Results of the experiments of vortex tube with different hot tube length from 15D to 50D. Temperature increment vs. cold mass fraction shown in (a), while temperature reduction vs. cold mass fraction presented in (b). In (c): the maximum isentropic efficiencies obtained with different tube lengths are shown..... 53

Figure 5.11. Conical nozzles used in the experiments shown in (a) and the apparatus for adjusting the position of the nozzles inside the hot end of the tube shown in (b). 55

Figure 5.12. Results of the experiments of vortex tube with different vortex cones having different cone angles from 40^0 to 75^0. Temperature increment vs. cold mass fraction shown in (a), while temperature reduction vs. cold mass fraction presented in (b). In (c): the maximum isentropic efficiencies obtained with different vortex cones are shown. 57

Figure 5.13. The insulation foam that used in this set of experiments. 58

Figure 5.14. Results of the experiments of vortex tube with and without insulation on the hot tube. Temperature increment vs. cold mass fraction shown in (a), while temperature reduction vs. cold mass fraction presented in (b). In (c): the maximum isentropic efficiencies obtained by these two conditions are shown in same graph. 59

Figure 5.15. Aluminum and steel pipes used in this set of experiments..... 60

Figure 5.16. Results of the experiments of vortex tube with steel and aluminum hot tubes. Temperature increment vs. cold mass fraction shown in (a), while temperature reduction vs. cold mass fraction presented in (b). In (c): the maximum isentropic efficiencies obtained by the each pipe are shown in same graph. 62

Figure 5.17. Aluminum pipes used in this set of experiments..... 63

Figure 5.18. Results of the experiments of vortex tube with different cold orifice ratios. Temperature increment vs. cold mass fraction shown in (a), while temperature reduction vs. cold mass fraction presented in (b). In (c): the maximum isentropic efficiencies obtained by the each ratio are shown..... 64

Figure 5.19. Temperature reduction and increment against cold mass fraction at different inlet pressures from 1.980 bar to 5.982 bar for vortex tube which has constant length (L=405 mm) 66

Figure 5.20. Results of the experiments of vortex tube with different inlet pressures. Temperature increment vs. cold mass fraction shown in (a), while temperature reduction vs. cold mass fraction presented in (b). In (c): the maximum isentropic efficiencies obtained by the each ratio are shown. At the last graph (d), the ratio of the maximum isentropic efficiency to inlet pressure is shown. 68

Figure 5.21. The ratio of the maximum isentropic efficiency to inlet pressure 69

Figure 5.22. The Maximum Isentropic Efficiency vs. Ln (P) Graph 71

LIST OF TABLES

Table 2.1. Summary of the data from the previous experimental studies 24

Table 2.2. Summary of computational studies on vortex tubes 26

Table 2.3. Initial conditions used in the research of W. Fröhlingsdorf and H. Unger 27

Table 5.1. Summary of the sets of experiments performed in current research including constant and variable parameters. 48

Table 5.2. Constant parameters and their values during the experiments of "Vortex generators with different inlet nozzle numbers" 49

Table 5.3. Constant parameters and their values during the experiments of "hot tube with different lengths from 15D to 50D". 52

Table 5.4. Constant parameters and their values during the experiments of "conical nozzles with different angles from 40^0 to 75^0". 55

Table 5.5 Constant parameters and their values during the experiments of "Effect of insulation on the hot tube" 58

Table 5.6. Constant parameters and their values during the experiments of “Vortex generators with different hot tube material”. 61

Table 5.7. Constant parameters and their values during the experiments of “Vortex generators with different cold orifice ratios”. 63

Table 5.8. Constant parameters and their values during the experiments of “Vortex tubes under different inlet pressures from 2 Bar (g) to 15,5 Bar (g)” 67

Table 5.9. Configurations increasing the performance of the vortex tube design and their optimum values. 73

LIST OF SYMBOLS / ABBREVIATIONS

A	Area
B	Diameter of the Inlet Nozzle
C	Compliance, Capacitance
C_p	Specific Heat Capacity at Constant Pressure
d	Cold Orifice Diameter
D	Diameter of the Hot Tube
G	Gravitational Acceleration
h_o	Total Enthalpy
h_s	Static Enthalpy
L	Tube Length
m	Mass
$\dot{m}$	Mass Flow Rate
$\dot{m}_{in}$	Inlet Mass Flow Rate
P	Pressure
P_i	Inlet Pressure
P_{ref}	Reference Pressure
Q	Heat Supplied to the System
$\dot{Q}$	Heat Flow Rate
Q_{act}	Actual Flow Rate
Q_{read}	Observed Flow Rate
R	Gas Constant
R_u	Universal Gas Constant
T	Temperature
T_{act}	Actual Temperature
T_o	Total Temperature
T_{ref}	Reference Temperature

U	Velocity
V	Volume
W	Work Input
$\dot{W}$	Work Rate
Z	Height
γ	Specific Heat Ratio
η_{is}	Isentropic Efficiency
μ_c	Cold Mass Fraction
RHVT	Ranque-Hilsch Vortex Tube

1. INTRODUCTION

The vortex tube, also known as Ranque-Hilsch vortex tube is a heat pump with no moving mechanical parts and it generates cold and hot gas from compressed gas. It was invented in 1933 by French physicist Georges J. Ranque [1]. Later, German physicist Rudolf Hilsch improved the design and published a paper in 1945, [2].

1.1. VORTEX TUBES

In a vortex tube, a pressurized gas is injected tangentially into a specially designed tube, both ends open, with a conical obstacle at one of the ends. It has been observed that the gas beam splits into two streams, which may have different temperatures. The warmer beam exits from the cone side, whereas the colder from the other end. The temperature difference could be significantly high. The flow inside the tube is suggested to be helical. Figure 1.1 shows a vortex tube and the flow inside it. In Figure 1.2 rotational motions of hot and cold beams are shown.

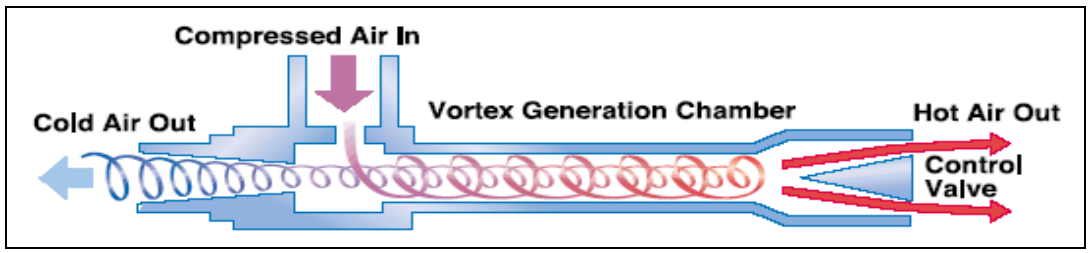

Figure 1.1. A vortex tube and flow inside it [3]

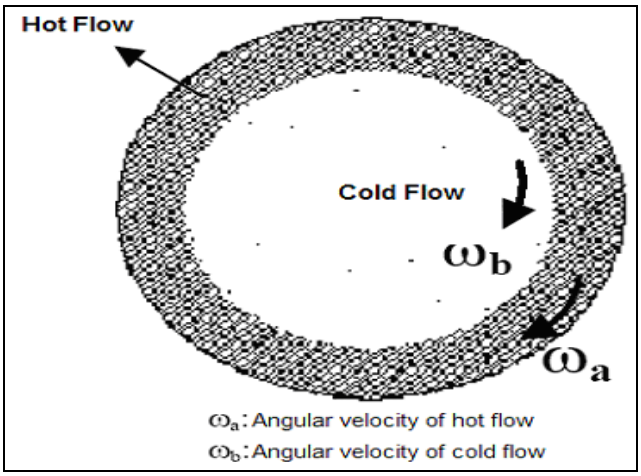

Figure 1.2. Rotational motions of hot and cold beams inside the vortex tube [4]

Basically, vortex tubes consist of one inlet in which a gas at pressure higher than the atmospheric pressure (usually 2–10 bar (g)) is tangentially injected via a nozzle into a vortex chamber. The fluid splits up into a hot portion that is exhausted at the right side and a cold portion that is exhausted at the left side of the vortex chamber. The fraction of the gas that leaves the tube in either direction is controlled by a valve. Because of the tangential injection, the gas velocity has a high rotational component in the vortex chamber.

Today, vortex tubes provide an alternative method for cooling applications. It has more advantages than classical cooling methods. First of all, because it has no moving parts, it can be used for years without any service or need for replacement parts or maintenance. The only need is compressed gas to run the vortex tube. Vortex tubes are small and lightweight. Thus, they can be used in all kinds of systems. Instant cold air (also hot air) at adjustable temperatures is produced by vortex tubes.

Although the overall efficiency of the vortex tubes are low, and the cost of providing pressurized gas is high in some countries, such as Turkey, vortex technologies are nevertheless rapidly developing and capacities are increasing. Nowadays, vortex tubes with a cooling capacity of 10000 btu/hour (~3 kW) are not uncommon. Vortex tubes are now commercially used for cooling (mainly for industrial spot cooling) applications, such as:

- cooling of machine parts and electrical enclosures
- setting solders
- dehumidifying gas samples
- chilling environmental chambers

Some examples of these applications are shown in Figure 1.3. and Figure 1.4.

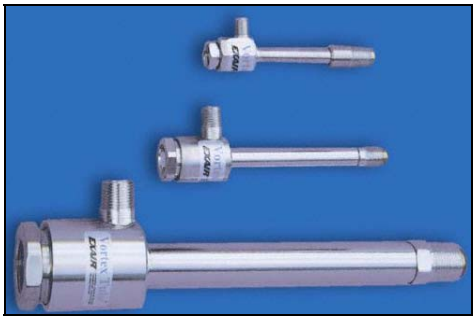

Figure 1.3. Examples of commercial vortex tubes [5]

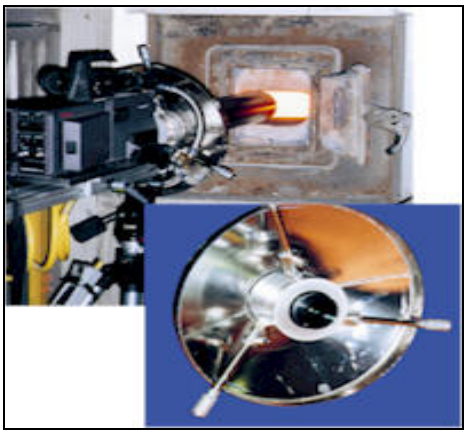

Figure 1.4. A vortex tube used for cooling of a camera lens [5]

Other practical applications of vortex tubes cover:

- Liquefaction of natural gas,
- Cooling of control rods in nuclear reactors and firemen's suits
- Cooling for low-temperature magic angle spinning nuclear magnetic resonance (NMR),
- Temperature control of divers' air suppliers, manned underwater habitats,
- Separating particles in waste gas industry,
- Low-pressure applications and snowmaking applications, and so on [6].

1.2. HISTORY OF VORTEX TUBES

History of vortex tubes started in the nineteenth century with an extra ordinary idea. The great physicist James Clerk Maxwell imagined that someday we might be able to get hot and cold air with the same device with the help of a "friendly little demon" who would sort out and separate the hot and cold molecules of air. In next century, his dream had come true by the vortex tube.

In 1933, George Ranque, a French physicist, accidentally found the phenomenon of energy separation in the vortex tube while he was doing an experiment with a vortex type pump. He realized that hot and cold air came out of opposite ends of a simple pipe but he could not explain the phenomenon. In 1945, Rudolph Hilsch, a German physicist, worked on vortex tubes and published his systematic experimental results on the thermal performances of vortex tubes with different geometrical parameters and under different inlet pressures [7]. Since then, the vortex tube has been the subject of much interest. In following years, many scientists focused on vortex tubes and did many experiments and tried to understand how energy separation process occurs in vortex tubes. Some of these ideas are explained in Section 2.

It has been accepted that although the vortex tube work and experiments help to understand the phenomenon, the actual mechanism of the energy separation in vortex tubes has not yet been completely understood. It still remains as a complex multi-physics problem and many researchers are still working on this phenomenon trying to explain the physics of it.

1.3. CLASSIFICATION OF VORTEX TUBES

Vortex tubes can be classified into two main groups according to the design characteristics and the flow characteristics.

1.3.1. Classification by Design Characteristics

In adiabatic vortex tubes, the entire body is well insulated and no heat transfer occurs between the body and the atmosphere.

In non-adiabatic vortex tubes, there is no insulation on the body of the tubes, so heat transfer occurs via conduction, convection, and radiation.

1.3.2. Classification by Flow Characteristics

1.3.2.1. Parallel Flow (Uni-Flow) Vortex Tubes

In parallel flow vortex tubes, shown in Figure 1.5, pressurized gas inserted tangentially to system from at least one inlet valve and due to the geometry, the inlet gas acquires a swirl velocity through the entire body. At the end of the system there is a nozzle, which has a hole at the center, provides the separation of cold and hot gases. Cold gas exits the system from this hole while hot gas exits through the outer surface of the nozzle. In these types of vortex tube, hot and cold gas ratios can be controlled by changing position of the nozzle. Because of disturbances in separation of flows and difficulties in controlling the flows by nozzle, parallel flow vortex tubes generally is not a preferred construction.

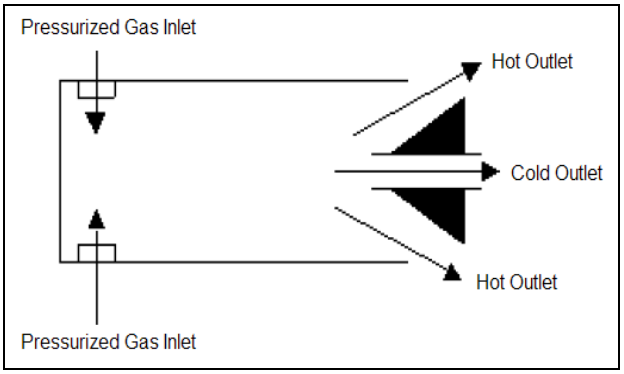

Figure 1.5. A parallel flow vortex tube [4]

1.3.2.2. Counter Flow Vortex Tubes

In counter flow vortex tubes, shown in Figure 1.6, pressurized gas is inserted to the system from one or more inlets, which are positioned close to one of the ends of the vortex

tube. Similarly to the parallel flow vortex tube, in this type, inlet gas gains a tangential velocity due to the inlet geometry and moves towards to the other end of the tube. A nozzle locates at the end of the tube, generally conical in shape, splits the incoming gas into two parts and reflects one part to the opposite end, while the other part, the hotter part, exits towards the outer surface of the nozzle. The reflected part, the colder flow, has also a swirl velocity and moves through the other end and exits the system by flowing inside an orifice with a diameter smaller then tube diameter. These types of vortex tubes are more advantageous than the parallel flow vortex tubes. Counter flow vortex tubes provide better temperature separation and control of the hot and cold gas beams. Thus, these types of vortex tubes are industrially preferred and common design. In Figure 1.7, schematic illustration of an industrial counter flow vortex tube is shown.

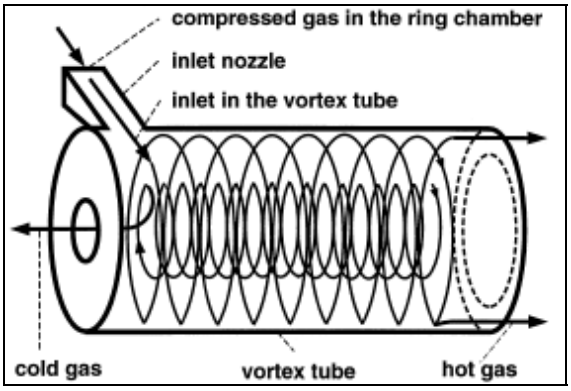

Figure 1.6. Counter flow vortex tube [8]

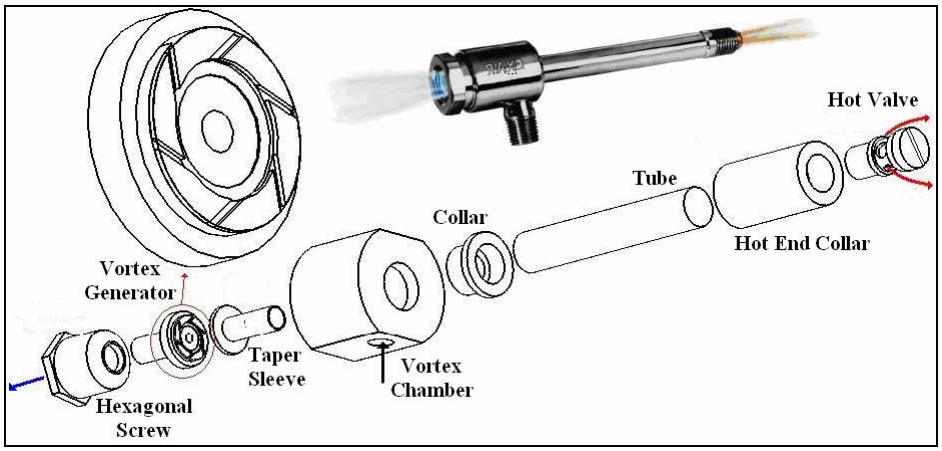

Figure 1.7. Schematic illustration of industrial counter flow vortex tube [5]

1.4. FUNDAMENTALS OF THE RANQUE – HILSCH VORTEX TUBE

Before exploring current published research papers, theses and articles on the RHVT, it is important to look at the fundamental aspects of the device to understand it better. This basic understanding of the RHVT draws from the well established principles of Thermodynamics and Fluid Dynamics, and it will be shown that the heat migration within the RHVT is not in conflict with long accepted aspects of both these engineering disciplines. This part of the thesis (Section 1.4) mainly refers to the study done by Oliver, [9].

1.4.1. Thermodynamics of the Ranque – Hilsch Vortex Tube

At first impression, it might appear that vortex tube phenomenon is a violation of the laws of thermodynamics. It would seem that there is an internal heat flux without any work input. As in any refrigeration process, work input is paramount to its operation.

The First Law of Thermodynamics can be written as follows, “When a system undergoes a thermodynamic cycle then the net heat supplied to the surroundings plus the net work input to the system from its surroundings is equal to zero”, [10].

Mathematically this statement is written as in Equation (1.1) where Q and W denote the heat supplied and work input to the system respectively. Using the First Law, the steady flow energy equation can be applied to the RHVT's boundary, as shown in Figure 1.8.

$$\sum Q + \sum W = 0 \tag{1.1}$$

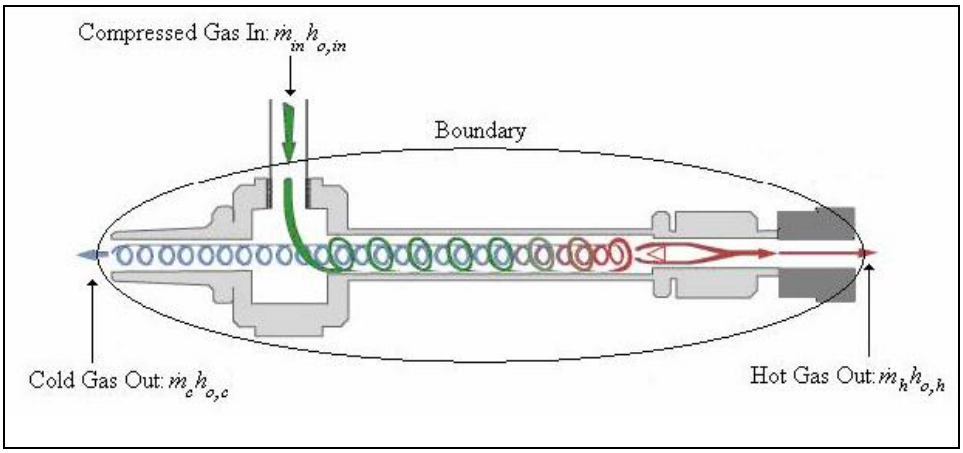

Figure 1.8. System Boundary applied to RHVT, [9].

Expanding Equation (1.1) results in Equation (1.2) where $\dot{m}$, h_o, h_s, $\mathbf{U}$, Z, $\dot{Q}$ and $\dot{W}$ denote the mass flow rate, the total enthalpy, the static enthalpy, the velocity, the height above the datum, the rate of heat, and, the rate of work, respectively. The subscripts in, c and h denote the inlet, and, cold and hot outlets, respectively.

$$\dot{m}_{in}\left(h_{s,in}+\frac{\mathbf{U}_{in}^{\,2}}{2}+Z_{in}\right)+\dot{Q}+\dot{W}=\dot{m}_c\left(h_{s,c}+\frac{\mathbf{U}_c^{\,2}}{2}+Z_c\right)+\dot{m}_h\left(h_{s,h}+\frac{\mathbf{U}_h^{\,2}}{2}+Z_h\right) \tag{1.2}$$

The steady - flow energy equation reduces to a reversed adiabatic mixing equation with use of the following steps:

1. Combining static enthalpies and kinetic energies into total enthalpy.
2. Acknowledging that the potential energies at each point are approximately the same.
3. There is no heat or work input.

In the resulting reversed adiabatic mixing equation, Equation (1.3), h_o denotes the total enthalpy. It is seen that the RHVT does indeed satisfy the first law.

$$\dot{m}_{in}h_{o,in}=\dot{m}_c h_{o,c}+\dot{m}_h h_{o,h} \tag{1.3}$$

This can be further reduced by introducing the ratio of cold gas flow to the supplied gas flow.

$$\mu_c = \frac{\dot{m}_c}{\dot{m}_{in}} \tag{1.4}$$

This ratio is called the cold gas (or mass) fraction and shown in Equation (1.4). After the Equation (1.3) is divided by the inlet mass rate, $\dot{m}_{in}$, the new form is obtained in terms of the cold gas fraction as in Equation (1.5).

$$h_{o,in} = \mu_c h_{o,c} + (1-\mu_c) h_{o,h} \tag{1.5}$$

If the gas flowing through the RHVT is treated approximately as an ideal gas and changes in kinetic energy are neglected, we can rewrite the conservation equation as in Equation (1.6). This is due to the fact that $h_o = c_p T_o$ where c_p and T_o are the specific heat capacity at constant pressure and the total temperature, respectively.

$$c_p T_{o,in} = \mu_c c_p T_{o,c} + (1-\mu_c) c_p T_{o,h} \tag{1.6}$$

Dividing Equation (1.6) across by c_p, results in a much simpler energy balance equation, as shown in Equation (1.7).

$$T_{o,in} = \mu_c T_{o,c} + (1-\mu_c) T_{o,h} \tag{1.7}$$

A much broader perspective of the system needs to be constructed to show that the Second Law of Thermodynamics is also satisfied, which states that “it is impossible to construct a device that operates in a cycle and produces no effect other than the transfer of heat from a cooler to a hotter body” [10].

As there is no mechanical work input to a RHVT, and yet there is a heat flux, to obey the above two classic laws of thermodynamics, there must be a supply of work of some

other form. The source of this work has been the main argument since the establishment of this technology [9].

1.4.2. Fluid Dynamics of the Ranque – Hilsch Vortex Tube

In a RHVT a high pressure fluid, mainly compressed air, enters the tube and passes through nozzles achieving a high angular velocity and hence causing a vortex-type flow, as can be seen in Figure 1.1. There are two outlets to the tube: the hot outlet is placed near the outer radius of the tube at the end away from the inlet nozzles and the cold outlet is placed at the centre of the tube at the same end as the air inlet.

By adjusting a control valve downstream of the hot outlet it is possible to vary the fraction of the incoming flow that leaves through the hot outlet on the periphery of the tube. The proportion of cold gas deflected back through the cold outlet is referred to as the cold fraction, μ_c, previously defined in Equation (1.4). By varying the cold fraction the cold outlet total temperature drop ($\Delta T_{o,c} = T_{o,in} - T_{o,c}$) can be adjusted accordingly, as can be seen, in the experimental results for example, in Figure 1.9, where the terms P_{in}, $T_{o,in}$, L, d_c, and D, denote static gauge pressure, total temperature at the inlet, the length of the RHVT, diameter of the cold outlet, and diameter of the RHVT, respectively.

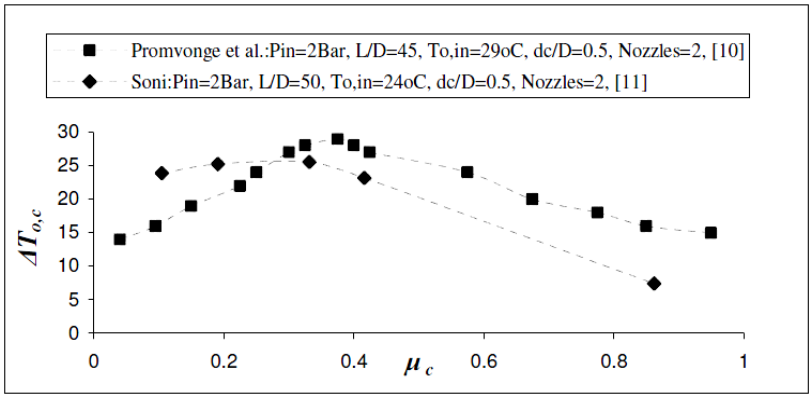

Figure 1.9. Variation of $\Delta T_{o,c}$ with μ_c for typical RHVT [11, 12]

An analysis of a basic axial velocity streamline plot gives a clearer understanding of the variance of both the axial and the tangential velocities throughout the RHVT. In Figure

1.10, the graphs of the axial and tangential velocities denote the axial direction and rotational strength of the vortex, at various axial and radial locations along the RHVT. As can be seen in same figure, in the streamline plot, the compressed air enters through the inlet nozzles and a proportion of this flow leaves through the hot and cold outlets respectively. In addition to the streamline plot, a graph of the tangential and axial velocities (denoted by *v* and *u* respectively) and their variance along the axial, x-direction, of the RHVT has been shown.

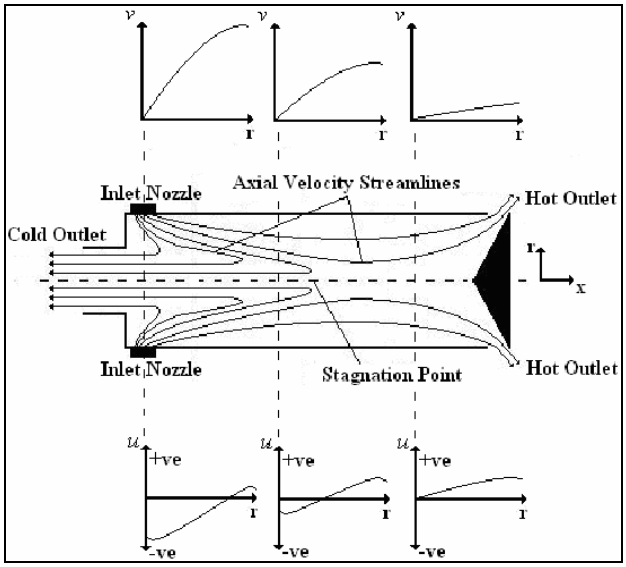

Figure 1.10. Axial velocity streamline plot and graphs of tangential and axial velocity and their distribution along the central axis of the RHVT [9]

It can be easily observed from the graphs in Figure 1.10, the tangential velocities, i.e. the swirling/rotating component of the vortex flow, is strongest at the entrance region (i.e. near the inlet nozzles) of the RHVT and decays significantly in magnitude towards the hot outlet. In the lower graphs it can be seen that, in the entrance region, the axial velocity of the vortex flow is positive (i.e. in a direction towards the hot outlet) at outer radial locations in the RHVT, and moves in a negative direction at inner radial locations of the vortex flow. What this means is that there are two vortices moving in opposite axial directions within this region. This reversal in flow towards the cold exit occurs in the positive x-direction from the inlet nozzles up to a point defined as the stagnation point, as highlighted in Figure 1.10.

The stagnation point also marks the limiting point where further increases of the vortex tube length beyond this point does not improve the energy separation, as observed by Aljuwayhel et al. [13]. This important aspect has been utilized later on in reducing the length of the computational domain of the vortex tube to that used by researchers in their experiments. Towards the hot outlet, the motion is no longer purely rotational due to friction from walls, slowing the tangential components of the flow substantially [9].

1.5. PREVIEW OF THESIS

In the next chapter, a substantial number of literature dealing with the vortex tube are reviewed and summarized. Previous experimental and computational studies are evaluated in historical order. At the end of that chapter, theoretical efforts involving energy separation process in the tube and its performance characteristics will be discussed.

In Chapter 3, physics of vortex tube will be investigated by considering the device as a thermodynamic system in steady state. The first and the second law analysis, energy separation process and the efficiency of the vortex tube are explained.

Although the Ranque-Hilsh Tube has very low efficiency compared to other commercial cooling and heating systems, its certain features make it attractive for some applications. Chapter 4 considers the potential of the tube to be used in a number of specific industrial applications.

Current experimental study to investigate the vortex phenomenon and to optimize its performance characteristics are presented in Chapter 5. Results gained from many different experiments that were conducted are presented and evaluated in order to increase the performance. Additional experiments are performed to examine the performance of the vortex tube under high inlet gas pressures starting from 10 Bar (g) and up, which was not attempted in any of the previous studies.

Last chapter represents information discussed in earlier chapters together and summarize the conclusions regarding the issues considered in this thesis. The suggestions and the future ideas for the device are presented in the closing part of the thesis.

2. LITERATURE SURVEY

The vortex tube was first discovered by Ranque, [1], a metallurgist and physicist who was granted a French patent for the device in 1933, and a United States patent "Method and apparatus for obtaining from a fluid under pressure two currents of fluids at different temperatures" in 1934. The first page of this patent is shown in Figure 2.1.

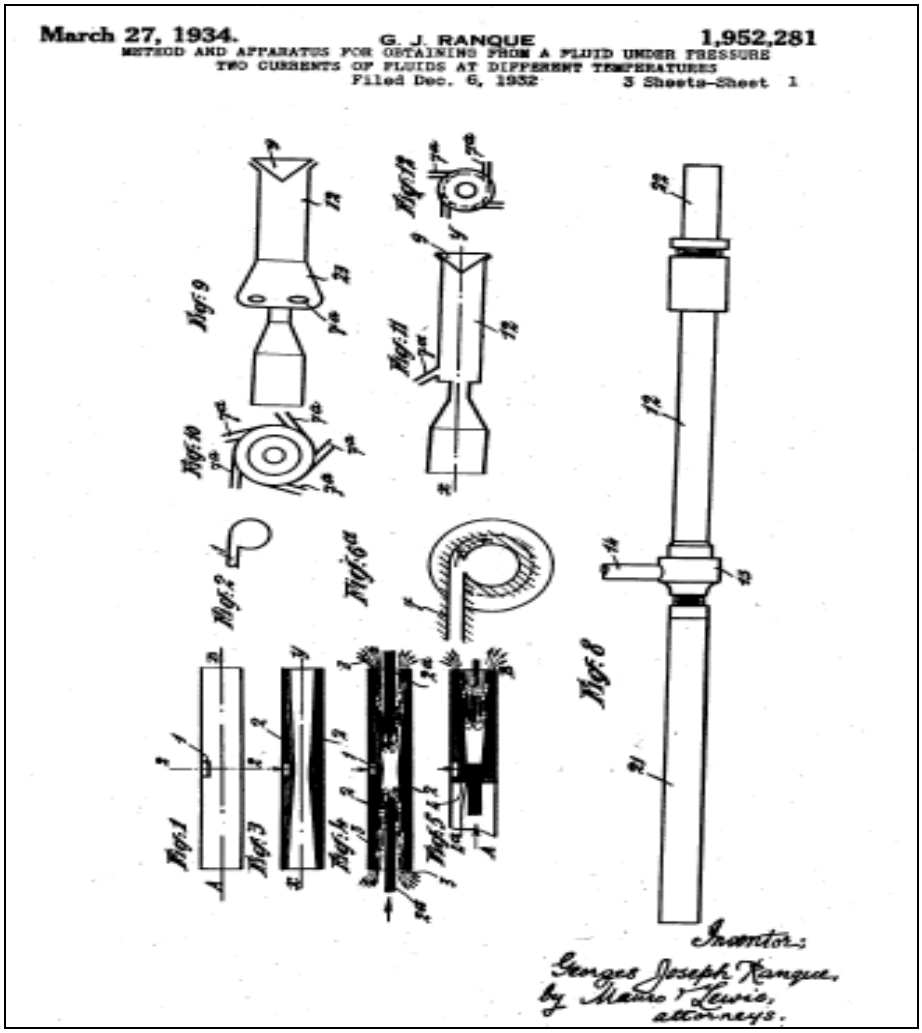
March 27, 1934. G. J. RANQUE 1,952,281
METHOD AND APPARATUS FOR OBTAINING FROM A FLUID UNDER PRESSURE TWO CURRENTS OF FLUIDS AT DIFFERENT TEMPERATURES
Filed Dec. 6, 1932 3 Sheets-Sheet 1
Inventor:
Georges Joseph Ranque,
by Mann & Lewis,
attorneys.

Figure 2.1. The first page of G. J. Ranque`s US patent received in 1934 [14]

The initial reaction of the scientific and engineering communities to his invention was mainly disbelief. Since the vortex tube was thermodynamically highly inefficient, it

was abandoned for several years. Interest in the device was revived by Hilsch [2], a German physicist, who reported an account of his own comprehensive experimental and theoretical studies aimed at improving the efficiency of the vortex tube. He systematically examined the effect of the inlet pressure and the geometrical parameters of the vortex tube on its performance and presented a possible explanation of the energy separation process. After World War II, Hilsch's tubes and documents were uncovered, which were later studied extensively [15].

For about 70 years, many investigators have been trying to find a theory which explains the whole vortex phenomena. The theoretical, experimental and computational methods improved the understanding of vortex tubes, their performance, and capacity. However, previous theoretical works are much rare than experimental and analytical studies for the reasons that vortex tube models are non-linear and very complex. Also, related equations, some of which mentioned before, are difficult to solve theoretically.

2.1. PREVIOUS EXPERIMENTAL STUDIES

Although the vortex tube phenomenon was discovered by Georges J. Ranque, [1], historically the first scientific work was done by German physicist Rudolf Hilsch, [2]. In 1945, Rudolph Hilsch published his systematic experimental results on the thermal performances of vortex tubes with different geometrical parameters and under different inlet pressures. In his works, he did many experiments by different set-ups. He had sketched the diagrams of parts that he used in his works. In Figure 2.2 one of the set-ups that he made is shown. In this figure, comparative lengths of hot and cold sides to the diameter of the main tube are shown. The "cold" pipe is about four inch-long and also has an inside diameter of half of an inch. The end of the pipe which butts up against the spiral piece is fitted with a washer, the central hole of which is about a quarter of an inch in diameter. Washers with larger or smaller holes can also be inserted to adjust the system.

In this set-up, three factors determine the performance of the Hilsch tube, the setting of the stopcock, the pressure of the inlet air, and the size of the hole in the washer. For each value of air pressure and washer opening there is a setting of the stopcock which results in a maximum difference in the temperature of the hot and cold pipes, as shown in Figure 2.4.

and Figure 2.5. The variation of temperature of the cold side at different inlet air pressures versus cold air ratio or cold mass fraction, μ_c, can be seen in Figure 2.5 too.

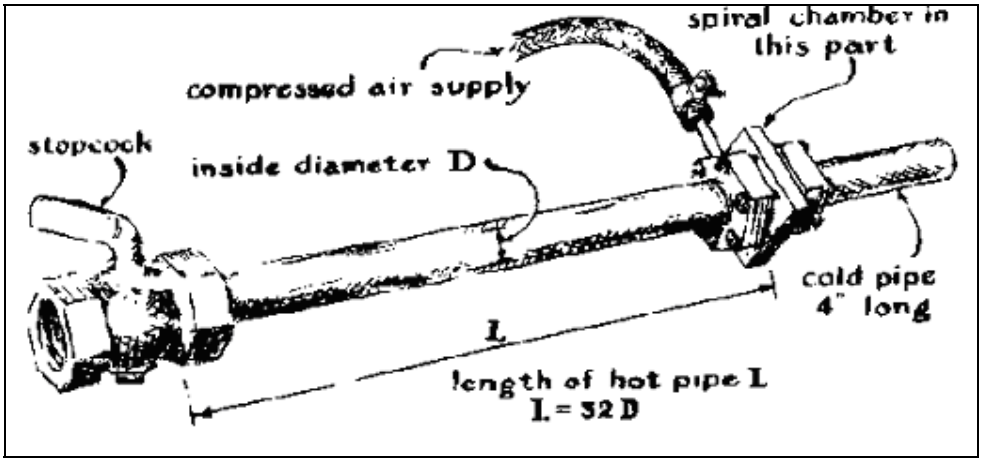

Figure 2.2. Relative lengths of hot and cold tubes of Hilsch device [2]

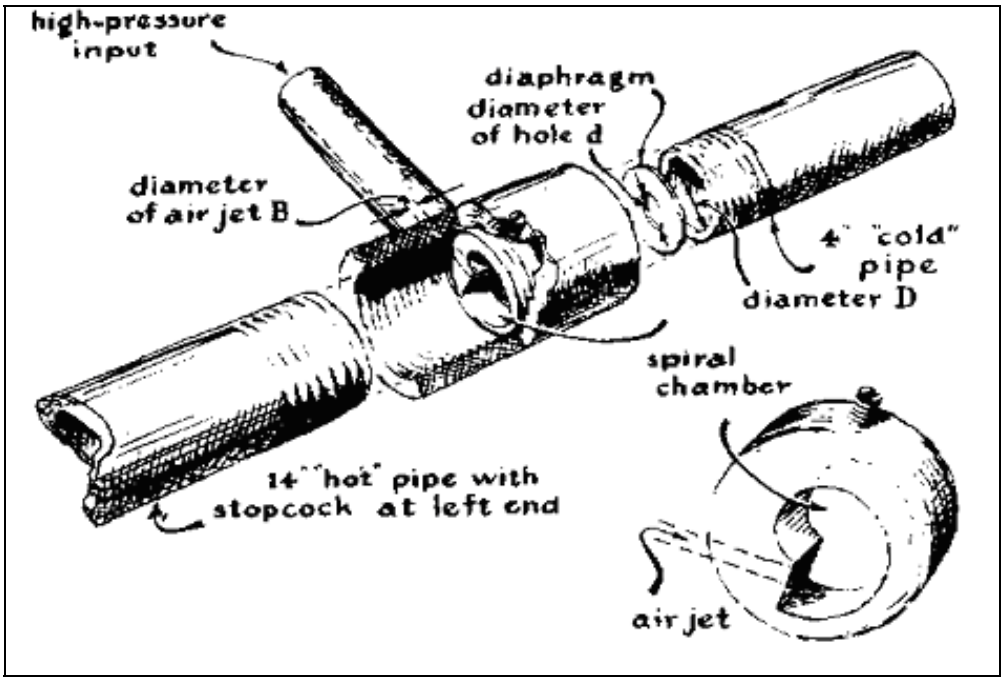

Figure 2.3. Cutaway view of Hilsch tube showing relation of spiral chamber to central pipe-coupling. Detail of spiral is at lower right [2]

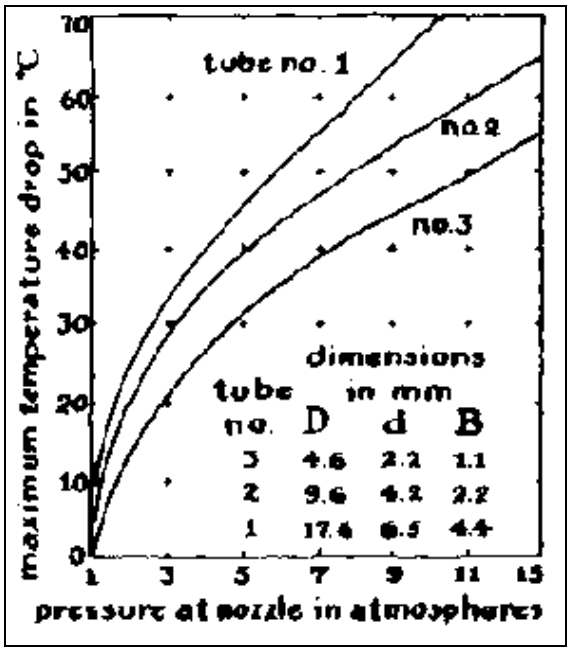

Figure 2.4. Graph of performance for three vortex tubes made by Rudolph Hilsch [2]

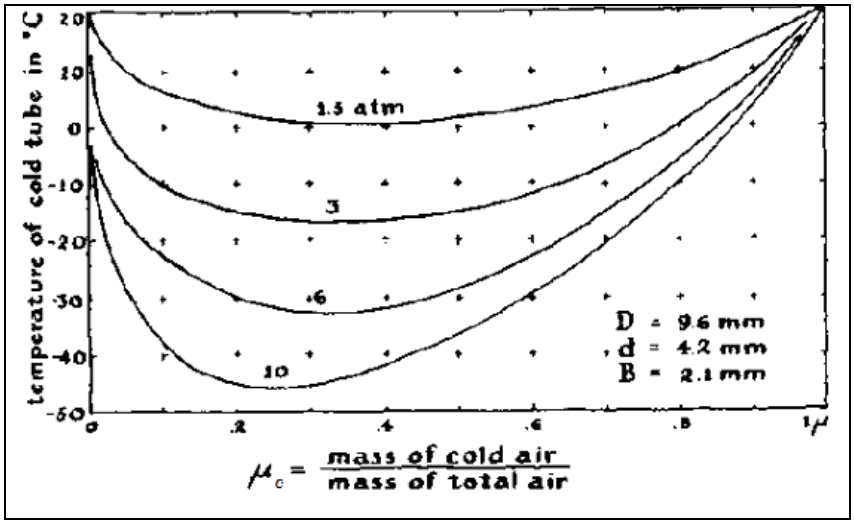

Figure 2.5. Performance graph of Hilsch tube showing effect of hot tube stopcock adjustment for various inlet pressure adjustments [2]

After Hilsch published his work, many scientists focused on vortex tubes and many experimental studies have been carried out in which attempts were concentrated on understanding the mechanism of energy separation in the vortex tube and several different explanations have been offered to explain this phenomenon.

After Hilsch [2], an experimental study was done by Scheper, [16], who measured the velocity, pressure, and total and static temperature gradients in a Ranque–Hilsch vortex tube, using probes and visualization techniques. He concluded that the axial and radial velocity components were much smaller than the tangential velocity. His measurements indicated that the static temperature decreased in a radially outward direction. This result was contrary to most other observations that were made later. Martynovskii and Alekseev, [17], studied experimentally the effect of various design parameters of vortex tubes.

Hartnett and Eckert [18], measured the velocity, total temperature, and total and static pressure distributions inside a uniflow vortex tube. They used the experimental values of static temperature and pressure to estimate the values of density and hence, the mass and energy flow at different cross sections in the tube. The results agreed fairly well with the overall mass and energy flow in the tube. Scheller and Brown [19] presented measurements of the pressure, temperature, and velocity profiles in a standard vortex tube and observed that the static temperature decreased radially outwards as in the work of Scheper [16], and hypothesized the energy separation mechanism as heat transfer by forced convection. Blatt and Trusch [20] investigated experimentally the performance of a uniflow vortex tube and improved its performance by adding a radial diffuser to the end of the shortened tube instead of a cone valve. The geometry of the tube was optimized to maximize the temperature difference between the cold and inlet temperatures by changing the various dimensions of the tube such as the gap of the diffuser, tube length, and entrance geometry. Moreover, the effects of inlet pressure and heat fluxes were examined. Linderstrom - Lang [21] studied in detail the application of the vortex tube to gas separation, using different gas mixtures and tube geometry and found that the separation effect depended mainly on the ratio of cold and hot gas mass flow rates. The measurements of Takahama [22] in a counter-flow vortex tube provided data for the design of a standard type vortex tube with a high efficiency of energy separation. He also gave empirical formulae for the profiles of the velocity and temperature of the air flowing through the vortex tube. Takahama and Soga [23] used the same sets of the vortex tubes of Takahama [22] to study the effect of the tube geometry on the energy separation process and that of the cold air flow rate on the velocity and temperature fields for the optimum proportion ratio of the total area of nozzles to the tube area. They also reported an axisymmetric vortex flow in the tube.

Vennos [24] measured the velocity, total temperature, and total and static pressures inside a standard vortex tube and reported the existence of substantial radial velocity. Bruun [25] presented the experimental data of pressure, velocity and temperature profiles in a counter-flow vortex tube with a ratio of 0.23 for the cold to total mass flow rate and concluded that radial and axial convective terms in the equations of motion and energy were equally important. Although no measurements of radial velocities were made, his calculation, based on the equation of continuity, showed an outward directed radial velocity near the inlet nozzle and an inward radial velocity in the rest of the tube. He reported that turbulent heat transport accounted for most of the energy separation.

Nash [26] used vortex expansion techniques for high temperature cryogenic cooling to apply to infrared detector applications. A summary of the design parameters of the vortex cooler was reported by Nash [27]. Marshall [28] used several different gas mixtures in a variety of sizes of vortex tubes and confirmed the effect of the gas separation reported by Linderstrom-Lang [21]. A critical inlet Reynolds number was identified at which the separation was a maximum. Takahama et al. [29] investigated experimentally the energy separation performance of a steam-operated standard vortex tube and reported that the performance worsened with wetness of steam at the nozzle outlet because of the effect of evaporation. Energy separation was absent with the dryness fraction less than around 0.98. The measurements of Collins and Lovelace [30] with a two-phase, liquid–vapor mixture, propane in a standard counter-flow vortex tube showed that for an inlet pressure of 0.791 MPa, the separation remained significant for a dryness fraction above 80% at the inlet. With a dryness fraction below 80%, the temperature separation became insignificant. But the discharge enthalpies showed considerable differences indicating that the Ranque–Hilsch process is still in effect.

Takahama and Yokosawa [31] examined the possibility of shortening the chamber length of a standard vortex tube by using divergent tubes for the vortex chamber. Earlier researchers such as Parulekar [32], Otten [33], and Raiskii and Tunkel [34] also employed divergent tubes for all or part of the vortex chamber in attempts to shorten the chamber and improve energy separation performance, but their emphasis was on the maximum and minimum temperatures in the outflowing streams. Therefore, Takahama and Yokosawa

[31] compared their results with those from the straight vortex chambers. They found that the uses of a divergent tube with a small angle of divergence led to an improvement in temperature separation and enable the shortening of the chamber. Kurosaka et al. [35] carried out an experiment to study the total temperature separation mechanism in a uniflow vortex tube to support their analysis and concluded that the mechanism of energy separation in the tube is due to acoustic streaming induced by the vortex whistle. Schlenz [36] investigated experimentally the flow field and the energy separation in a uniflow vortex tube with an orifice rather than a conical valve to control the flow. The velocity profiles were measured by using laser-Doppler velocimetry (LDA), supported by flow visualization. Experimental studies of a large counter-flow vortex tube with short length by Amitani et al. [37] indicated that the shortened vortex tube of 6 tube diameters length had the same efficiency as a longer and smaller vortex tube when perforated plates are equipped to stop the rotation of the stream in the tube. Stephan et al. [38] measured temperatures in the standard vortex tube with air as a working medium in order to support a similarity relation of the cold gas exit temperature with the cold gas mass ratio, established using dimensional analysis. Negm et al. [39, 40] studied experimentally the process of energy separation in the standard vortex tubes to support their correlation obtained using dimensional analysis and in a double stage vortex tube which found that the performance of the first stage is always higher than that of the second stage tube. Lin et al. [41] made an experimental investigation to study the heat transfer behavior of a water-cooled vortex tube with air.

Ahlborn et al. [42] carried out measurements in standard vortex tubes to support their models for calculating limits of temperature separation. They also attributed the heating to the conversion of kinetic energy into heat and the cooling to the reverse process. Ahlborn et al. [43] studied the temperature separation in a low-pressure vortex tube. Based on their recent model calculation [42], they concluded that the effect depends on the normalized pressure ratio ($\mu_c = (P_i - P_c)/P_c$) rather than on the absolute values of the entrance pressure, P_i and exhaust pressure, P_c. In 1997, Ahlborn and Groves [44] measured axial and azimuthal velocities by using a small pitot probe and found that the existence of secondary air outward flow in the vortex tube. Ahlborn et al. [45] identified the temperature splitting phenomenon of a Ranque–Hilsch vortex tube in which a stream of gas divides itself into a hot and a cold flow as a natural heat pump mechanism, which is

enabled by secondary circulation. Ahlborn and Gordon [46] considered the vortex tube mass a refrigeration device which could be analyzed as a classical thermodynamic cycle, replete with significant temperature splitting, refrigerant, and coolant loops, expansion and compression branches, and natural (or built-in) heat exchangers.

Arbuzov et al. [47] concluded that the most likely physical mechanism (the Ranque effect) was viscous heating of the gas in a thin boundary layer at the walls of the vortex chamber and the adiabatic cooling of the gas at the centre on account of the formation of an intense vortex braid near the axis. Gutsol [48] explained that the centrifugal separation of ‘‘stagnant’’ elements and their adiabatic expansion causes the energy separation in the vortex tube system. Piralishvili and Polyaev [49] made experimental investigations on this effect in so-called double-circuit vortex tubes. The possibility of constructing a double-circuit vortex tube refrigeration machine as efficient as a gas expansion system was demonstrated. Lewins and Bejan [50] have suggested that angular velocity gradients in the radial direction give rise to frictional coupling between different layers of the rotating flow resulting in a migration of energy via shear work from the inner layers to the outer layers. Trofimov [51] verified that the dynamics of internal angular momentum leads to this effect. Guillaume and Jolly [52] demonstrated that two vortex tubes placed in series by connecting the cold discharge of one stage into the inlet of the following stage. From their results, it was found that for similar inlet temperatures, a two-stage vortex tube could produce a higher temperature reduction than one of the vortex tubes operating independently. Manohar and Chetan [53] used a vortex tube for separating methane and nitrogen from a mixture and found that there was partial gas separation leading to a higher concentration of methane at one exit in comparison to the inlet and a lower concentration at the other exit.

Saidi and Valipour [54] presented on the classification of the parameters affecting vortex tube operation. In their work, the thermo-physical parameters such as inlet gas pressure, type of gas and cold gas mass ratio, moisture of inlet gas, and the geometry parameters, i.e., diameter and length of main tube diameter of outlet orifice, shape of entrance nozzle were designated and studied. Singh et al. [55] reported the effect of various parameters such as cold mass fraction, nozzle, cold orifice diameter, hot end area of the tube, and L/D ratio on the performance of the vortex tube. They observed that the effect

of nozzle design was more important than the cold orifice design in getting higher temperature separations and found that the length of the tube had no effect on the performance of the vortex tube in the range 45 – 55 L/D. Riu et al. [56] investigated dust separation characteristics of a counter flow vortex tube with lime powders whose mean particle sizes were 5 and 14.6 mm. They showed that a vortex tube can be used as an efficient pre-skimmer to separate particles from the waste gas in industry.

Promvonge and Eiamsa-ard [57] experimentally studied the energy and temperature separations in the vortex tube with a snail entrance. In their experimental results, the use of snail entrance could help to increase the cold air temperature drop and to improve the vortex tube efficiency in comparison with those of original tangential inlet nozzles. Promvonge and Eiamsa-ard [11] again reported the effects of (1) the number of inlet tangential nozzles, (2) the cold orifice diameter, and (3) tube insulations on the temperature reduction and isentropic efficiency in the vortex tube. In their experiments, different cold orifice diameters ranging from 0.4D to 0.9D was used (see Figure 2.6.) and results showed that highest temperature reduction can be achieved by using the cold orifice diameter of 0.5 D. Researhers explanations for this result as follows: using the cold orifice diameter ranging from 0.6D to 0.9D (larger than that of 0.5D) would allow some hot air and cold air to mixed together thus these diameters cause lower temperature reduction. On the other hand, using a small cold orifice diameter of 0.4D produces higher back pressure than other diameters do and makes the temperature reduction at the cold tube lower.

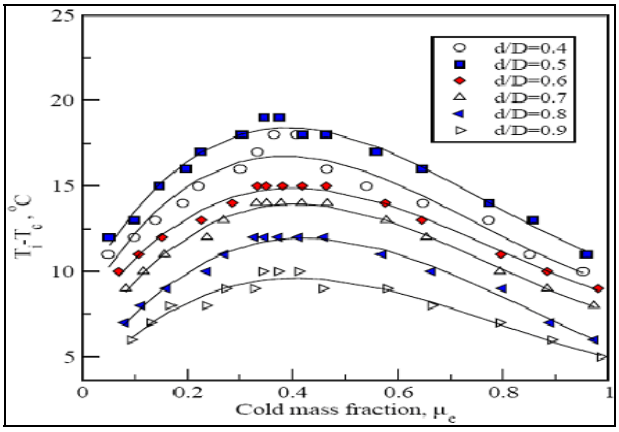

Figure 2.6. Effect of the cold orifice diameters on temperature reduction in the insulated vortex tube, Ti =29°C and P_i=3.5 bar [11]

In the Figure 2.7 below, Promvonge and Eiamsa-ard also showed the effect of the number of inlet nozzles on temperature reduction in an insulated vortex tube by comparing the performances of a single inlet nozzle, 2 nozzles and 4 nozzles. Results show that the increase in the number of inlet nozzles increases the temperature reduction in vortex tube. In the figure, the use of 4 inlet nozzles resulted in a higher temperature reduction in the cold tube than that of 1 and 2 inlet nozzles for the cold orifice diameter of 0.5D. They evaluated the results as that changing the number of inlet nozzles from 1 to 2 and 4 helped to speed up the flow and to increase the mass flow rate and strong swirl flow into the vortex tube. Moreover, these gave rise to higher friction dissipation between the walls and air that flows inside and a higher momentum transfer from the core region to the wall region. This reduced temperature in the center of the tube while increased temperature in the tube wall area [11].

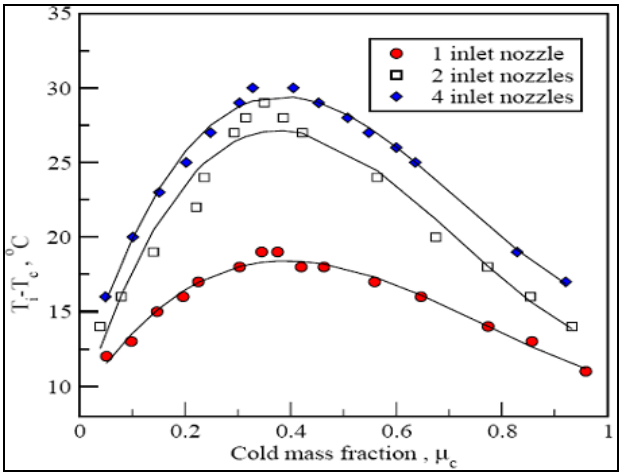

Figure 2.7. Effect of the number of inlet nozzles on temperature reduction in the insulated vortex tube, Ti=29°C and Pi =3.5 bar [11]

The effect of tube insulations on the temperature reduction and isentropic efficiency in the vortex tube was also investigated on this research. As it was mentioned before, insulated vortex tubes work adiabatically and cause higher temperature separation performance than non-insulated once. Because in adiabatic process there is no heat transfer between the system and its environment thus heat is transferred only between hot and cold flows. The comparison results of using insulated or non-insulated tubes on temperature separation are seen Figure 2.8. In this experiment, inlet air temperature (T_i) was 29 ^{0}C

while inlet pressure was 3.5 bar. A single-inlet nozzle and a cold orifice which has a diameter of 0.5 D were used. As it can be seen in this figure, insulation increases the performance of a vortex tube on both temperature reduction and increment [11].

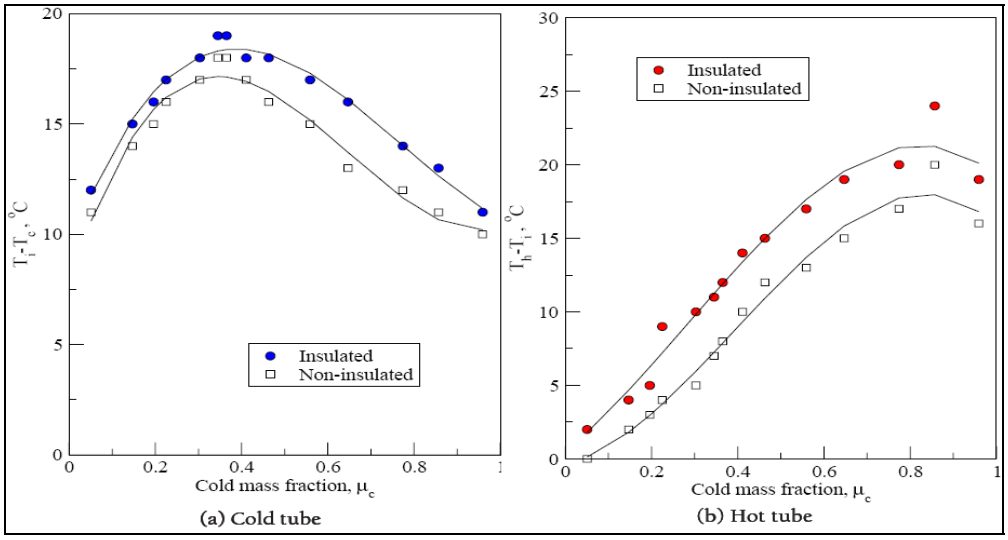

Figure 2.8. Effect of the insulated and non-insulated tubes on temperature variation in (a) cold tube and (b) hot tube, for T_i =29°C and P_i= 3.5 bar, [11].

Gao et al. [58] used a special pitot tube and thermocouple techniques to measure the pressure, velocity and temperature distribution inside the vortex tube, in which the pitot tube has only a diameter of 1mm with one hole (0.1mm diameter). In their work, the influence of different inlet conditions was studied. They found that rounding off the entrance can be enhanced and extended the secondary circulation gas flow, and improved the system's performance. Aydin and Baki [59] investigated experimentally the energy separation in a counter-flow vortex tube with various geometrical and thermo-physical parameters. The geometry of the tube was optimized to maximize the temperature difference between the cold and inlet temperatures by changing the various dimensions of the tube such as the length of the vortex tube, the diameter of the inlet nozzle, and the angle of the control valve. Moreover, the effects of various inlet pressure and different working gases (air, oxygen, and nitrogen) on temperature different in a tube were also studied.

The relevant data from the experimental work are summarized in Table 2.1. It is found that various tube dimensions and operating conditions are used, for example, from diameters as low as 4.6mm and as high as 800 mm. Table 2.1. presents variations in the maximum temperature difference between the inlet and the hot and cold streams. In this table for the same standard tube type, Scheper [16] used an inlet pressure of 2.0 atm (absolute) and obtained a temperature difference of about 8 ^{o}C between the hot and cold streams while Vennos [24] employed inlet pressure of 5.8 atm (absolute) but obtained only a temperature difference of about 12 ^{o}C. This means that, at this point, it is nearly impossible to predict how a given tube will perform because the exact nature of flow inside the tube is in doubt. However, it can be achieved if the energy separation mechanisms are understood [11].

Table 2.1. Summary of the data from the previous experimental studies [11, 60]

YEAR	INVESTIGATOR	D (mm)	P_i (abs.) (atm)	$T_h - T_i$ ($^{\circ}C$)	$T_c - T_i$ ($^{\circ}C$)	μ_c
1933	Ranque	12	7	38	-32	-
1947	Hilsch	4.6	11	140	-53	0.23
1950	Webster	8.7	-	-	-	-
1950	Blaber	9.6	5	68	-40	-
1951	Elser and Hoch	14.5	7	46	-35	-
1951	Scheper	38.1	2	3.9	-12	0.26
1956-7	Hartnett and Eckert	76.2	2.4	3.5	-40	-
1957	Martynoskii and	4.4/28	12	-	-65	-
1957	Scheller and Brown	25.4	6.1	15.6	-23	0.506
1958	Otten	20	8	40	-50	0.43
1959	Lay	50.8	1.68	9.4	-16	0
1960	Suzuki	16	5	54	-30	1
1960	Takahama and	52.8	-	-	-	-
1962	Sibulkin	44.5	-	-	-	-
1962	Reynolds	76.2	-	-	-	-
1965	Takahama	28 & 78	-	-	-	-
1966	Takahama and Soga	28 & 78	-	-	-	-
1968	Vennos	41.3	5.76	-1	-13	0.35
1969	Bruun	94	2	6	-20	0.23
1972	Syred and Beer	25.4	4.95	43	-2	-
1973	Soni	6.4 & 32	1.5 & 3	-	-	-
1982	Schlenz	50.8	3.36	-	-	-
1983	Stephan et al.	17.6	6	78	-38	0.3
1983	Amitani et al.	800	3.06	15	-19	0.4
1988	Negm et al.	11 & 20	6	30	-42	0.38

1994	Ahlborn et al.	18	4	40	-30	-
1996	Ahlborn et al.	25.4	2.7	30	-27	0.4
1999	Fröhlingsdorf and	94	3	-	-17.37	-
2000	Boucher and Tippetts	9.53	4	-	-43	0.4
2001	Guillaume and Joly	9.5	6	-	-37	0.4
2003	Saidi and Valipour	18	2.0-4.0	-	(-20) & (-38)	0.7
2004	Promvonge and	16	3.5		-33	0.33
2005	Promvonge and	16	3.5	25	-30	0.38
2004	Shannak	20	6	15	-50	0.4
2005	Gao	16	6.3	5.7	-15	0.27
2005	Alhuwayhel et al.	19	3	1.2	-11	0.1
2006	Aydin and Baki	18	5	15	-50	0.2
2007	Dincer et al.	9	2-3.20	5 & 45	(-8) & (-23)	-

2.2. PREVIOUS COMPUTATIONAL STUDIES

Today, computational analysis methods are used intensively in many applications such as in scientific researches, in production and development and so on. Indeed, these methods have more advantages than classical methods in some areas. First of all they are more economical than doing complex experiments, they are time-effective and they are applicable to many applications which are difficult to work on with classical methods.

Vortex tube is a very simple device, but physics behind the whole phenomenon is very complex. Vortex tubes deal with fluids which are in motion. Understanding mass and energy flows inside the vortex tube is very important and this is very difficult by classical methods. Computational fluid dynamics (CFD) techniques have revolutionized engineering design in several important areas, notably in analysis of fluid flow technology. CFD can also be used as a minimal adequate tool for design of engineering components. Generally in computational studies about vortex tubes, numerical solution methods are applied to solve Navier - Stokes and other balance equations and CFD softwares such as Fluent, CFX, Star CD, Flow 3D, and so on are used to analyze the vortex tube. However, because there is no exact theory to explain the vortex phenomenon and the computational results always include errors. Thus, experimental data are more valid than computational ones for vortex tube. In previous numerical investigations on the mechanism of thermal separation in vortex tubes indicate that barring a few, [8], no serious attempts have been made to use CFD techniques to simulate the flow patterns of vortex tubes [61].

Most of the past work efforts based on theoretical and analytical studies have been unsuccessful to explain the energy separation phenomenon in the tube. Also, a few attempts of applying numerical analysis to the vortex tube (see Table 2.2) have failed to predict the flow and temperature fields due to the complexity of the flow and energy separation process inside the tube. The failure of those calculations of vortex-tube flows was due to the choice of oversimplified models to describe the flow. In view of the recent computational work, the use of various turbulence models in predicting the temperature separation such as the first-order or the second-order turbulence models, leads to fairly good agreement between the predicted and the experimental results better than those found in the past decades, especially for those using second-order turbulence model [15].

Table 2.2: Summary of computational studies on vortex tubes [57]

Investigators	**Flow considered**	**Model**	**Method or software used**	**Results compared with measurements**
Linderstrom-Lang (1971)	Incompressible	Zero-equation	Stream-function	Poor but just trend
Schlenz (1982)	2D compressible	Zero-equation or mixing length	Galerkin's technique	Poor but qualitative trend
Amitani et al. (1983)	2D compressible	Neglected	Finite difference	Fair but assumptions in doubt
Borissov et al. (1993)	Incompressible	–	Velocity field induced by helical vortex	Qualitative agreement
Guston and Bakken (1999)	2D compressible	k– ε model	FLUENT^{TM} code	Fairly good
Frohlingsdorf and Unger (1999)	2D compressible	k– ε model	CFX code	Fairly good
Promvonge (1999)	2D compressible	ASM and k– ε model	Finite volume	Good
Behera et al. (2005)	3D compressible	k– ε and RNG k– ε model	Star-CD code	Fairly good
Aljuwayhel et al. (2005)	2D compressible	k– ε and RNG k– ε model	FLUENT^{TM} code	Fairly good
Skye et al. (2006)	2D compressible	k– ε and RNG k– ε model	FLUENT^{TM} code	Fairly good
Eiamsa-ard and Promvonge (2006)	2D compressible	ASM and k– ε model	Finite volume	Good

One of the most well known computational studies about vortex tube was done by W. Fröhlingsdorf and H. Unger [8]. In this study, they predicted the compressed flow and energy separation phenomena in vortex tube numerically using CFX. The basic set of

equations solved by CFX (finite volume program from AEA technologies) comprises conservation of mass, momentum and energy, expressed as balance equations for the change of mass, momentum and energy per unit volume with respect to time, [8]. Initial conditions for their study can be seen in the Table 2.3.

Table 2.3. Initial conditions used in the research of W. Fröhlingsdorf and H. Unger [8]

tube length, L	520 mm
tube radius, D	47 mm
radius of cold gas outlet orifice, d	17.5 mm
inlet area, A_i (4 nozzles)	252 mm
inlet mass stream, $\dot{m}_{in}$	0.12 kg/s
inlet pressure, P_i (absolute)	2 bar
inlet total temperature, T_i	294K
cold mass fraction, μ_c	0.23
temperature reduction	20 K
temperature increment	6 K

After the computation was conducted with the given initial conditions, they found the velocity profiles and axial and radial flow patterns as in Figure 2.9.

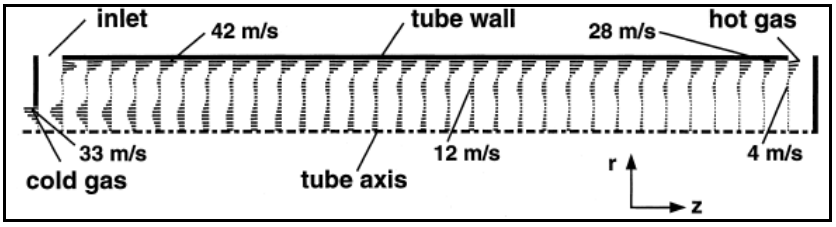

Figure 2.9. Velocity profiles of CFX calculation [8]

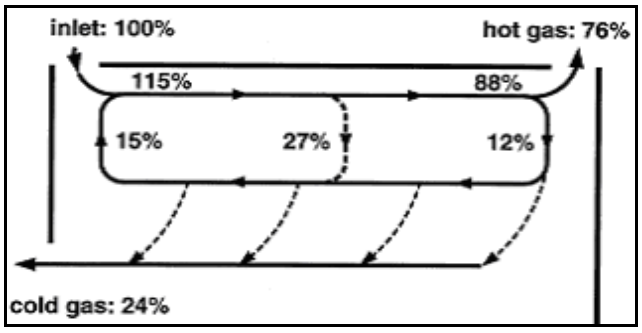

Figure 2.10. Axial and radial flow patterns of the flow inside the vortex tube by CFX calculation [8]

In velocity profile, lengths of the lines are proportional to the magnitude of velocity and the outer stream is directed to the hot gas outlet and inner stream to the cold gas outlet. The mass flow fractions given in Figure 2.10 are related to the inlet mass flow and flow patterns with mass flow fractions are easily seen from this figure.

In another computational study by Behera et al. [61], the CFD techniques were used to simulate the phenomenon of flow pattern, thermal separation, and pressure gradient. Results were used for optimizing the parameter of vortex tube. Different types of nozzle profiles and number of nozzles are evaluated by CFD analysis. The swirl velocity, axial velocity and radial velocity components as well as the flow patterns including secondary circulation flow have been evaluated. The optimum cold end diameter, d, and the length to diameter, L/D ratios and optimum parameters for obtaining the maximum hot gas temperature and minimum cold gas temperature are obtained through CFD analysis and validated through experiments. For all analysis fixed diameter of 12 mm was chosen and at inlet, the inlet pressure, $P_i = 0.5422\,\text{MPa}$, and inlet temperature, $T_i = 300\,\text{K}$, were specified. The three-dimensional model showing the boundary regions used in calculations is represented in Figure 2.11. (a) and (b). The tube walls are considered to be adiabatic and no slip conditions were used. For the numerical solution of the equation for compressible flow, a variant of well-known simple algorithm method is used [61].

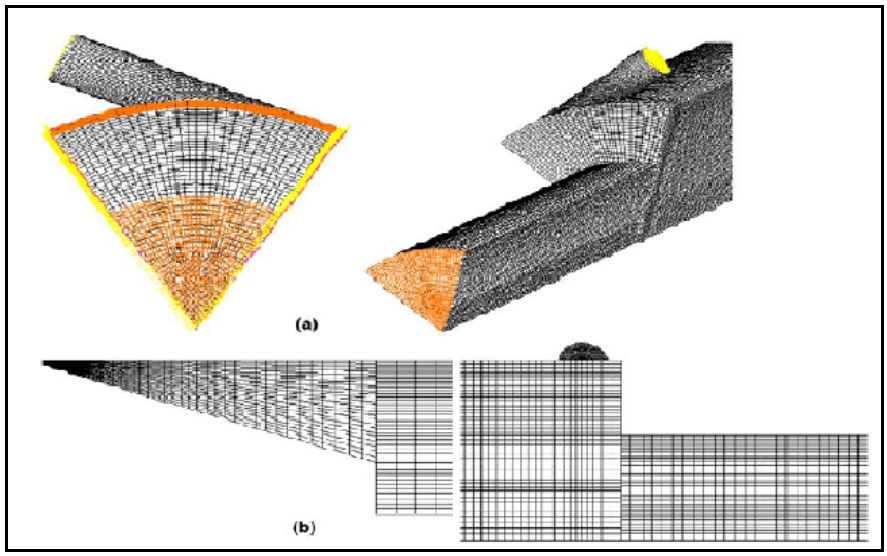

Figure 2.11. (a) Three-dimensional model of vortex tube in sector, (b) the hot end and cold end of vortex tube in sector provided with refinement in mesh [61]

In this study, to find velocity and temperature profiles by CFD analysis, a specific vortex tube of diameter, $D = 12\,\text{mm}$, length to diameter ratio $L/D = 20$, cold end diameter, $d = 7\,\text{mm}$, with six numbers of convergent nozzles was used and swirl, radial and axial velocity component were found. Moreover temperature distribution of vortex tube as shown in Figure 2.9. and it shows that the peripheral flow is hot while core flow is cold. Also the swirl velocity pattern for different type of nozzles were found and for a 12 mm diameter vortex tube this study has shown that swirl generator with six convergent nozzles gives the best performance [61].

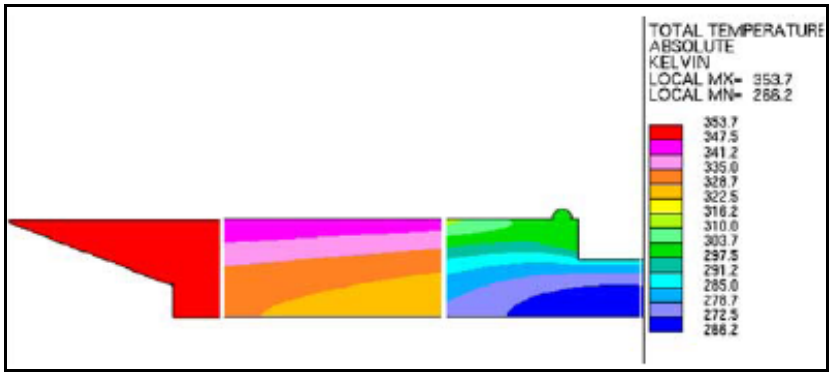

Figure 2.12. Temperature distribution of vortex tube in axial direction [61]

2.3. PREVIOUS THEORITICAL STUDIES

Early workers, including Hilsch [2], attributed the energy separation in the vortex tube to a change in the swirl velocity profile from a free vortex near the inlet nozzles to a forced vortex further along the tube. Viscous dissipation was predicted as producing the final radial temperature separation. While such a transformation would indeed presents an energy transfer from the center of flow to the periphery, as shown by Kassner and Koernschild [62], it seems extremely unlikely that it is in fact the mechanism responsible for the behavior of the Ranque - Hilsch tube. For one thing, none of the experimental studies of vortex tubes have found any evidence of a free vortex near the inlet. For another, there doesn't seem to be any physical process that could be responsible for such an effect. Kurosaka's [63] acoustic streaming comes close, but does not show the axial development assumed by others.

Deissler and Perlmutter [64] consider a planar, axially symmetric compressible vortex. Employing a turbulent diffusivity, ε, they produce an analytical solution of the swirl equation by specifying an axial velocity distribution and using continuity to realize a compatible radial flow profile. The result gives Rankine like profiles qualitatively comparable to those obtained experimentally. Using an energy equation modified to use for the expansion and contraction of eddies within the radial pressure gradient produces stagnation temperature curves broadly comparable with the result of Hartnett and Eckert [18]. A similar analysis is given by Van Deemter [65] who reaches the same conclusion.

$$pu\frac{\partial v}{\partial t}+\frac{puv}{r}=p\varepsilon\left(\frac{\partial^2 v}{\partial r^2}+\frac{1}{r}\frac{\partial v}{\partial r}-\frac{v^2}{r}\right) \tag{2.1}$$

Hinze [66] also cites the behavior of eddies in the radial pressure gradient as involved in the energy separation. The relationship between the mean radial temperature and pressure distribution is other than what might be named *adiabatic*, given for an ideal gas by the Equation (2.2). Assuming that the turbulent motion of the air particles is approximately adiabatic, then their expansion or contraction in the radial pressure gradient will cause them to adopt a temperature different than the temperature of their surroundings.

Once the fluid particle reaches its destination, it will come into thermal equilibrium with its surroundings, resulting in net heat flux.

$$\frac{T}{T_1} = \left(\frac{P}{P_1}\right)^{\frac{\gamma-1}{\gamma}} \tag{2.2}$$

Sibulkin [67] includes axial variations in his solutions by replacing variations in z with a variation in time t. By assuming the Mach number to be much less than unity throughout the flow field, the Navier – Stokes equations are decoupled from the energy equation, as the gas density no longer depends on temperature. This allows calculation of velocity profiles at points along the axis of a vortex tube (i.e. with increasing time) using numerical methods previously developed by Sibulkin [68, 69]. An initial velocity profile is required to represent the behavior of the gas at the tangential inlets. Sibulkin assumes that the inflowing gas occupies an annulus of the same height as the inlet nozzles, while the gas at the core remains undisturbed. Performance curves of the behavior of a vortex tube with the cold gas fraction are estimated by integrating the energy equation for a fluid element travelling along the centre-line of a counter flow tube. Comparison of the results with some experimental data appears favorable, and Sibulkin concludes that the Ranque – Hilsch effect is due to the differential expansion of the core and peripheral gas as it travels axially up the tube from the inlet and to thermal conduction from the quiescent core to the high speed periphery.

Linderstrom – Lang [70] presents an incompressible, axisymmetric potential solution of the Navier – Stokes equations, based on a method developed by Lewellen [71]. An order of magnitude analysis reduces the turbulent energy equation to a balance between four terms, namely axial and radial convection by the mean flow, turbulent conduction radially, and a turbulent dissipation term. The radial conduction term is evaluated with a thermal eddy viscosity is also used to model the dissipation. A parameter study based on his results shows that the Energy number, the cold mass flow fraction, the turbulent Reynolds number and the amount of radial flow in the overall flow pattern are all strong influences on the energy separation. The results stand comparison with experiment.

Linderstrom – Lang also explores that a heat exchanger analogy for vortex tube operation, originally proposed by Scheper [72]. Considering the work of Cohen [73] in the field of isotopic enrichment, a value of function to represent the effect of the tube on the gas passing through it is derived.

In a comprehensive general discussion of the Ranque – Hilsch tubes, Gulayev [74] reviews a number of works. Using a semi – empirical theory of the vortex tube, he shows that turbulent heat transfer between the parallel streams of flow is responsible for the effect.

A radical departure from conventional theories is offered by Kurosaka [63] who proposes acoustic streaming as the mechanism of energy separation. A perturbation analysis suggests that acoustic energy generated by the vortex whistle could be deposited at the periphery of the flow, thereby transforming a base Rankine vortex into a forced vortex.

Lay [75, 76] gives a flow-field solution by superposing independent potential type calculations of the axial and swirl velocity fields. No solution for the temperature field is provided, although Lay suggests that there is evidence of a transformation in the swirl velocity profile from a free to forced vortex [77].

3. PHYSICS OF VORTEX TUBES

Although the vortex phenomenon is a multi-physics problem, it can be mainly considered as a thermodynamic system. To analyze the whole phenomenon, one needs to solve the related equations which are mass balance, energy balance, continuity, Navier - Stokes equations and so on. First of all, mass is conserved in vortex tube and before writing mass balance equation, it is better to remember the definition of the parameter cold mass fraction, μ_c, which describes the amount of incoming mass flow rate that exits the tube from cold side as previously described in Equation (1.4).

The mass balance equation can be written as,

$$\dot{m}_{in} = \dot{m}_c + \dot{m}_h \tag{3.1}$$

By substituting cold mass fraction, μ_c, the mass balance equation becomes as in Equation (3.2).

$$\dot{m}_{in} = \mu_c \dot{m}_{in} + (1 - \mu_c)\dot{m}_{in} \tag{3.2}$$

For all closed systems total energy is always conserved (except in the case of nuclear reactions). According to first law of thermodynamics, the internal energy, E_{int}, of a system increases if energy is added as heat, Q, and tends to decrease if energy is lost as work, W, done by the system, as shown below.

$$\Delta E_{\text{int}} = \Delta Q - \Delta W \tag{3.3}$$

The vortex tubes have only one inlet and two outlets. Therefore, the energy balance equation can be rewritten as in Equation (3.4) where $\dot{Q}$, $\dot{W}$, $\dot{m}$, Δh, Δke, and Δpe denotes heat flow rate, net work done, mass flow rate, net enthalpy change, net kinetic energy change, and net potential energy change, respectively.

$$\dot{Q} - \dot{W} = \dot{m}\left(\Delta h + \Delta ke + \Delta pe\right) \tag{3.4}$$

There is no net work done on the vortex tube system and the change in potential energy can also be neglected. Considering these, energy balance equation for vortex tubes can be written as follows.

$$\dot{Q} = \dot{m}\left(\Delta h + \Delta ke\right) \tag{3.5}$$

As it is expressed in the Equation (3.5), if the enthalpy and kinetic energy change between inlet and outlets of the vortex tube is measured, net heat flow rate can be calculated.

Another important equation for the vortex tube is the continuity equation. The continuity equation in cylindrical coordinate system is shown in Equation (3.6). First part of the equation is the change in density with respect to time and the other parts are the derivatives of velocity in cylindrical components. In this equation, υ_x, υ_y and υ_z are *x*, *y* and *z* components of the velocity vector.

$$\frac{\partial \rho}{\partial t} + \frac{1}{r}\frac{\partial (\rho r \upsilon_r)}{\partial r} + \frac{1}{r}\frac{\partial (\rho \upsilon_\theta)}{\partial \theta} + \frac{\partial (\rho \upsilon_z)}{\partial z} = 0 \tag{3.6}$$

Because the vortex tubes deal with gases, the Navier - Stokes equations which describe the motion of fluid substances should also be used. These equations state that the changes in momentum (acceleration) of fluid particles are simply the product of changes in pressure and viscous forces (similar to frictional forces) acting inside the fluid. Thus, the Navier - Stokes equations are the dynamical statement of the balance of forces acting at any given region of the fluid [78]. The general form of the Navier - Stokes equations in cylindrical coordinate system for the directions r, θ and z are given in Equations (3.7), (3.8) and (3.9), respectively.

$$\rho\left(\frac{\partial \upsilon_r}{\partial t}+\upsilon_r\frac{\partial \upsilon_r}{\partial r}+\frac{\upsilon_\theta}{r}\frac{\partial \upsilon_r}{\partial \theta}-\frac{\upsilon_\theta{}^2}{r}+\upsilon_z\frac{\partial \upsilon_z}{\partial z}\right)=$$
$$-\frac{\partial \rho}{\partial r}+\mu\left(\frac{1}{r}\frac{\partial}{\partial r}\left(r\frac{\partial \upsilon_r}{\partial r}\right)-\frac{\upsilon_r}{r^2}+\frac{1}{r^2}\frac{\partial^2 \upsilon_r}{\partial \theta^2}-\frac{2}{r^2}\frac{\partial \upsilon_\theta}{\partial \theta}+\frac{\partial^2 \upsilon_r}{\partial z^2}\right)+\rho G_r \tag{3.7}$$

$$\rho\left(\frac{\partial \upsilon_\theta}{\partial t}+\upsilon_r\frac{\partial \upsilon_\theta}{\partial r}+\frac{\upsilon_\theta}{r}\frac{\partial \upsilon_\theta}{\partial \theta}+\frac{\upsilon_r\upsilon_\theta}{r}+\upsilon_z\frac{\partial \upsilon_\theta}{\partial z}\right)=$$
$$-\frac{1}{r}\frac{\partial \rho}{\partial \theta}+\mu\left(\frac{1}{r}\frac{\partial}{\partial r}\left(r\frac{\partial \upsilon_\theta}{\partial r}\right)-\frac{\upsilon_\theta}{r^2}+\frac{1}{r^2}\frac{\partial^2 \upsilon_\theta}{\partial \theta^2}+\frac{2}{r^2}\frac{\partial \upsilon_r}{\partial \theta}+\frac{\partial^2 \upsilon_\theta}{\partial z^2}\right)+\rho G_\theta \tag{3.8}$$

$$\rho\left(\frac{\partial \upsilon_z}{\partial t}+\upsilon_r\frac{\partial \upsilon_z}{\partial r}+\frac{\upsilon_\theta}{r}\frac{\partial \upsilon_z}{\partial \theta}+\upsilon_z\frac{\partial \upsilon_z}{\partial z}\right)=$$
$$-\frac{\partial \rho}{\partial z}+\mu\left(\frac{1}{r}\frac{\partial}{\partial r}\left(r\frac{\partial \upsilon_z}{\partial r}\right)+\frac{1}{r^2}\frac{\partial^2 \upsilon_z}{\partial \theta^2}+\frac{\partial^2 \upsilon_z}{\partial z^2}\right)+\rho G_z \tag{3.9}$$

In these equations, μ denotes the viscosity coefficient. It is a property of a fluid and it shows how viscous a fluid is. It can be regarded as a friction coefficient and like friction, it causes resistance while the fluid is flowing. Generally gases have smaller μ value than liquids. G_r, G_θ and G_z are gravitational acceleration in these directions and for the vortex tubes, the gravitational effects are usually neglected, so the last terms of all three equations above are zero. ρ is the density of fluid. In many cases, the constant density assumption is used to simplify the equation. However, the flow inside the vortex tube is compressible and assumed to be turbulent, thus, the constant density assumption is not valid for the exact outcome.

3.1. EFFICIENCY OF VORTEX TUBES

Because the vortex tubes are mainly used for cooling applications, the cooling efficiencies are more important. The cooling efficiencies are calculated by using the principle of adiabatic expansion of ideal gas. The ideal gas law is as shown in Equation (3.10) where P is the pressure, V is the specific volume, T is the temperature of the gas and R is the gas constant which is defined in Equation (3.11).

$$PV = nRT \tag{3.10}$$

$$R = \frac{R_u}{M} \tag{3.11}$$

In Equation (3.11), R_u is the universal gas constant, which is $8.314\,\text{kJ/(kmol.K)}$ or $8.314\,\text{kPa.m}^3\text{/(kmol.K)}$, and M is the molar weight of the gas.

Efficiency of a vortex tube is defined as,

$$\eta_{\text{is}} = \frac{T_i - T_c}{(\Delta T)_{is}} \tag{3.12}$$

Where η_{is} is the isentropic efficiency, T_i and T_c are the actual inlet and cold end temperatures, respectively, and $(\Delta T)_{is}$ is the isentropic temperature difference.

$(\Delta T)_{is}$ occurs as follows: If the vortex tube is assumed to work isentropically (ideal case with no loss), then as air flows into the vortex tube and an isentropic (no entropy chance) expansion occurs. This case can be expressed as

$$(\Delta T)_{is} = T_i \left(1 - \left(\frac{P_{atm}}{P_{in}} \right)^{\frac{\gamma - 1}{\gamma}} \right) \tag{3.13}$$

In this equation, P_{atm} and P_{in} are atmospheric and inlet pressures, respectively, and γ is the specific heat ratio of the gas (γ is known for different gases and for air, $\gamma_{air} \approx 1.4$). Thus, isentropic efficiency of a vortex tube can be calculated by measuring pressure and temperature of the inlet and cold side temperature, [11].

4. APPLICATIONS OF VORTEX TUBES

In the section 1.1, general information about applications of vortex tube are presented. This chapter considers the potential of the tube to be used in a number of specific industrial applications in detail, by focusing on simple heating and cooling, gas liquefaction, and mixture separation processes.

4.1. SIMPLE HEATING AND COOLING APPLICATIONS

Although the efficiency of the device is poor compared to conventional techniques, its low capital cost can overcome this disadvantage. It is particularly useful where there is a ready supply of compressed gas, as in these circumstances, the heating and cooling required can be obtained almost free. Some applications, considering heating and cooling, are correcting for the aerodynamic heating experienced by thermometers in high speed aircrafts [80], cooling sensitive materials undergoing machining operations [81], cooling experiments in laboratories dealing with explosive chemicals [82], use in conjunction with thermocouples to improve the performance of a Peltier refrigerator [83] and temperature of control of divers' air supplies [84], manned underwater habitats [86], and hyperbaric chambers [87]. In Figure 4.1, some examples of industrial vortex tube applications are shown [77].

4.2. GAS LIQUEFACTION APPLICATIONS

The simplest application of the vortex tube to gas liquefaction would be as a supplement to the throttle cooling of the Linde process as suggested in Figure 4.2. Inclusion of a vortex tube in the Linde process could have a number of advantages. Most notable is that all gases would effectively have an artificially enhanced isenthalpic Joule – Thomson coefficient. Expansion would automatically give a cooling effect, and then any pre – cooling system would be unnecessary. This saving would have to be offset against the reduction in yield produced by venting off a substantial proportion of the inlet flow.

Figure 4.1. Cooling of electrical control cabinets by using commercial vortex tubes (a) and (b). In (c), spot cooling of a cutting tool in milling operation and vortex tube as a personal air-conditioner (d) [85]

It is quite possible that the throttle could be entirely replaced by a vortex tube. In the Claude and Heylandt processes, care has to be taken to avoid condensation within the expansion engine, and the final cooling stage is always a throttle. Such precautions are not necessary with the vortex tube, which can quite happily cool saturated gases. That gas liquefaction which is possible in Ranque – Hilsch tubes has been demonstrated by Fin'ko [88] who operated a counter flow vortex tube on air pre-cooled with liquid nitrogen. His experiments found liquid air running from the cold outlet, although the two phase nature of the flow seemed to degrade the performance [77].

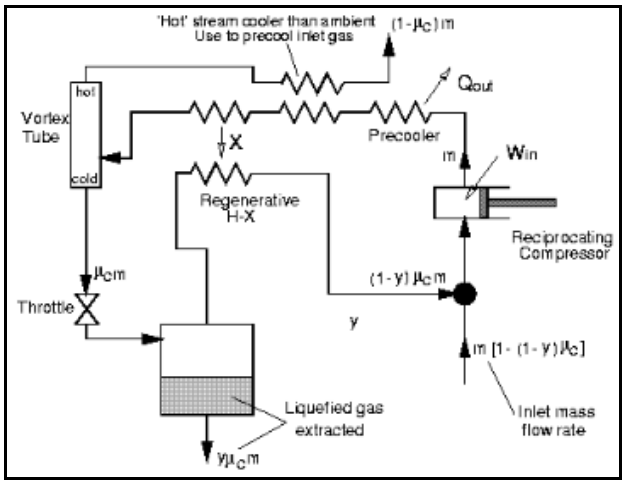

Figure 4.2. Linde-type gas liquefaction process incorporating a vortex tube [77]

4.3. MIXTURE SEPERATION APPLICATIONS

The first attempts to use the vortex tubes in the separation of gas mixtures were done by Johnson [89] and Wenig [90], but unfortunately they both failed. On the other hand, Elser and Hoch [91] finalized a small accurate suspension balanced separation of air and air – carbon dioxide mixtures successfully. Keyes realized gas separation using helium and C_8F_{16} in a specially designed vortex tube. In 2001, Raterman *et al.* [92] used vortex tubes to separate carbon dioxide. Kulkarni and Sadesai [93] employed vortex tubes to enrich the methane concentration in 2002. In 2004, Khodorkov *et al.* [94] used natural gas as the working fluid and liquefied natural gas with a vortex tube [77].

5. CURRENT EXPERIMENTAL RESEARCH

This chapter presents the current experimental study to investigate vortex phenomenon and to optimize its performance characteristics. Results gained from many different experiments that were conducted will be shown and evaluated to improve the device performance. Although there was no previous attempts, additional experiments were performed to examine the performance of the vortex tube under high inlet gas pressures starting from 10 Bar (g) and up.

5.1. GOALS OF THIS STUDY

This study has following main goals:

- Design and manufacture an experimental prototype that is very modular and easy to operate,
- Change geometrical parameters of prototype and inlet conditions,
- Investigate the effects of vortex tube geometry (such as the length and diameter of the hot tube, number of generator inlet nozzles, angles of the vortex cones), inlet pressure, material of the cold tube and insulation on performance of the vortex tube.
- Examine the performance of the vortex tube under high inlet gas pressures starting from 10 Bar (g) and up.
- Calculating isentropic efficiencies in each case for performance comparison
- Finding an improved vortex tube design.

5.2. DESIGN OF THE EXPERIMENTAL PROTOTYPE

Designing of the prototype was started with the decision of the type of the vortex tube. Because of its high efficiency and ease in design, manufacture and control, counter-flow vortex tube was selected. All of the parts of the prototype were designed and tested by using Pro Engineer WF4.0 software. 3D design pictures of the prototype are shown in Figure 5.1.

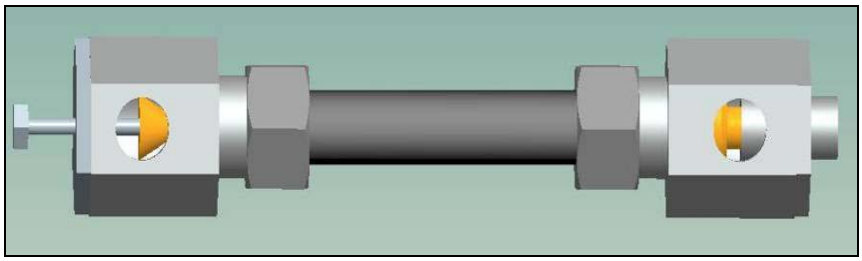

(a)

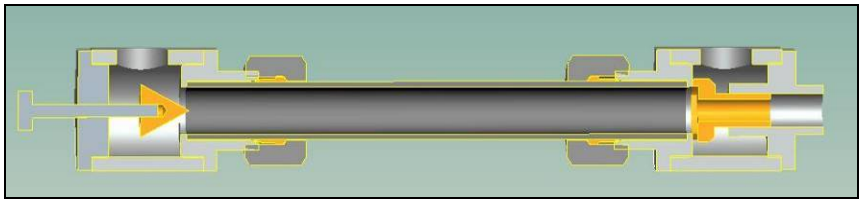

(b)

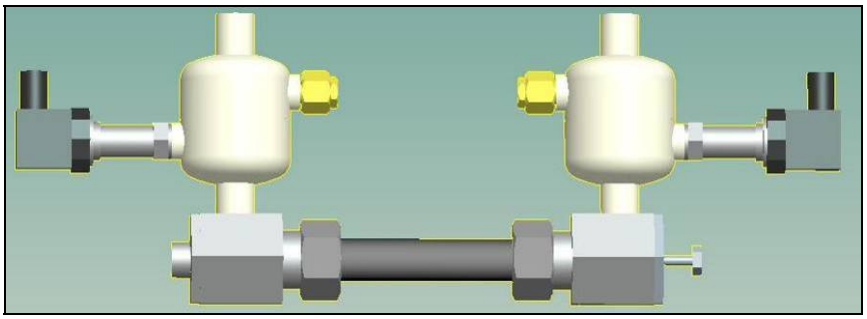

(c)

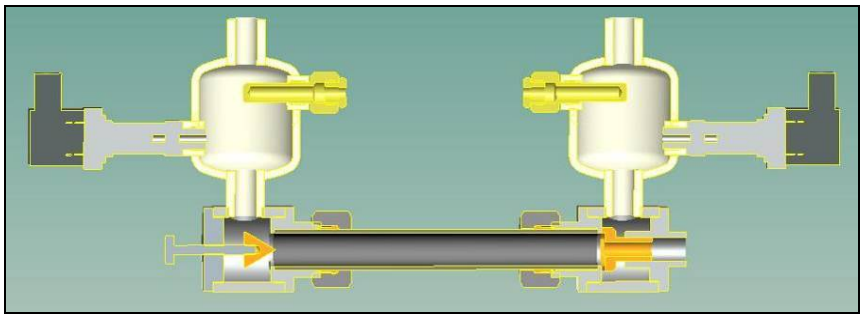

(d)

Figure 5.1. Design pictures of the prototype: general view (a) and cross-sectional view of the vortex tube (b). Inlet and hot outlet collectors are shown in (c) and its cross-sectional view in (d).

Parts like vortex generators and vortex cones that are used in experiments can be seen in Figure 5.2. Main parts such as inlet and outlet ports, adjustment screw of vortex cone, adapters, and measurement collectors were made of steel. The parts which must have high surface quality and resistance to corrosion, such as vortex generators and cones, were manufactured from brass. Seamless aluminum and steel pipes were used as hot tubes.

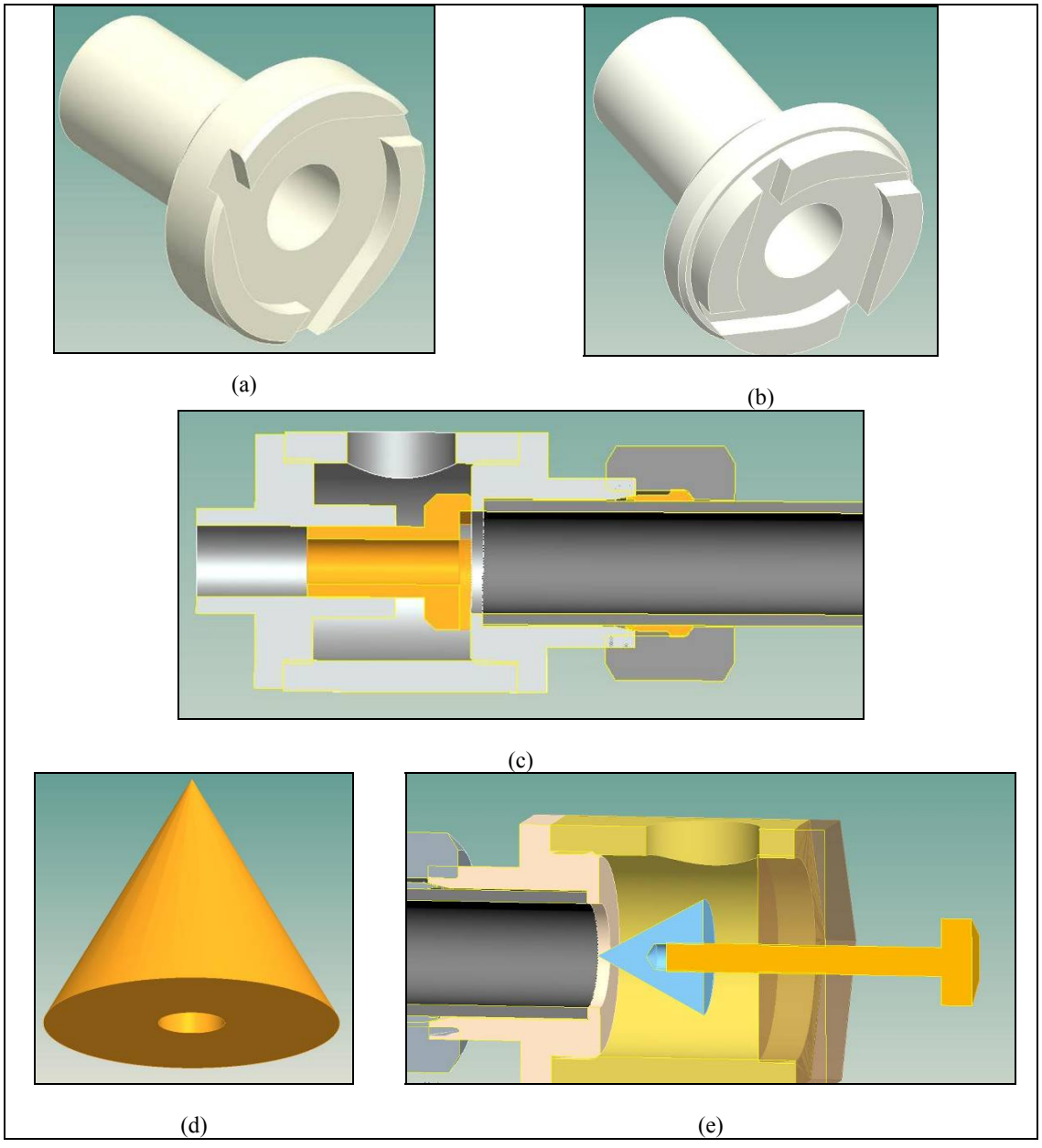

Figure 5.2. (a), (b): Design pictures of generators with 3 and 4 inlet nozzles, and its detailed view in tube assembly (c). One of vortex cone pictures (d) and its detailed, cross-sectional view in hot side of the tube (e).

5.3. EXPERIMENTAL APPARATUS

During the experiments, two different experimental setups were used. The first set-up shown in Figure 5.3 was constructed for all experiments except high pressure case.

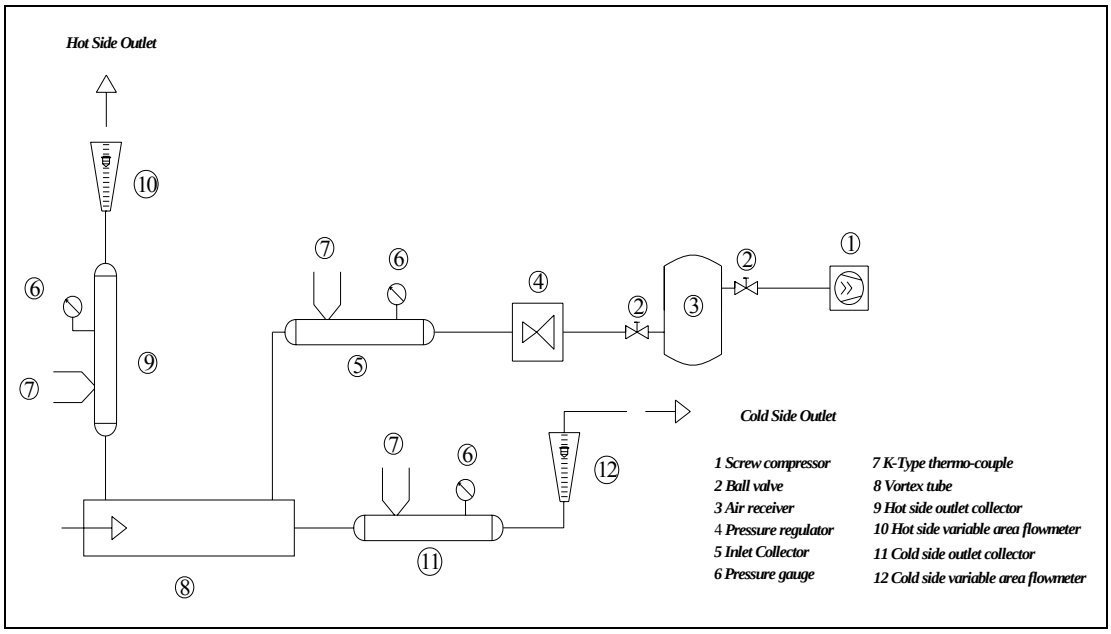

Figure 5.3. Experimental apparatus used in all experiments except high pressure case.

Commercial Rotary-Screw Compressors have very high efficiencies and flow rates with uniform pressure profile. However, these compressors have maximum working pressure of 14.5 bar (g). During high pressure experiments, at least 15 bar (g) or higher pressures were needed at the inlet of the vortex tube after the pressure regulator. This means, 20 bar (g) or higher pressures must be supplied to the second-stage air receiver tank to provide uniform pressure profile at the inlet. To do so, a reciprocating compressor installed to the new experimental set-up as the second-stage compressor. Also, the second-stage air receiver with its accessories installed the system too.

Figure 5.4. and Figure 5.5. show this modified apparatus and the simplified representation of the vortex tube with significant parameters and parts, respectively. Most of the parts that were used during the experiments are also presented in Figure 5.6.

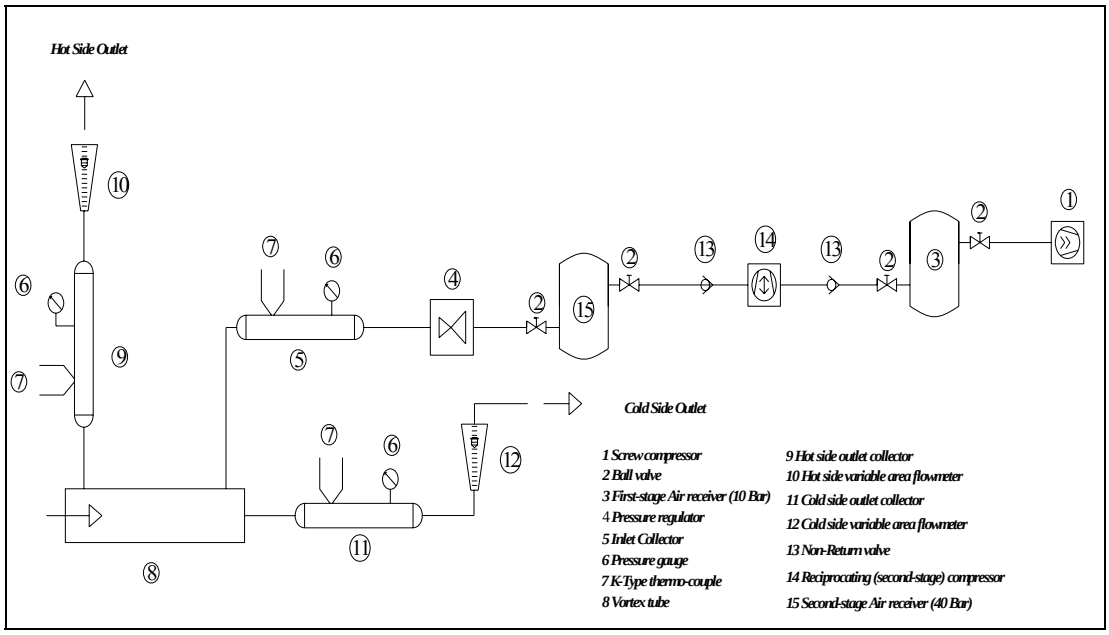

Figure 5.4. Experimental apparatus used in high pressure case.

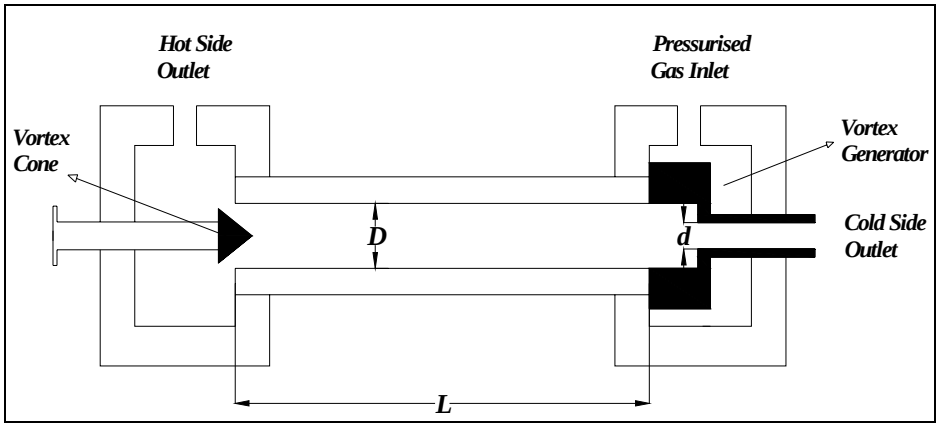

Figure 5.5. Simple representation of the vortex tube including main parts and dimensions.

Figure 5.6. Main parts used in experiments: Vortex Tube Prototype (a), VT with installed collectors and measurement devices (b), Rotary-Screw Compressor (c), Reciprocating 'Booster' Compressor (d), pressure regulator (e) and general parts used in (f).

In the first setup, air is compressed to 10 bar (g) and stored in the air receiver. After passing through the pressure regulator and inlet collector, the air reaches the vortex tube inlet. During the experiments, ratio of the hot and cold flows is adjusted by vortex cone adjustment screw. Hot and cold outlet collectors were equipped with pressure gauges, k-type thermocouples and variable area flow meters to measure pressure, temperature and the flow rates at the outlets respectively.

In the second setup, the only difference is installation of the second-stage compressor and receiver with equipments to the system to provide high enough pressures.

5.4. EXPERIMENTAL RESULTS

In previous sections, experimental prototype and set-ups were explained in detail. Because of the quantity and the complexity of the experiments, focusing on the important steps and organizing the experiments for this research were needed. Table 5.1. shows the summary of the sets of experiments and their constant and variable parameters.

In each sets of experiments, some parameters were kept constant during the experiments. Variable parameters were changed in every step. Cold mass fraction is the crucial parameter to understand the flow characteristics of the vortex tube and to calculate its performance. Through the experiments, inlet pressure (P_i), outlet pressures (P_h, P_c), temperatures of the inlet (T_i) and outlets (T_h, T_c) were measured simultaneously. Flows at the hot and cold outlets of the tubes were measured by variable area flowmeters (shown in Figure 5.6.-b and f).

These flowmeters are calibrated to operate at a specific set of conditions, and deviations from those standard conditions require corrections in measurements. In practice, the reading taken from the flowmeter scale must be corrected back to standard conditions to be used with the scale units. The correct location to measure the actual pressure and temperature is at the exit of the flowmeter, except under vacuum applications where they should be measured at the flowmeter inlet. The equation to correct for nonstandard operating conditions is as follows:

$$Q_{act} = Q_{read}\sqrt{\frac{P_{act}T_{ref}}{P_{ref}T_{act}}} \tag{5.1}$$

where Q_{act} is the actual (calibrated) while Q_{read} is the observed value from flow meter, P_{act} and T_{act} actual pressure and temperature at the conditions while the readings taken, and P_{ref} and T_{ref} are the reference pressure and temperature for the flow meter respectively.

After calculating the actual flows at the ends of the tube, density of the air and mass flow rates at each end are calculated. Then cold mass fraction is calculated by using Equation (1.4).

Although the temperatures at the condition of $\mu_c = 1$ (all the inlet gas flow directly from cold end of the vortex tube) were measured, the results were ignored and not considered in the graphs. Because, the measured temperatures in this case were collector inside temperatures and had no relationship with hot flow. As a result of closing all the areas in hot side by vortex cones, no hot flow occurs inside the hot side outlet collector, so the temperature in this condition, should not be considered.

Finally, the isentropic efficiency is calculated by using Equation (3.12) and (3.13) to find the most efficient condition and improve the vortex tube. Appendices include all the experimental data and calculations for all sets of experiments.

All the experiments were performed in DALGAKIRAN KOMPRESOR R&D Laboratory while the ambient temperature was +16 C^0.

Table 5.1. Summary of the sets of experiments performed in current research including constant and variable parameters.

#	Sets of Experiments	Constant Parameters	Variable Parameter	Experimental Data and Calculations
1	# of inlet nozzles at vortex generator	P_i, L, D, d, material of the hot tube, and Vortex Cone Angles	Number of inlet nozzles at generator from 1 to 4.	APPENDIX A
2	Length of the Hot Tube (L)	P_i, D, d, Vortex Cone Angles, material of the hot tube, and # of inlet nozzles in generator	Length of the Hot Tube from 10D to 50D	APPENDIX B
3	Vortex Cone Angles	P_i, L, D, d, material of the hot tube, and # of inlet nozzles in generator	Vortex Cone Angle changing from 40^0 to 75^0.	APPENDIX C
4	Insulation Effect	P_i, D, d, Vortex Cone Angles, material of the hot tube, and # of inlet nozzles in generator	Insulation of the Hot tube	APPENDIX D
5	Material of The Hot Tube,	P_i, D, d, Vortex Cone Angles, and # of inlet nozzles in generator	Material of The Hot Tube changing from Aluminum to Steel	APPENDIX E
6	Cold Orifice Ratio (d/D)	P_i, D, d, Vortex Cone Angles, material of the hot tube, and # of inlet nozzles in generator	Cold Orifice Ratio (d/D) changing by using pipe different diameter (D) and keeping cold orifice diameter (d) constant.	APPENDIX F
7	Inlet Pressure (P_i)	D, d, Vortex Cone Angles, material of the hot tube, and # of inlet nozzles in generator	Inlet Pressure (P_i) changing from 2 bar(g) to 15,5 bar(g)	APPENDIX G

5.4.1. Effect of the Number of Inlet Nozzles in Vortex Generator

Since the Vortex Tube was invented in 1933, all previous researchers have accepted that increasing swirl (tangential) velocities inside the tube led to higher temperature separation and increases the efficiency of the RHVT.

In this sets of experiments, four different vortex generators, shown in Figure 5.7, each having different number of nozzles from one to four were used. Because of some manufacturing defects (seen in center of cold orifice) in generator with three inlet nozzle, results were ignored and not shown in comparison graphs.

Figure 5.7. Vortex generators with inlet nozzle numbers from 1 to 4. Other geometrical parameters of the generators are all the same.

In the generators, all geometrical dimensions are kept same, except number of inlet nozzles. Especially, cold orifice diameter, which is the diameter of the hole at the center of the generator, is kept at a value of d= 7.94 mm. Table 5.2. shows constant parameters during this set of experiments and their values. Results of this section can be seen in Figure 5.8.

Table 5.2. Constant parameters and their values during the experiments of 'Vortex generators with different inlet nozzle numbers.

	PARAMETER	**VALUE**
1	Length of the Hot Tube (L)	20 D
2	Inlet Pressure (P_i)	6 Bar(g)
3	Diameter of the Hot Tube (D)	19 mm
4	Cold Orifice Diameter (d)	7.94 mm
5	Vortex Cone Angle	40^0
6	Material of the Hot Tube	Seamless Aluminum pipe

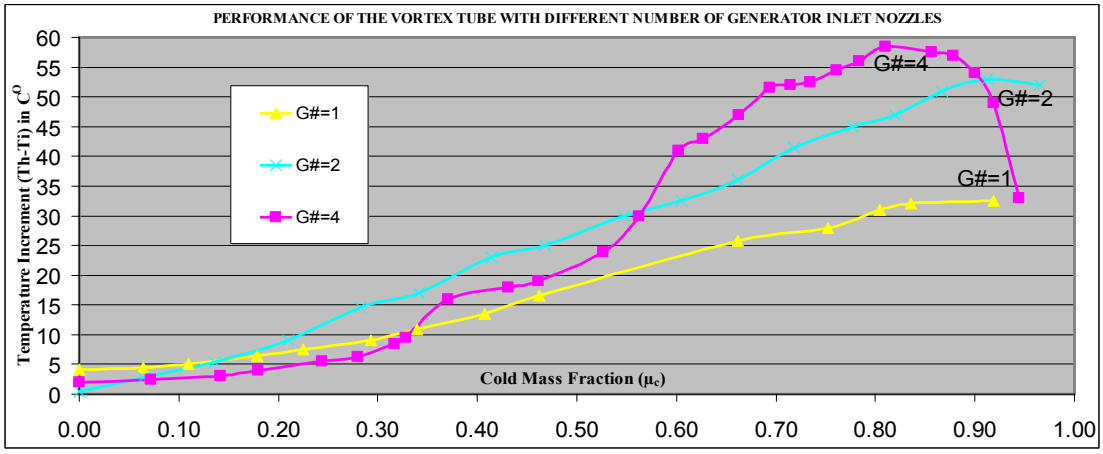

(a)

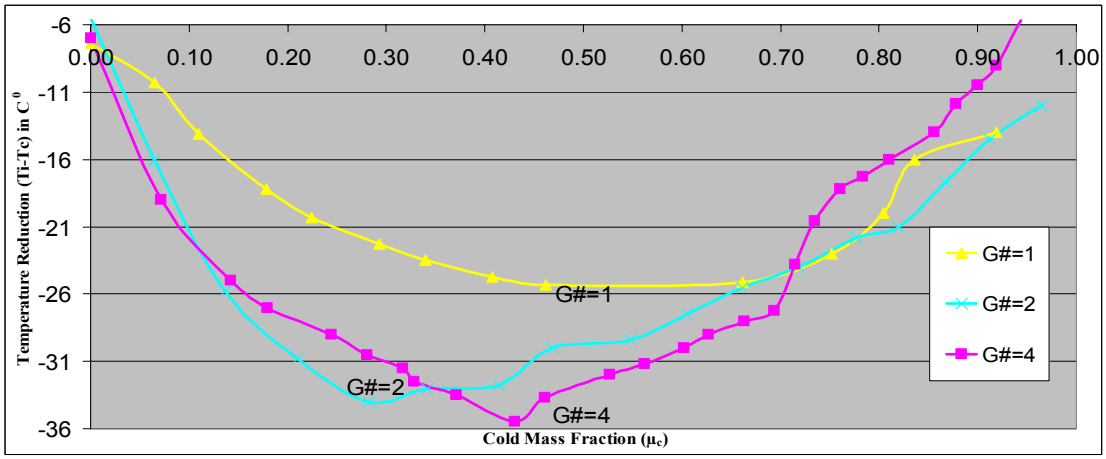

(b)

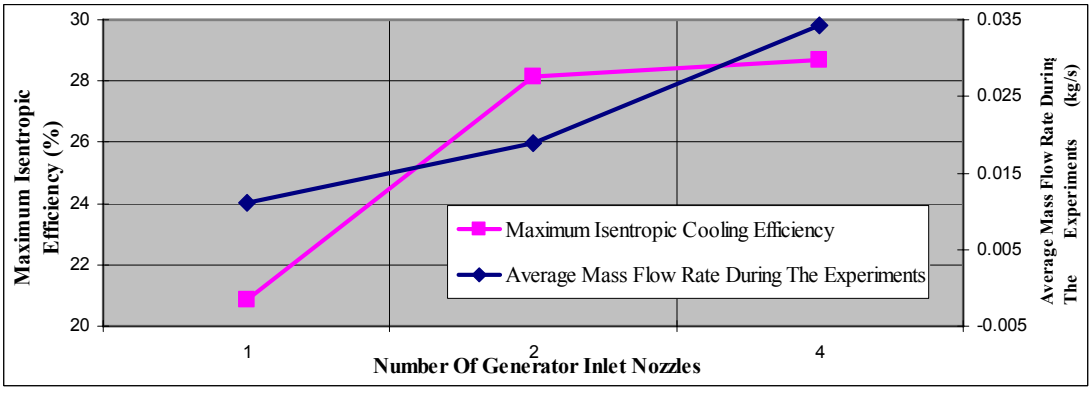

(c)

Figure 5.8. Results of the experiments of vortex generators with inlet nozzle numbers from 1 to 4. Temperature increment vs. cold mass fraction shown in (a), while temperature reduction vs. cold mass fraction presented in (b). In (c): the maximum isentropic efficiencies obtained by generators and average mass flow rate during the experiments are shown.

The first two graphs show that temperature separation effect increases with number of inlet nozzles. Four inlet nozzles case is the most efficient case in both temperature increment and reduction. Increasing the number of nozzles creates better flow profile in the generator and helps to speed up the rotational flow speeds and to increase the mass flow rate and strong swirl flow into the vortex tube. In addition, this gave rise to higher friction dissipation between the boundary of the flows and a higher momentum transfer from the core region to the wall region. This reduced temperature in the tube core while increased temperature in the tube wall area, [11]. The last graph not only shows the isentropic efficiencies of the generators, but also average mass flow rates during these experiments.

5.4.2. Effect of the Length of the Hot Tube

The length of the hot tube is another important geometrical parameter of the vortex tube. Many previous experimental studies were conducted to understand the effect of the hot tube length on the performance of the RHVT and to find optimum value. Most of the researchers believe that performance of the vortex tube is very low when $L/D < 20$ and almost constant when $L/D > 55$.

In this sets of experiments eight different seamless aluminum pipes, shown in Figure 5.9, were used as hot tube each having diameter of 19 mm. Length of the tubes were varying form 15D to 50D. Table 5.3, also shows constant parameters during this set of experiments and their values. Results of this section can be seen in Figure 5.10.

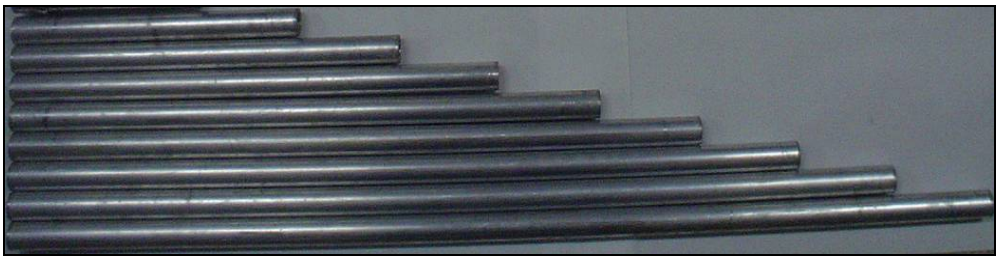

Figure 5.9. Length of the hot tubes were changed from 15D to 50D. The seamless aluminum pipes had constant diameter of 19 mm during this group of experiments.

Table 5.3. Constant parameters and their values during the experiments of "hot tube with different lengths from 15D to 50D".

	PARAMETER	VALUE
1	Number of inlet nozzle	1
2	Inlet Pressure (P_i)	6 Bar(g)
3	Diameter of the Hot Tube (D)	19 mm
4	Cold Orifice Diameter (d)	7.94 mm
5	Vortex Cone Angle	40^0
6	Material of the Hot Tube	Seamless Aluminum pipe
7	Average Mass Flow Rate	0.0110 kg/s

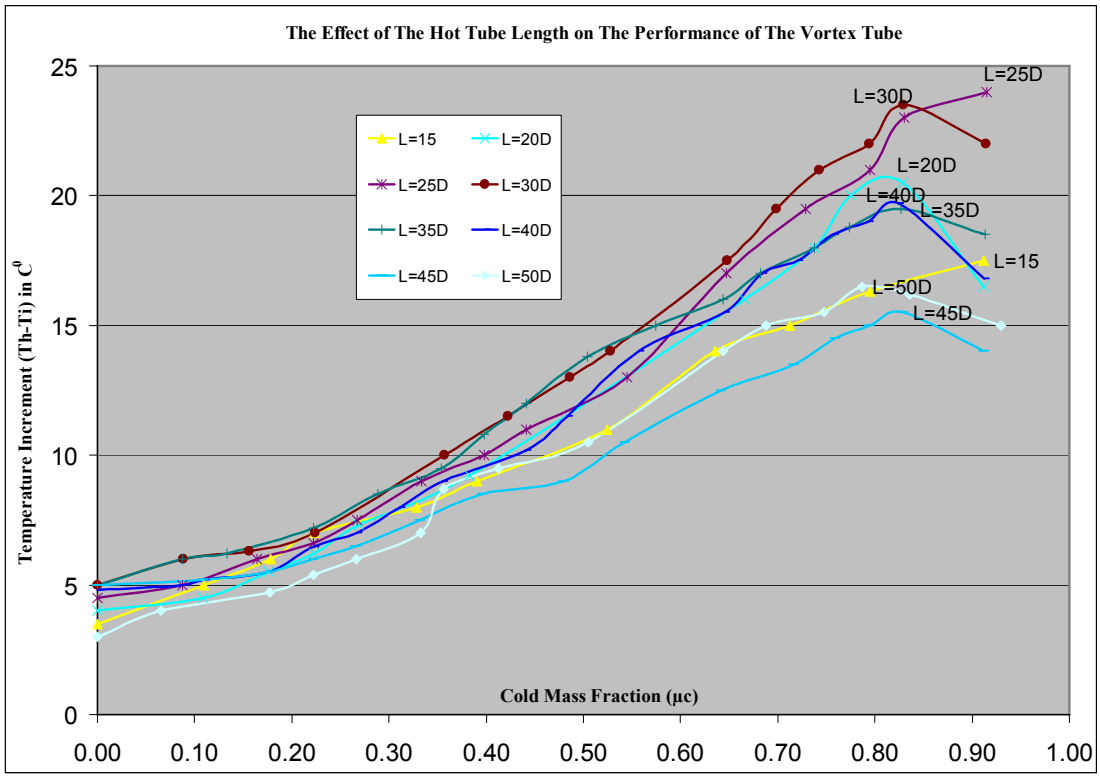

(a)

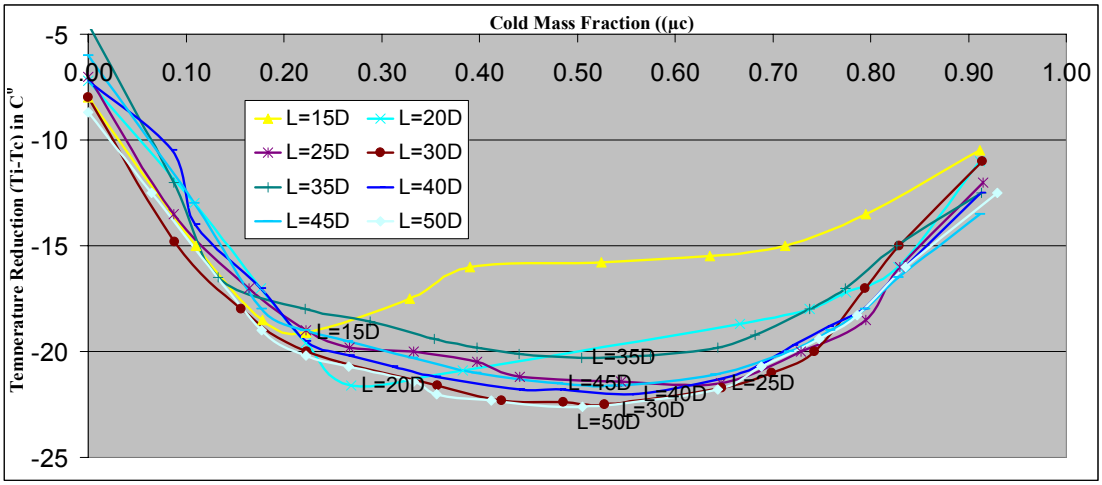

(b)

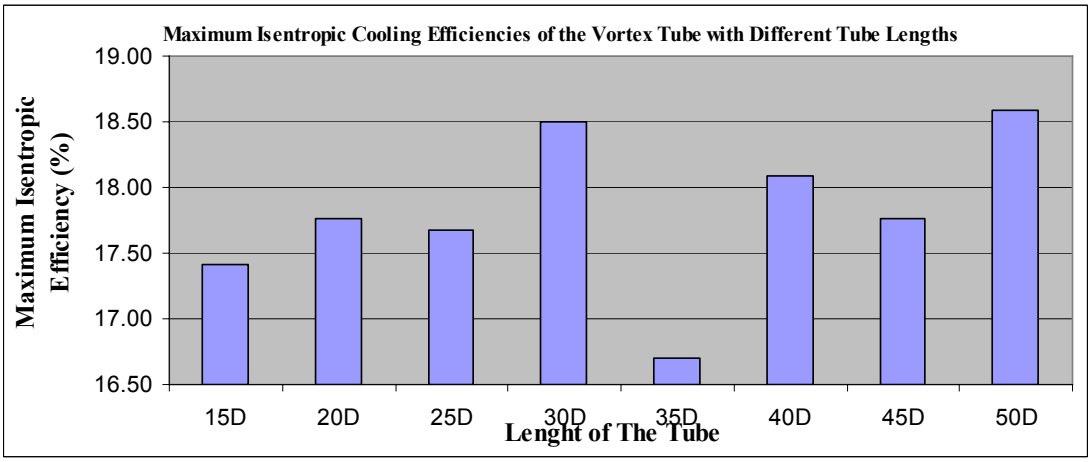

(c)

Figure 5.10. Results of the experiments of vortex tube with different hot tube length from 15D to 50D. Temperature increment vs. cold mass fraction shown in (a), while temperature reduction vs. cold mass fraction presented in (b). In (c): the maximum isentropic efficiencies obtained with different tube lengths are shown.

The first two graphs show that temperature increment and reduction versus cold mass fraction for the vortex tube with different hot tube length from 15D to 50D. L=50D is the most efficient geometry for temperature reduction. On the other hand, this pipe has low temperature increment performances, while L=25D and L=30D have much better performances. L=30D case also has high efficiency in temperature reduction, too. This result can also be realized easily in the last graph. This length has isentropic efficiency which is very close that of L=50D. During the experiments, heat transfer rate between hot tube and the environment is much higher in L=50D than L=30D. As the surface of the pipe

increases, amount of the heat energy loss to the ambient increases too. This explains the reason of L=50D having better cooling performance while having worse heating performance than L=30D. The unclear point of this group of experiments is that observing very low efficiency and thermal separation characteristics of L=35D pipe, this could happen if there was a leakage in that combination during the experiments. The average mass flow rates of the pressurized air were constant during these experiments. Because it is a function of the inlet area, inlet pressure, inlet temperature, and internal pressure of the prototype. Thus, length of the tube does not change the mass flow rate.

5.4.3. Effect of the Vortex Cone Angles

In a vortex tube, after a pressurized gas is injected tangentially from the inlet of the tube, the gas beam splits into two streams, by the help of a conical obstacle. This blockage inside the tube lets a part of the incoming stream to reflect and flow to the opposite direction. In the preliminary researches, investigators had used some stopcocks to create reverse flow to observe the vortex phenomenon. A good example to these is the Hilsch`s investigation which was presented and discussed in chapter 2. After that, researchers preferred using spherical and conical obstacles instead of using stopcocks at the end of the hot side of the vortex tube. Now with a common acceptance, conical obstacles are used in all vortex tubes. However, there are not sufficient previous efforts showing the effect of the cone geometry, mainly cone angle, on the performance of the vortex tube.

The aim of this set of experiments is to observe the effect of the cone angle on the performance of the tube. Therefore, 4 different conical obstacle both having same material properties and same base diameter (20 mm) was used. Cone angle of these obstacles were 40^0, 45^0, 60^0 and 75^0 respectively. Figure 5.11. shows these conical nozzles and the apparatus that was used for adjusting the position of the cones inside the tube. By using this equipment, positions of the conical nozzles were adjusted precisely and thus ratio of the flows in each end of the tube was changed. Hence, cold mass fractions in each adjustment also changed. Table 5.4. also shows constant parameters during this set of experiments and their values.

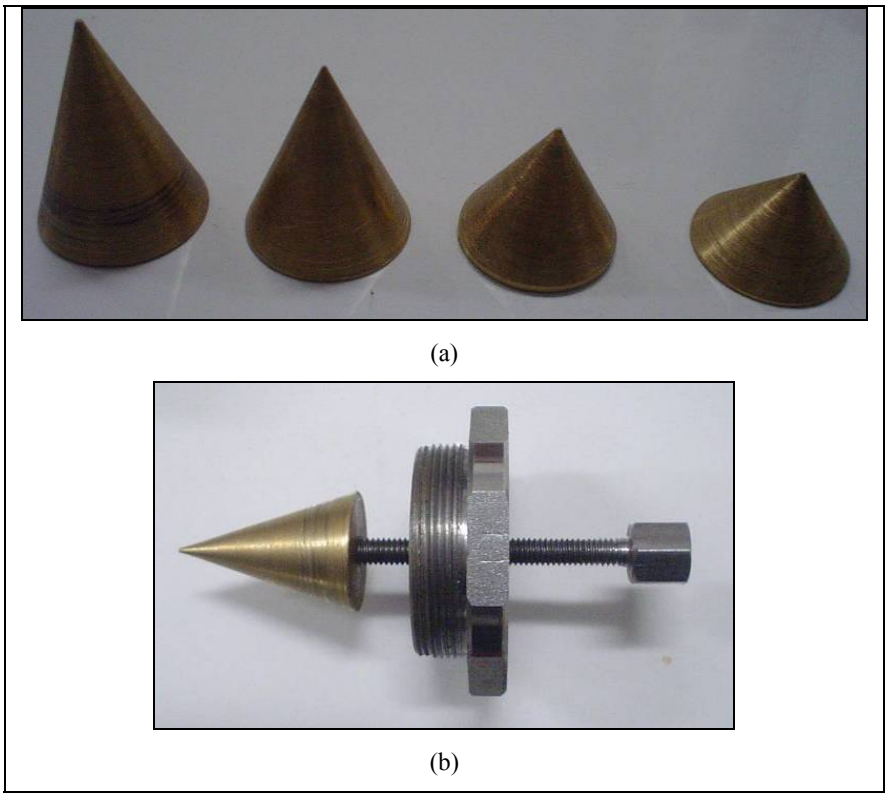

(a)

(b)

Figure 5.11. Conical nozzles used in the experiments shown in (a) and the apparatus for adjusting the position of the nozzles inside the hot end of the tube shown in (b).

Table 5.4. Constant parameters and their values during the experiments of "conical nozzles with different angles from 40^0 to 75^0".

	PARAMETER	VALUE
1	Number of inlet nozzle	1
2	Inlet Pressure (P_i)	6 Bar(g)
3	Diameter Of the Hot Tube (D)	16 mm
4	Cold Orifice Diameter (d)	7.94 mm
5	Length Of the Hot Tube (L)	20 D
6	Material Of the Hot Tube	Seamless Aluminum pipe
7	Average Mass Flow Rate	0.0110 kg/s

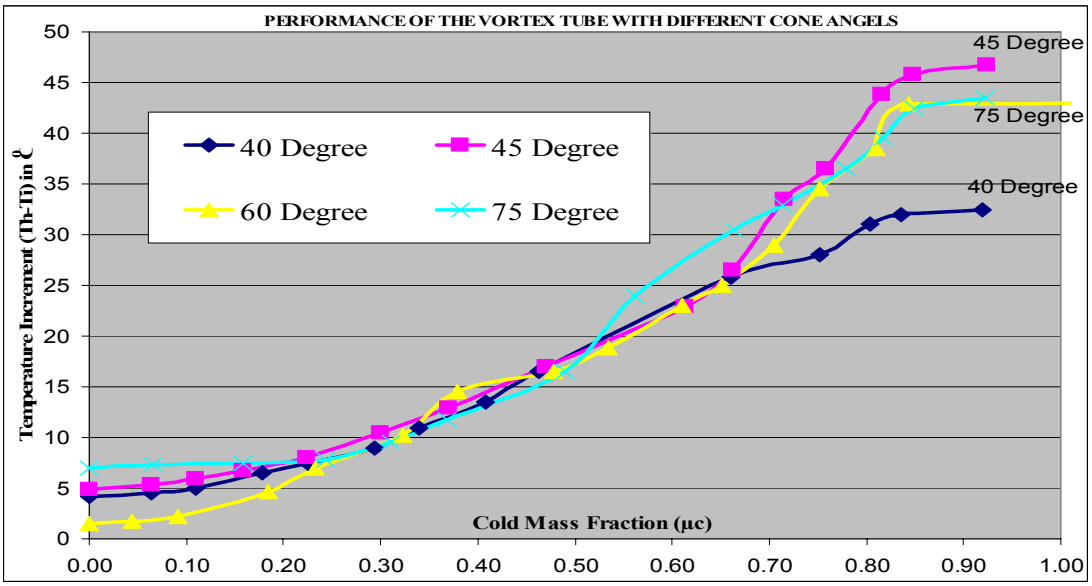
PERFORMANCE OF THE VORTEX TUBE WITH DIFFERENT CONE ANGELS
Temperature Increment (Th-Ti) in ℃
Cold Mass Fraction (μc)
40 Degree
45 Degree
60 Degree
75 Degree
45 Degree
75 Degree
40 Degree
0
5
10
15
20
25
30
35
40
45
50
0.00
0.10
0.20
0.30
0.40
0.50
0.60
0.70
0.80
0.90
1.00

(a)

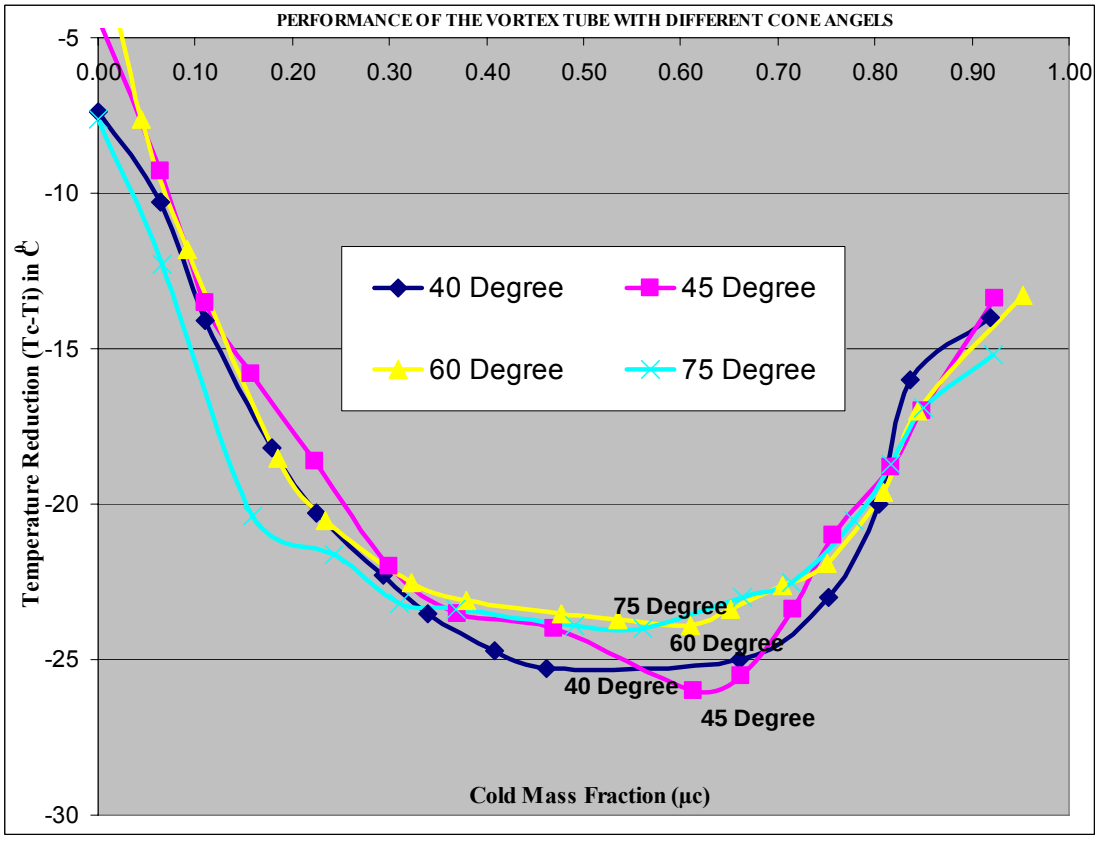
PERFORMANCE OF THE VORTEX TUBE WITH DIFFERENT CONE ANGELS
Temperature Reduction (Tc-Ti) in ℃
Cold Mass Fraction (μc)
40 Degree
45 Degree
60 Degree
75 Degree
75 Degree
60 Degree
40 Degree
45 Degree
-5
-10
-15
-20
-25
-30
0.00
0.10
0.20
0.30
0.40
0.50
0.60
0.70
0.80
0.90
1.00

(b)

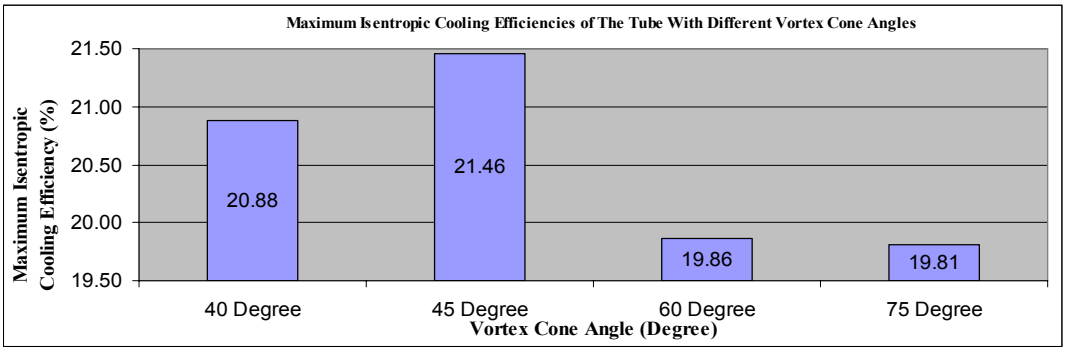

(c)

Figure 5.12. Results of the experiments of vortex tube with different vortex cones having different cone angles from 40^0 to 75^0. Temperature increment vs. cold mass fraction shown in (a), while temperature reduction vs. cold mass fraction presented in (b). In (c): the maximum isentropic efficiencies obtained with different vortex cones are shown.

Results of this section can be seen in Figure 5.12. with in three graphs. The first two graphs show that temperature increment and reduction versus cold mass fraction for the vortex tube with different conical obstacles having different cone angles. It is easily seen that, the angle of 45^0 gives better energy separation in both temperature increment and reduction case. The cones having 60^0 and 75^0 have similar characteristic on both heating and cooling. Smaller angles may yield less reflection while larger angles causing higher reflection on the main flow stream thus in both two cases, one of the flow is more dominant with respect to the other. So cold stream and hot stream can not produce a homogeneous and steady flow inside the tube. This explains why nozzle with 45^0 are more efficient in all case and the reason of the nozzle with 40^0 has better temperature reduction performance while it has worse performance on temperature increment. Because in 40^0, due to the angle of the cone, it caused stronger and dominant cold flow as it created weaker hot flow. Thus, the final observation of these experiments is that to increase the energy separation performance of the tube, both cold and hot flows should have similar structure. In case of 45^0 nozzle angle, because of the geometry of the nozzle is symmetric inside the cylinder, main stream is reflected equally and symmetrically, so the performance in this situation is higher than other angles.

5.4.4. Insulation Effect

To observe the insulation effect on the performance of the vortex tube, a 5 mm thick thermal and acoustic insulation foam (model called as FIREX) shown in Figure 5.13. was used for hot tube of the vortex tube.

Figure 5.13. The insulation foam that was used in this set of experiments.

A seamless aluminum with diameter of 16 mm and length of 15D was used during the experiments. After the first test completed, hot tube of the vortex tube was coated by this foam. Then a second test was performed. Table 5.5. shows constant parameters during this set of experiments and their values, and Figure 5.14. shows the results of this section.

Table 5.5.Constant parameters and their values during the experiments of "Effect of insulation on the hot tube"

	PARAMETER	**VALUE**
1	Length of the Hot Tube (L)	15 D
2	Inlet Pressure (P_i)	6 Bar(g)
3	Diameter of the Hot Tube (D)	16 mm
4	Cold Orifice Diameter (d)	7.94 mm
5	Vortex Cone Angle	40^0
6	Material of the Hot Tube	Seamless Aluminum pipe
7	Number of inlet nozzle	1
8	Average Mass Flow Rate	0.0103 kg/s

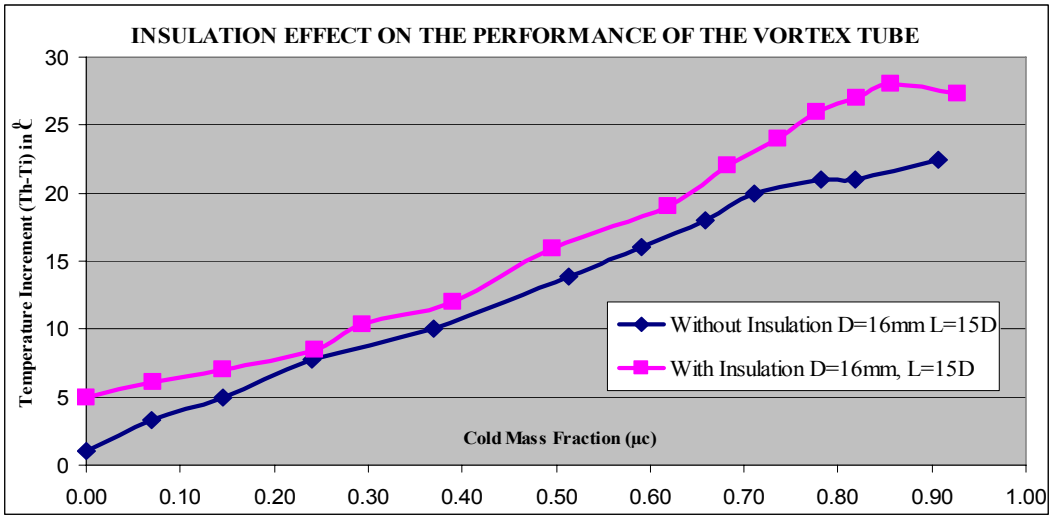

(a)

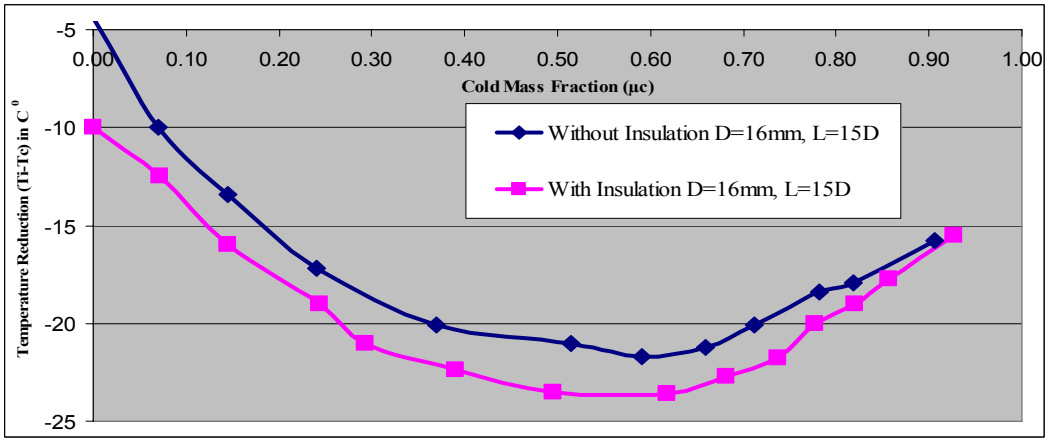

(b)

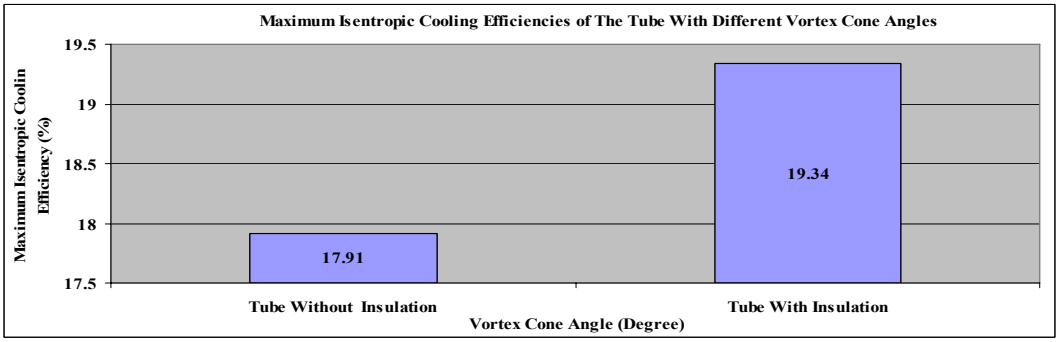

(c)

Figure 5.14. Results of the experiments of vortex tube with and without insulation on the hot tube. Temperature increment vs. cold mass fraction shown in (a), while temperature reduction vs. cold mass fraction presented in (b). In (c): the maximum isentropic efficiencies obtained by these two conditions are shown in same graph.

The first two graphs of Figure 5.14. show that insulation on the hot tube of the vortex tube increases temperature separation effect. This increment of the performance is not at a single measurement point but effective during all cold mass fraction ratios. The last graph also shows the maximum isentropic efficiencies of the vortex tube which about 1.7% of the isentropic efficiency increased just by insulation in this case. This is because the insulated tube gave less energy to the surroundings than the non-insulated one, causing the higher temperature difference within the tube.

5.4.5. Material Of the Hot Tube

In the preceding investigations, including Ranque`s and Hilsch`s efforts, almost all the parts of the experimental prototypes were made of steel or iron. Nowadays there are many alternative materials for manufacturing vortex tubes. Composite or plastic materials like plexiglass or teflon, have advantages in machining and forming and high surface quality. Also price can be lower than working with metals. On the other hand, metals are so common to use and high strength and robustness are their pluses. However, there are many alternatives for vortex tube manufacturing. Aluminum, copper, brass, and steels can be used in RHVT. In this part, two different material, aluminum and steel will be used as hot tube. Both these two pipes are seamless and have similar internal surface quality. These pipes (Figure 5.15.) had diameter of 19 mm diameter and length of 15D was used. Table 5.6. also shows constant parameters during this set of experiments and their values. Results of this section can be seen in Figure 5.16.

Figure 5.15. Aluminum and steel pipes used in this set of experiments

Table 5.6. Constant parameters and their values during the experiments of "Vortex generators with different hot tube material".

	PARAMETER	VALUE
1	Length of the Hot Tube (L)	15 D
2	Inlet Pressure (P_i)	6 Bar(g)
3	Diameter of the Hot Tube (D)	19 mm
4	Cold Orifice Diameter (d)	7.94 mm
5	Vortex Cone Angle	40^0
6	Material of the Hot Tube	Seamless Aluminum and steel pipes
7	Number of inlet nozzle	1
8	Average Mass Flow Rate	0.0110 kg/s

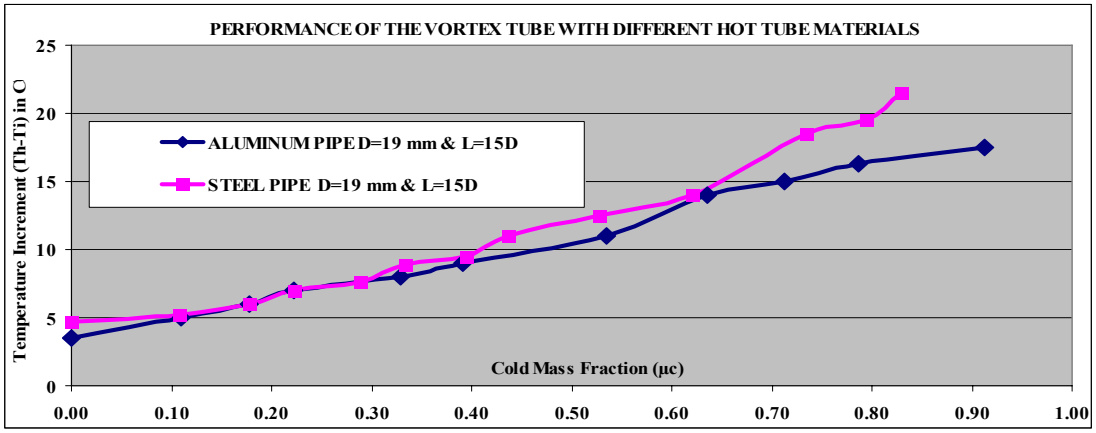

(a)

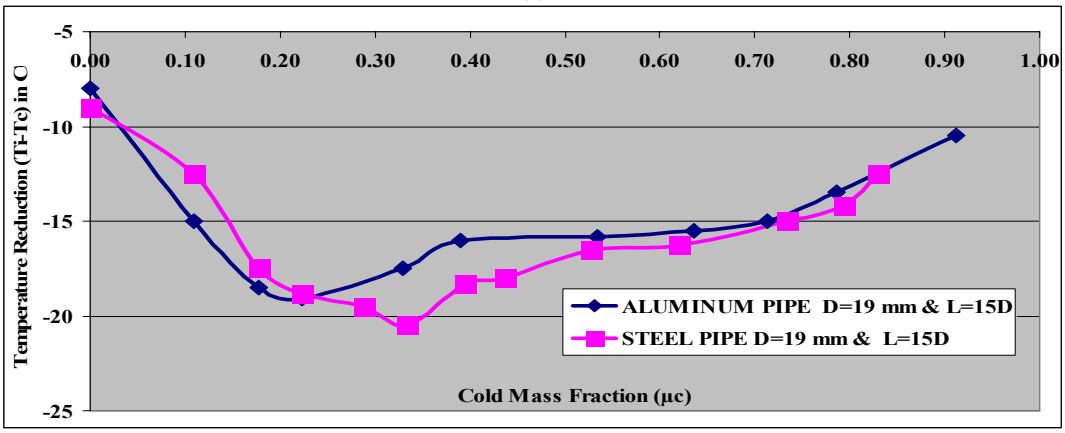

(b)

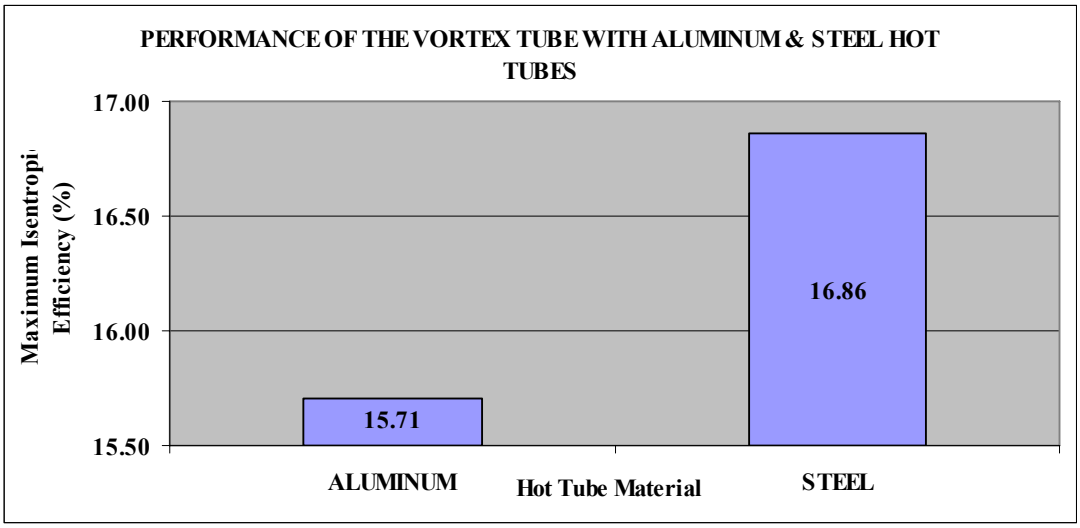

(c)

Figure 5.16. Results of the experiments of vortex tube with steel and aluminum hot tubes. Temperature increment vs. cold mass fraction shown in (a), while temperature reduction vs. cold mass fraction presented in (b). In (c): the maximum isentropic efficiencies obtained by the each pipe are shown in same graph.

In this part of the current study, steel and aluminum pipes were used as hot tube. Both steel and aluminum pipes were seamless and cold-drawn with similar internal surface quality. The first 2 graphs show that temperature increment and reduction versus cold mass fraction for the vortex tube with these hot tubes. It is easily seen that, steel pipe gives better energy separation in both temperature increment and reduction case. This increment of the performance is not at a single measurement point but effective during almost all of cold mass fraction ratios. The last graph also shows the steel pipe has about 1.15% higher maximum isentropic efficiencies than aluminum pipe. In case of both pipes are having similar internal surface quality, this difference can be explained similarly to the insulation effect. Standard steel has a thermal conductivity of about 40 W/m.K whereas aluminum has a thermal conductivity of 240 W/m.K. This means aluminum has almost 6 times higher thermal conductivity than steel. Thus, same as the results seen in previous part, steel tube gave less energy to the surroundings than the aluminum, and causing the higher temperature difference within the tube. After seeing these results, one can say that, if the other parameters are same, the material with lower thermal conductivity causes better thermal separation than metals having higher thermal conductivity.

5.4.6. Cold Orifice Ratio

Cold orifice ratio (d/D) is the fraction of the diameter of the cold pipe (d) to the diameter of the hot pipe. Similarly to the length of the hot tube, cold orifice diameter is also expressed in unit of diameter of hot tube D. This is also a very important parameter that affects the performance of the vortex tube. There are many previous attempts to investigate the influence of this ratio on vortex tube performance. Hilsch`s [2] and Promvonge and Eiamsa-ard`s [11] efforts (see at section 2.1) are good examples. To investigate this relation, three different pipes having the same length and material properties, but different diameters have been used to change the cold orifice ratio. Figure 5.17. shows these pipes and Table 5.7. also shows constant parameters during this set of experiments and their values. Results of this section can be seen in Figure 5.18.

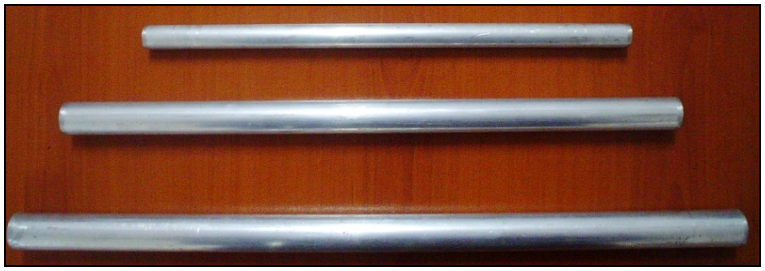

Figure 5.17. Aluminum pipes used in this set of experiments.

Table 5.7. Constant parameters and their values during the experiments of "Vortex generators with different cold orifice ratios".

	PARAMETER	VALUE
1	Length of the Hot Tube (L)	20 D
2	Inlet Pressure (P_i)	6 Bar(g)
3	Diameters of the Hot Tube (D)	19, 16 and 12 mm
4	Cold Orifice Diameter (d)	7.94 mm
5	Vortex Cone Angle	40^0
6	Material of the Hot Tube	Aluminum pipes
7	Number of inlet nozzle	1
8	Average Mass Flow Rate	0.0110 kg/s

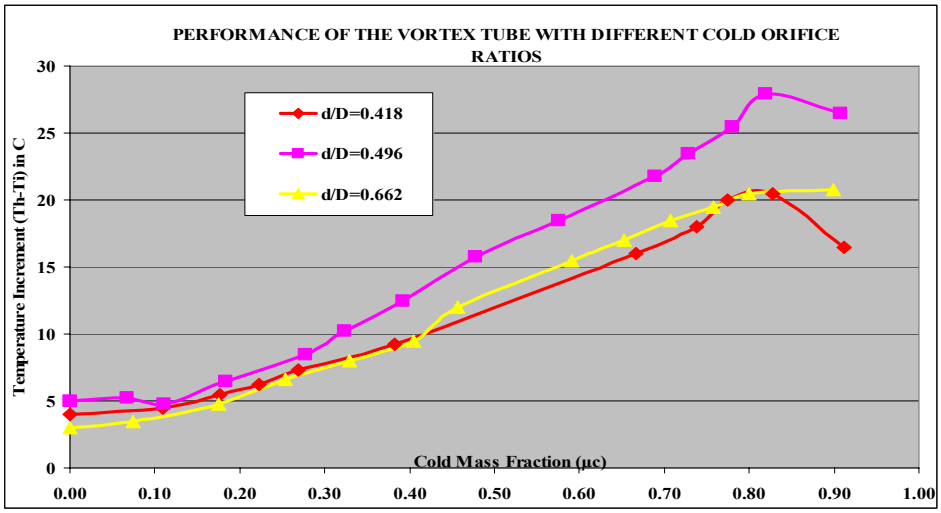

(a)

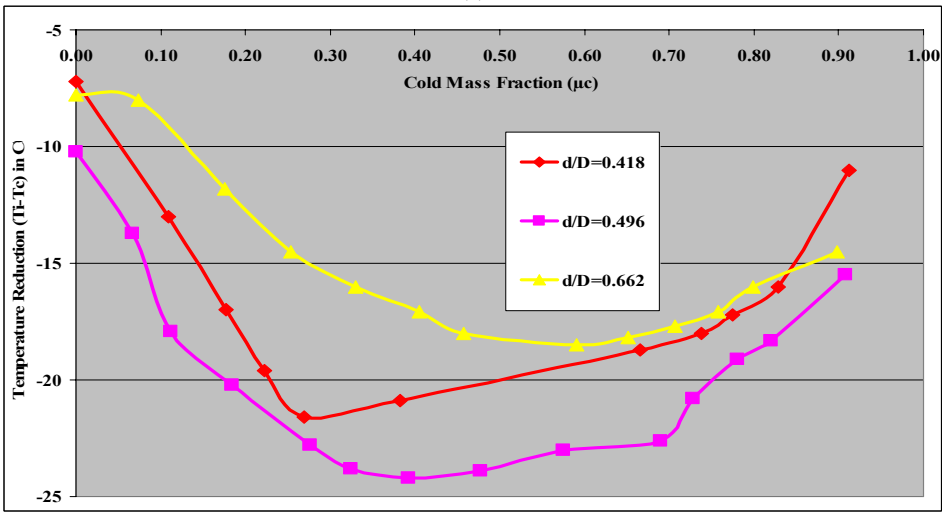

(b)

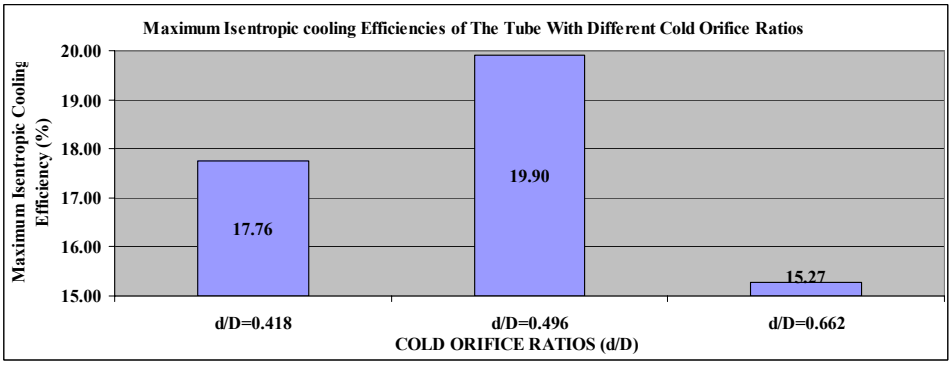

(c)

Figure 5.18. Results of the experiments of vortex tube with different cold orifice ratios. Temperature increment vs. cold mass fraction shown in (a), while temperature reduction vs. cold mass fraction presented in (b). In (c): the maximum isentropic efficiencies obtained by the each ratio are shown.

In this part of the current research, effect of the cold orifice ratio on the performance of the vortex tube is investigated. Three different ratios were demonstrated by using three different pipes having diameters of 19, 16, and 12 mm respectively. By keeping cold orifice diameter of 7.94 mm constant, d/D ratios of 0.662, 0.496 and 0.418 were realized. The first two graphs show that temperature increment and reduction versus cold mass fraction for the vortex tube with these cold orifice ratios. It is easily seen that the ratio of 0.496 gives better energy separation in both temperature increment and reduction case. This increment of the performance is not at a single measurement point but effective during almost all of cold mass fraction ratios.

The last graph also shows the ratio of 0.496 has much higher maximum isentropic efficiencies when compared to the other ratios. As in mentioned in some of previous studies such as Promvonge and Eiamsa-ard`s [11], optimum cold orifice diameter ratio should be in between 0.4 to 0.6. Using the cold orifice diameter ranging from 0.6D to 0.9D (bigger than that of 0.5D) would allow some hot air in vicinity of the tube wall to exit the tube with the cold air. Both the hot air and cold air as flowing out were mixed together which further affected the cold air to have higher temperature. On the other hand, for a small cold orifice diameter of 0.4D, it has a higher back pressure and makes the temperature reduction at the cold tube lower. Thus, as in found in current results, the cold orifice diameter of 0.5D yielded the highest potential of temperature reduction in the cold tube than the others.

5.4.7. Inlet Pressure

All of researchers working on vortex tube accept that the most important parameter that affects the performance of the vortex tube is the inlet pressure. Because of the working principle of the device, the pressurized gas expands inside the vortex chamber and its speed increases while the pressure decreases. If the vortex tube assumed to work isentropically, expansion process occurs isentropically too. This case can be expressed as in Equation (3.13). During the expansion phase, internal energy of the gas converted to kinetic energy with assumptions of no heat and work input to the system and the change in potential energies are neglected. The magnitude of the thermal separation is related to the pressure reduction from initial to final case according to this equation.

Almost all researchers who worked on vortex tubes experimentally were tried to see the relation between inlet pressure and thermal separation. Hilsch`s [2] graph shown in Figure 2.5. and study of J. U. Keller et al. [95] shows the thermal separation performances of their prototypes an different inlet pressure in Figure 5.19. below.

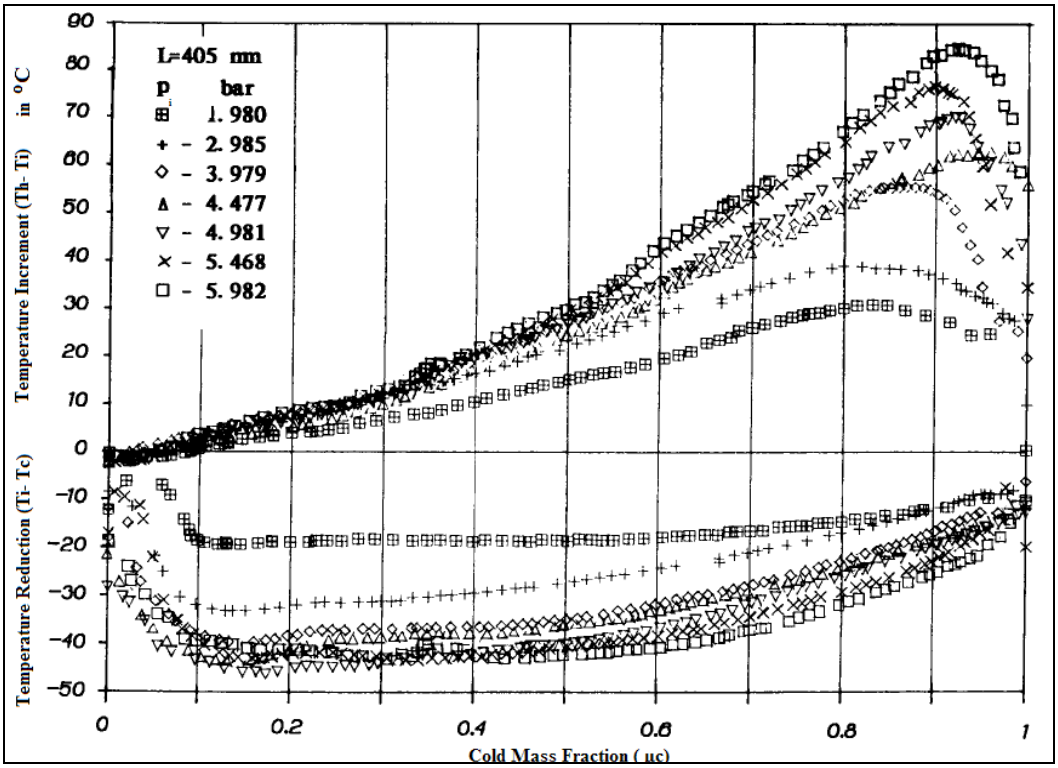

Figure 5.19. Temperature reduction and increment against cold mass fraction at different inlet pressures from 1.980 bar to 5.982 bar for vortex tube which has constant length (L=405 mm) [95]

In the current study, performance of the prototype vortex tube under different inlet pressures from 2 Bar (g) to 15,5 Bar (g) will be investigated in this section the thesis. Experimental set-up presented in Figure 5.4 had been used for these set of experiments. The reason of using high pressure compressor and receiver tank was explained in section 5.3. Table 5.8 shows constant parameters during this set of experiments and their values. Results of this section can be seen in Figure 5.20.

Table 5.8. Constant parameters and their values during the experiments of "Vortex tubes under different inlet pressures from 2 Bar (g) to 15,5 Bar (g)".

	PARAMETER	VALUE
1	Length of the Hot Tube (L)	20 D
2	Inlet Pressure (P_i)	Variable, from 2 Bar(g) to 15,5 Bar (g)
3	Diameters of the Hot Tube (D)	19mm
4	Number of inlet nozzle	1
5	Cold Orifice Diameter (d)	7.94 mm
6	Vortex Cone Angle	40^0
7	Material of the Hot Tube	Aluminum pipe

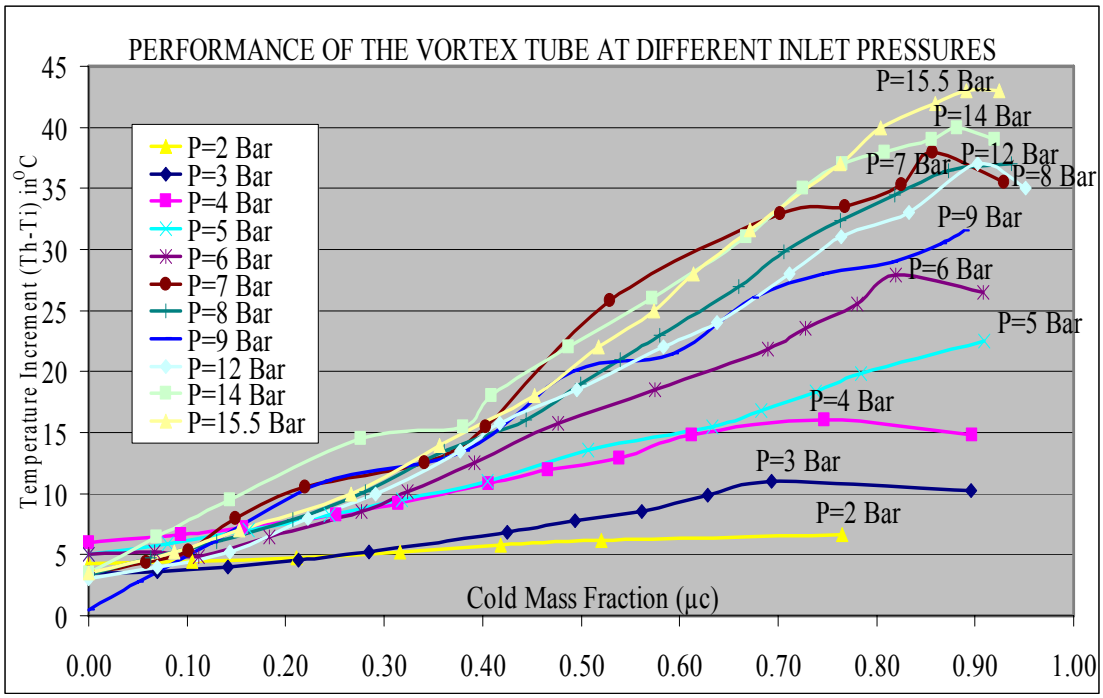

(a)

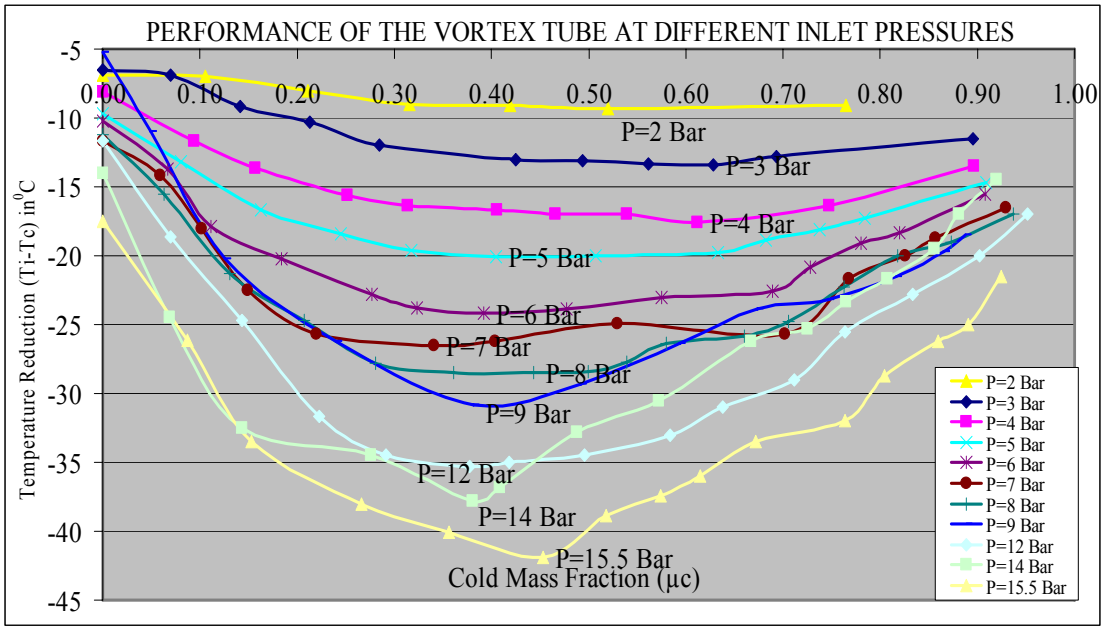

(b)

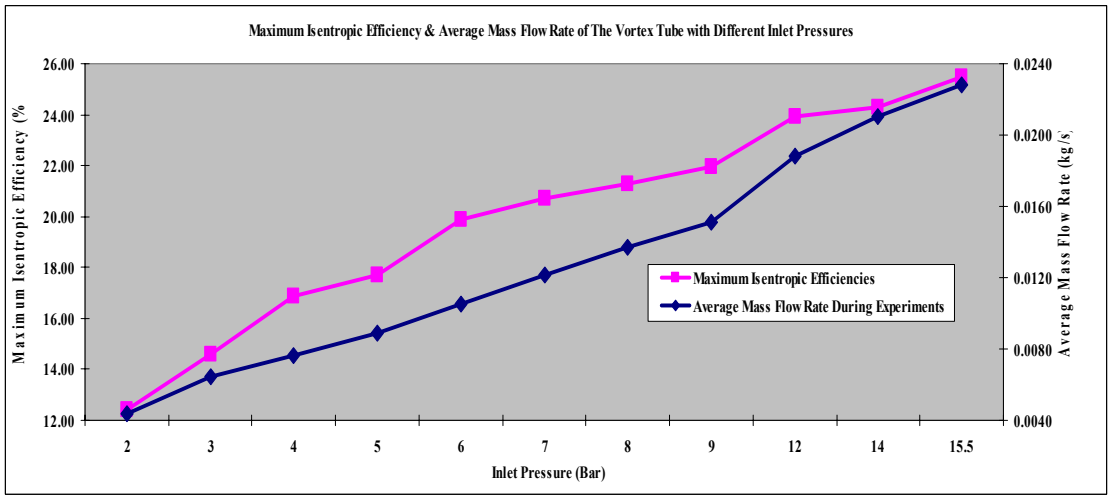

(c)

Figure 5.20. Results of the experiments of vortex tube with different inlet pressures. Temperature increment vs. cold mass fraction shown in (a), while temperature reduction vs. cold mass fraction presented in (b). In (c): the maximum isentropic efficiencies obtained by the each ratio are shown. At the last graph (d), the ratio of the maximum isentropic efficiency to inlet pressure is shown.

The effect of the inlet pressure on performance of the vortex tube was investigated in this part of the current research. As it seen from Figure 5.20, temperature increment and reduction performance of the prototype vortex tube increases while the inlet pressure increases. Figure 5.20.c. shows the maximum isentropic efficiencies and average mass

flow rate with respect to inlet pressure. After considering these results, another graph was created to understand the relationship between the maximum isentropic efficiency and inlet pressure. Figure 5.21, the ratio of the maximum isentropic efficiency achieved by given inlet pressure versus inlet pressure is shown.

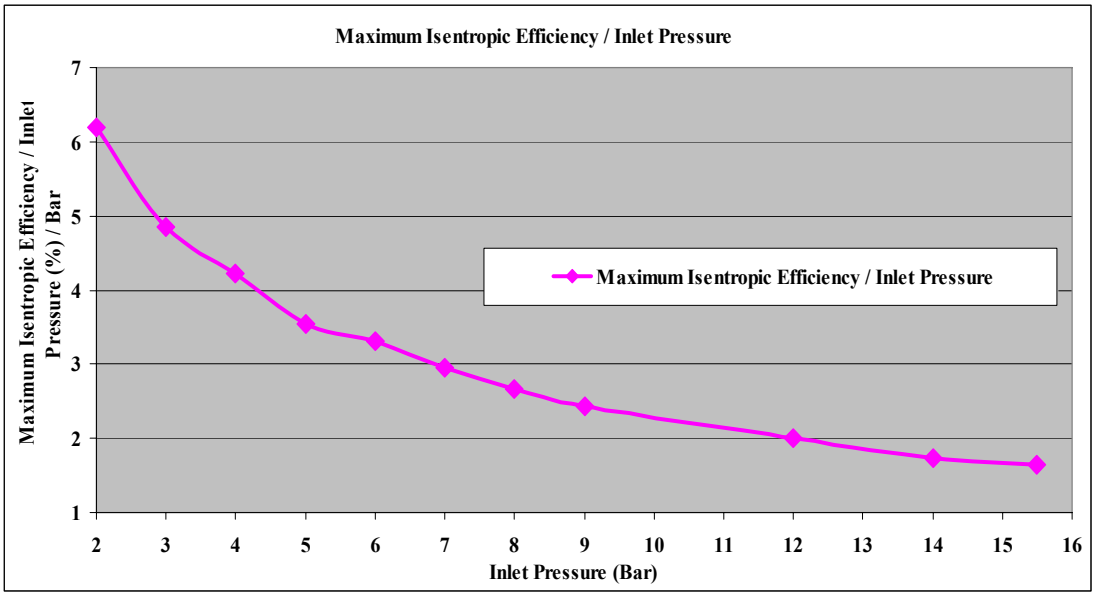

Figure 5.21. The ratio of the maximum isentropic efficiency to inlet pressure

Since the vortex tube was invented by George Ranque in 1933, many investigators had worked on it and tried to find optimum geometry to get maximum performance from the device. In the literature, maximum inlet pressure that applied to the vortex tube was 11 Bar (g) by Martynoskii and Alekseev [17] in 1957 (see Table 2.1). In this study, 15.5 Bar was achieved at the inlet of the prototype vortex tube. This pressure is still very low compared to the higher pressures up to 2000 – 3000 Bar needed to reach near the absolute 0 K at the cold end of the device. As the inlet pressure is the most important parameter that affects the performance and efficiency directly, a formula that gives the maximum isentropic efficiency at given inlet pressure would be helpful.

In Figure 5.20.c, a steady growth is seen whereas in Figure 5.21. a steady decrease is observed. The profiles seem logarithmic. However, to be sure, one needs to consider the isentropic efficiency definition given in equations 3.12 and 3.13.

$$\eta_{\text{is}} = \frac{T_i - T_c}{(\Delta T)_{is}} \tag{3.12}$$

$$(\Delta T)_{is} = T_i \left(1 - \left(\frac{P_{atm}}{P_{in}} \right)^{\frac{\gamma-1}{\gamma}} \right) \tag{3.13}$$

$$\eta_{\text{is}} = \frac{T_i - T_c}{T_i \left(1 - \left(\frac{P_{atm}}{P_{in}} \right)^{\frac{\gamma-1}{\gamma}} \right)} \tag{5.2}$$

$$\underset{P_{in}\to\infty}{Lim}\, \eta_{\text{is}} = \frac{T_i - T_c}{T_i \left(1 - \left(\frac{P_{atm}}{P_{in}} \right)^{\frac{\gamma-1}{\gamma}} \right)} = \frac{T_i - T_c}{T_i} = 1 - \frac{T_c}{T_i} \tag{5.3}$$

It is clear that, if the inlet pressure increases, temperature separation performance of the device is also increased. Thus colder temperatures will occur at cold side outlet. According to the profiles of the results in Figure 5.21.c. and Figure 5.22, the maximum isentropic efficiency is a function of $\ln(P)$ (see Equation 5.4).

$$y = a \ln(x) + b \tag{5.4}$$

To obtain the exact formula, a new graph was drawn to show the relationship between η_{is} and $\ln(P)$ in Figure 5.23.

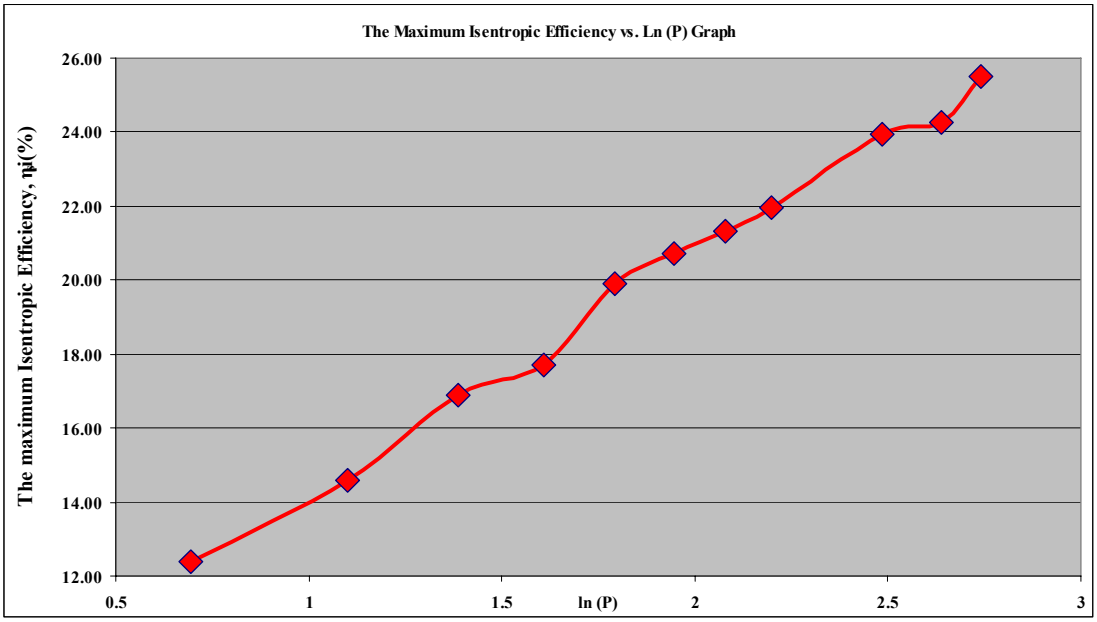

Figure 5.22. The Maximum Isentropic Efficiency vs. Ln (P) Graph

The trendline of this graph, formulates the relationship between η_{is} and $\ln(P)$. According to result η_{is} in (%) is formulated as:

$$\eta_{is} = 6.40\ln(P) + 7.89 \tag{5.5}$$

The coefficient of correlation value of the the trendline is 0.99 which indicates nearly perfect linear fit to the given experimental data. By this equation, the actual temperature reduction and maximum isentropic efficiency of the prototype vortex tube can be calculated at any given inlet pressure. To formulate this relation:

$$\eta_{is} = \frac{T_i - T_c}{(\Delta T)_{is}} \tag{3.12}$$

$$(\Delta T)_{is}\,\eta_{is} = T_i - T_c \tag{5.6}$$

$$T_c = T_i - T_i\left(1 - \left(\frac{P_{atm}}{P_{in}}\right)^{\frac{\gamma-1}{\gamma}}\right)\frac{\left[6.40\ln(P_{in}) + 7.89\right]}{100} \tag{5.7}$$

$$T_c = T_i\left(1-\left(\frac{[6.40\ln(P_{in})+7.89]}{100}\right)\left(1-\left(\frac{P_{atm}}{P_{in}}\right)^{\frac{\gamma-1}{\gamma}}\right)\right) \quad (5.8)$$

By using Equation (5.8), actual temperature reduction in the vortex tube at given inlet temperature and pressure can be calculated. For example, inlet air having pressure of 25 Bar (g) and temperature of 25 C^0 results the cold side temperature of – 26.92 C^0 and temperature reduction of 51.92 C^0 in the prototype vortex tube.

5.5. OPTIMUM VORTEX TUBE DESIGN

The most important goal of this study is to find an improved vortex tube design that will result in better temperature separation performances and higher isentropic efficiencies.

Results of the experiments conducted in this study, helped to determine the improved vortex tube designs. The parameters obtained by the current study, which give better performance on vortex tube, are summarized in Table 5.9.

Using these parameters on the prototype and performing a final experiment to achieve maximum temperature reduction and isentropic efficiency was planned previously. However, during the experiments, it was observed that as the efficiency and performance of the device by changing the parameters and components as expected. Thus, lower temperatures achieved in the cold end of the vortex tube. Because of there was a lack of an air dryer on the experimental set-up, water vapor inside the atmospheric air, could not be removed from compressed air completely. Then, excessive water inside the pressurized air, either in the liquid or vapor phase, condenses or freezes at the cold end side of the vortex tube. Cold side outlet collector and variable are flowmeter lose their functions in this case. As a result, performing the final optimization experiment was cancelled.

Table 5.9. Configurations increasing the performance of the vortex tube design and their optimum values.

#	Parameter	Results	Optimum Value
1	# of inlet nozzles at vortex generator	Investigated in section 5.4.1. Generators with one to four nozzles were used and results showed that increasing the number of inlet nozzles led to higher temperature separation and increased the isentropic efficiency.	4 or more number of inlet nozzles
2	Length of the Hot Tube (L)	Investigated in section 5.4.2. Aluminum seamless pipes without insulation and having length from 15D to 50D were used and results showed that performance of the vortex tube are also affected by hot tube length. 25D≤L≤50D is the optimum range for hot tube length.	L=50D gave the optimum value for temperature reduction and highest isentropic efficiency. On the other hand, 25D≤L≤30D range causes better temperature increment performance.
3	Vortex Cone Angles	Investigated in section 5.4.3. Vortex cones having cone angles of 40^0, 45^0, 60^0 and 75^0 were used and results showed that using vortex cone having angle of 45^0 causes higher temperature separation and increases the isentropic efficiency.	Vortex Cone Angle of 45^0 is the optimum value.
4	Insulation Effect	Investigated in section 5.4.4. The hot tube of the vortex tube was insulated and results compared with the same vortex tube without insulation. Results showed that the insulated tube gave less energy to the surroundings than the non-insulated one. It causes higher temperature separation within the tube and increases the isentropic efficiency.	Insulation of the Hot tube increases the temperature separation performance and isentropic efficiency of the vortex tube.
5	Material of The Hot Tube,	Investigated in section 5.4.5. Seamless aluminum and steel pipes were used and results showed that if the other parameters are same, the material with lower thermal conductivity causes better thermal separation than metals having higher thermal conductivity.	If all the other parameters are same, the material with lower thermal conductivity causes better thermal separation than metals having higher thermal conductivity.

6	Cold Orifice Ratio (d/D)	Investigated in section 5.4.6. By keeping cold orifice diameter of 7.94 mm constant, d/D ratios of 0.662, 0.496 and 0.418 were established. Using smaller or higher orifice diameters than 0.5D decreases the performance and isentropic efficiency of the RHVT.	Cold Orifice Ratio (d/D) of 0.5D is about the best.
7	Inlet Pressure (P_i)	Investigated in section 5.4.7. Inlet pressures from 2 Bar (g) to 15.5 Bar (g) applied to the same prototype. Results had showed that if the inlet pressure increases, temperature separation performance and isentropic efficiency of the device is also increased. Thus colder temperatures will occur at cold side outlet. By further evaluations and calculations, equations (5.5) and (5.8) are found. By these equations, the actual temperature reduction and maximum isentropic efficiency of the prototype vortex tube can be calculated at any given inlet pressure and temperature.	As the inlet pressure (P_i) increases, temperature separation performance and isentropic efficiency of the device is also increased in a logarithmic manner.

6. CONCLUSION AND FUTURE WORKS

In this thesis, an experimental investigation on vortex tubes is performed. Counter-flow type vortex tubes were designed by using Pro Engineer WF 4.0 software, manufactured by CNC machining centers, and tested at several different conditions for improvement of performance characteristics of the device.

In previous studies, experimental and computational methods have been used for explaining temperature separation process and flow inside the vortex tube. Results of these studies show that temperature separation is strongly dependent to inlet parameters and geometry of the tube. Pressure of the inlet gas is the most important inlet parameter and directly related to the performance. Also geometrical parameters such as length and diameter of the tube, number of inlet nozzle and cold orifice diameter etc. also affect the performance. In chapter 2, substantial quantity of literature dealing with the vortex tube were reviewed and summarized. Previous experimental and computational studies, tried to be evaluated by historical order. At the end of this chapter included the theoretical efforts which try to explain energy separation process in the tube and its performance characteristics.

In Chapter 3, physics of vortex tube investigated by considering the device as a thermodynamic system in steady state. The first and the second law analysis, energy separation process and the efficiency of the vortex tube will be explained.

Although the Ranque-Hilsh Tube has very low efficiency considering commercial cooling and heating systems, its intrinsic features that make it attractive for some applications. Chapter 4 considered the potential of the tube to be used in a number of specific industrial applications in detail, by focusing on simple heating and cooling, gas liquefaction, and mixture separation processes.

Current experimental study to investigate vortex phenomenon and improve its performance characteristics are presented in Chapter 5. Results obtained from numerous different experiments that were conducted are shown and evaluated to improve the device

performance. Additional experiments have been performed to examine the performance of the vortex tube under high inlet gas pressures up to 15.5 Bar (g), a first in literature.

The main objective of this study was to find an improved vortex tube design that would result in enhanced temperature separation performances and higher isentropic efficiencies. The parameters obtained by current study, which give optimum performance of vortex tube, are summarized in Table 5.9. Because of the reason that was explained in Section 5.5, using these parameters on the prototype and performing the final optimization experiment was cancelled.

The following results have been obtained from current research:

- Increasing the number of inlet nozzles in vortex generators led to higher temperature separation and increases the isentropic efficiency. In this study, generators with 1, 2 and 4 inlet nozzles had been used. It was determined that four inlet nozzles creates higher temperature separation and have higher efficiency.
- Length of the hot tube also affects the performance of the device and results showed that L=50D is the optimum value for temperature reduction and highest isentropic efficiency. On the other hand, $25D \leq L \leq 30D$ range causes better temperature increment performance.
- Vortex Cone Angle = 45^0 is the optimum value for increasing the vortex tube performance.
- Insulation has positive effect on the temperature seperation process. Results showed that insulation of the hot tube increases the temperature separation performance and isentropic efficiency of the vortex tube. Similarly, using a material with lower thermal conductivity causes better thermal separation than metals having higher thermal conductivity.
- According to the results of current study and some previous efforts, Cold Orifice Ratio (d/D) of 0.5D yields better results.
- Inlet pressure (P_i) is the most important parameter that affects the performance of RHVT. Results have proven that if the inlet pressure increases temperature separation performance and isentropic efficiency of the device are also increased. Thus colder temperatures will occur at cold side outlet. By further evaluations and calculations,

relations of $\eta_{is} = 6.40\ln(P) + 7.89$ and $T_c = T_i\left(1 - \left(\frac{[6.40\ln(P_{in}) + 7.89]}{100}\right)\left(1 - \left(\frac{P_{atm}}{P_{in}}\right)^{\frac{\gamma-1}{\gamma}}\right)\right)$ are found. By these equations, the actual temperature reduction and maximum isentropic efficiency of the prototype vortex tube can be calculated at any given inlet pressure and temperature.

Vortex tubes are very simple but promising devices. Although the efficiencies achieved by current industrial models are very low comparing to the other refrigeration method, its ease of use, low investment cost and possibility of reaching very high and low temperatures instantly makes the device still attractive for scientists and industry.

To develop the vortex tube technology, following aspects should be considered. The performance of the tube under inlet pressures up to 40 Bar (g) should be considered. Moreover, by applying higher inlet pressures to the devices, colder temperatures close to the absolute 0 K can be achieved. Acoustic characteristics of the device should be investigated by performing similar experiments performed in chapter 5, in an acoustically insulated test room. Fast frequency response of the device under variable flow condition should be found. Another future problem is finding solution for the noise problem of vortex tubes. Generally vortex tubes operate with 100 dB (A) noise level in case of no silencers mounted on the ends of the device and it must be reduced to more comfortable noise levels.

The most important future work for vortex tubes is performing similar researches on “Parallel-flow type vortex tube”. Since the device was discovered in 1933, almost all studies were performed on counter flow vortex tube because of its simplicity and ease of manufacturing the device and control. Thus, there is no relevant data on parallel flow vortex tubes and comparison of the performances can not be done because of this.

REFERENCES

1. Ranque, G. J., *Experiences sur la detente giratoire avec productions simultanes d`un echappement d`air chaud et d`un echappement d`air froid"*, J. Phys. Radium Vol. 4 (7), pp. 112–114, 1933.

2. Hilsch, R., *"The use of the expansion of gases in a centrifugal field as cooling process"*, The Review of Scientific Instruments, Vol. 18(2), pp. 108, February 1947.

3. Pelmar Engineering Ltd. Online. Available at http://www.pelmareng.com.

4. Usta, H., K. Dincer and V. Kirmaci, *"Vorteks tüpünde akışkan olarak kullanılan hava ile karbondioksitin soğutma sıcaklık performanslarının deneysel incelenmesi"*, C.U. Fen-Edebiyat Fakültesi Fen Bilimleri Dergisi 24, Sayı 2, 2003.

5. Exair Vortex Tubes. Online. Available at http://www.exair.com.

6. Aydin O. and M. Baki, *"An experimental study on the design parameters of a counter-flow vortex tube"*, Energy, Article in Press, Elsevier 2005.

7. Ting-Quan, M., Qing-Guo ZHAO, Jian YU, Fang YE, and Chong-Fang MA, *"Experimental investigation on energy separation by vortex tubes"*, College of Environmental and Energy Engineering, Beijing Polytechnic University, Beijing 100022, P. R. China.

8. Fröhlingsdorf, W. and H. Unger, *"Numerical investigations of the compressible flow and the energy separation in Ranque–Hilsch vortex tube"*, International Journal of Heat and Mass Transfer, Vol 42, pp. 415-422, 1999.

9. Oliver, R., *"Numerical prediction of primary and secondary flows in a Ranque-Hilsch vortex tube"*, Master's thesis, Dublin Institute of Technology, 2008.

10. Eastop, T.D. and A. McConkey, *"Applied thermodynamics for engineering technologists"*, Prentice Hall, 5th Edition, 1993.

11. Promvonge, P. and S. Eiamsa-ard, *"Investigation on the vortex thermal separation in a vortex tube refrigerator"*, Science Asia Vol. 31, pp. 215-223, 2005.

12. Soni, Y., *"A parametric study of the Ranque-Hilsch tube"*, University of Idaho, 1973.

13. Aljuwayhel, N. F., G. F. Nellis and S. A. Klein, *"Parametric and internal study of the vortex tube using a CFD model"*, International Journal of Refrigeration, Vol.28, pp. 442-450, 2005.

14. Ranque, G. J., "Method and apparatus for obtaining from a fluid under pressure two currents of fluids at different temperatures", U.S. Patent Office, Filed on Dec. 6, 1932.

15. Eiamsa-ard S. and P. Promvonge, *"Review of Ranque – Hilsch effects in vortex tubes"*, Renewable and Sustainable Energy Reviews, Vol. 12, pp. 1822 – 1842, 2008.

16. Scheper, G. W., *"The vortex tube; internal flow data and a heat transfer theory"*, J ASRE Refrig Eng, Vol. 59: 985–9, 1951.

17. Martynovskii V. S. and V. P. Alekseev, *"Investigation of the vortex thermal separation effect for gases and vapors"*, Sov Phys-Tech Phys, Vol. 1, pp. 2233–43, 1956.

18. Hartnett J. P. and E. R. G. Eckert, *"Experimental study of the velocity and temperature distribution in a high-velocity vortex-type flow"*, Heat Transfer and Fluid Mechanics Institute, Stanford University Press pp. 135–50, 1956.

19. Scheller W.A. and G. M. Brown, *"The Ranque–Hilsch vortex tube"*, J Ind Eng Chem, Vol. 49(6), pp. 1013–6, 1957.

20. Blatt T. A. and R. B. Trusch, *"An experimental investigation of an improved vortex cooling device"*, American Society of Mechanical Engineers, Winter Annual Meeting, America, 1962.

21. Linderstrom-Lang C. U., *"Gas separation in the Ranque–Hilsch vortex tube"*, Int J Heat Mass Transfer Vol.7, pp. 1195–206, 1964.

22. Takahama, H., *"Studies on vortex tubes"*, Bull Jpn Soc Mech Eng, Vol. 8(31), pp. 433–40, 1965.

23. Takahama, H. and N. Soga, *"Studies on vortex tubes 2nd report, Reynolds no. the effects of the cold air rate and partial admission of nozzle on the energy separation"*, Bull Jpn Soc Mech Eng, Vol. 9(33), pp. 121–30, 1966.

24. Vennos, S. L. N., *"An experimental investigation of the gaseous vortex"*, PhD thesis. Rensselaer Polytechnic Institute, 1968.

25. Bruun, H. H., *"Experimental investigation of the energy separation in vortex tubes"*, J Mech Eng Sci, Vol. 11(6), pp. 567–82, 1969.

26. Nash, J. M., *"Vortex heat exchanger cooling for infrared detectors"*, USA: Annual Meeting of the Optical Society of America, 1974.

27. Nash, J. M., *"Design of the vortex cooler"*, American Society of Mechanical Engineers, Annual Design Engineering Conference, New York, USA, 1975.

28. Marshall, J., *"Effect of operating conditions, physical size and fluid characteristics on the gas separation performance of the Linderstrom–Lang vortex tube"*, Int J Heat Mass Transfer, Vol. 20, pp. 227–31, 1977.

29. Takahama, H., M. Kawamura, B. Kato and H. Yokosawa, *"Performance characteristics of energy separation in a steam operated vortex tube"*, Int J Eng Sci, Vol. 17, pp. 735–744, 1979.

30. Collins, R. L. and R. B. Lovelace, *"Experimental study of two-phase propane expanded through the Ranque–Hilsch tube"*, Trans ASME J Heat Transfer, Vol. 101, pp. 300–5, 1979.

31. Takahama, H. and H. Yokosawa, *"Energy separation in vortex tubes with a divergent chamber"*, Trans ASME J Heat Transfer, Vol. 103, pp. 196–203, 1981.

32. Parulekar, B. B., *"The short vortex tube"*, J Refrig Vol. 4, pp. 74–80, 1961.

33. Otten, E. H., *"Production of cold air"*, London: Engineering, pp. 154, 1958.

34. Raiskii, Yu D. and L. E. Tankel, *"Influence of vortex-tube saturation and length on the process of energetic gas separation"*, J Eng Phys, Vol. 27(6), pp. 1578–81, 1974.

35. Kurosaka, M., J. Q. Chu, and J. R. Goodmann, *"Ranque Hilsch effect revisited: temperature separation effect traced to orderly spinning waves or vortex whistle"*, In: AIAA 82-0952, AIAA/ASME third joint thermo-physics of fluids plasma and heat transfer conference, USA, 1982.

36. Schlenz, D., *"Kompressible strahlgetriebene drallstromung in rotations-symmetrischen Kanalen"*, PhD thesis. Technische Fakultat Universitat, Erlangen-Nurnberg, 1982.

37. Amitani, T., T. Adachi and T. Kato, *"A study on temperature separation in a large vortex tube"*, Trans JSME, Vol. 49, pp. 877–84, 1983.

38. Stephan, K., S. Lin, M. Durst, F. Huang and D. Seher, *"An investigation of energy separation in a vortex tube"*, Int J Heat Mass Transfer, Vol. 26, pp. 341–8, 1983.

39. Negm,M. I. M., A. Z. Serag and S. M. Abdel Ghany, *"Performance characteristics of energy separation in double stage vortex tubes"*, Model Simulat Control B: Mech Therm Eng Mater Resour Chem, Vol. 14, pp. 21–32, 1988.

40. Negm,M. I. M., A. Z. Serag and S. M. Abdel Ghany, *"Generalized correlations for the process of energy separation in vortex tubes"*, Model Simulat Control B: Mech Therm Eng Mater Resour Chem, Vol. 14, pp. 47–64, 1988.

41. Lin, S., J. R. Chen and G. H. Vatistas, *"A heat transfer relation for swirl flow in a vortex tube"*, Can J Chem Eng J, Vol. 68(6), pp. 944–7, 1990.

42. Ahlborn, B., J. U. Keller, R. Staudt, G. Treitz and E. Rebhan, *"Limits of temperature separation in a vortex tube"*, J Phys D: Appl Phys, Vol. 27, pp. 480–8, 1994.

43. Ahlborn, B., J. Camire and J. U. Keller, *"Low-pressure vortex tubes"*, J Phys D, Appl Phys, Vol. 29, pp. 1469–72, 1996.

44. Ahlborn, B. and S. Groves, *"Secondary flow in a vortex tube"*, Fluid Dyn Res, Vol. 21(2), pp. 73–86, 1997.

45. Ahlborn, B., J. U. Keller and E. Rebhan, *"The heat pump in a vortex tube"*, J Non-Equilib Thermodyn, Vol. 23(2), pp. 159–65, 1998.

46. Ahlborn, B. and J. M. Gordon, *"The vortex tube as a classic thermodynamic refrigeration cycle"*, J Appl Phys, Vol. 88(6), pp. 3645–53, 2000.

47. Arbuzov, V. A., Y. N. Dubnishchev, A. V. Lebedev, M. Kh. Pravdina and N. L. Yavorskii, *"Observation of large-scale hydrodynamic structures in a vortex tube and the Ranque effect"*, Tech Phys Lett, Vol. 23(12), pp. 938–40, 1997.

48. Gutsol, A. F. *"The Ranque effect"*, Phys–Uspekhi, Vol. 40(6), pp. 639–58, 1997.

49. Piralishvili, S. A. and V. M. Polyaev, *"Flow and thermodynamic characteristics of energy separation in a double circuit vortex tube - an experimental investigation"*, Int J Exp Therm Fluid Sci, Vol. 12(4), pp. 399–410, 1996.

50. Lewins, J. and A. Bejan, *"Vortex tube optimization theory"*, Energy J, Vol. 24, pp. 931–43, 1999.

51. Trofimov, V. M. *"Physical effect in Ranque vortex tubes"*, JETP Lett, Vol. 72(5), pp. 249–52, 2000.

52. Guillaume, D. W. and J. L. Jolly, *"Demonstrating the achievement of the lower temperatures with two-stage vortex tubes"*, Rev Sci Instrum, Vol. 72(8), pp. 3446–8, 2001.

53. Manohar, R. and R. Chetan, *"Enrichment of methane concentration via separation of gases using vortex tubes"*, J Energy Eng, Vol. 128(1), pp. 1–12, 2002.

54. Saidi, M. H. and M. S. Valipour, *"Experimental modeling of vortex tube refrigerator"*, Appl Therm Eng, Vol. 23, pp. 1971–80, 2003.

55. Singh, P. K. *"An experimental performance evaluation of vortex tube"*, IE(I) J-MC, Vol. 84, pp. 149–53, 2004.

56. Riu, K., J. Kim and I. S. Choi, *"Experimental investigation on dust separation characteristics of a vortex tube"*, Trans JSME Ser B: Therm Fluid Mech, Vol. 47(1), pp. 29–36, 2004.

57. Promvonge, P. and S. Eiamsa-ard, *"Experimental investigation of temperature separation in a vortex tube refrigerator with snail entrance"*, ASEAN J Sci Technol Dev, Vol. 21(4), pp. 297–308, 2004.

58. Gao, C. M., K. J. Bosschaart, J. C. H. Zeegers and A. T. A. M. Waele, *"Experimental study on a simple Ranque–Hilsch vortex tube"*, Cryogenics, Vol. 45(3), pp. 173–83, 2005.

59. Aydin, O. and M. Baki, *"An experimental study on the design parameters of a counter flow vortex tube"*, Energy J, Vol. 31(14), pp. 2763–72, 2006.

60. Yilmaz, M., O. Comakli, O. Ozyurt, S. Erdogan, K. Bakirci, M. Kaya, S. Karagoz, *"Vorteks tüplerin sogutma tekniginde kullanilmasi"*, TUBITAK Proje No: 105M028, 2007.

61. Behera, U., P.J. Paul, S. Kasthurirengan, R. Karunanithi, S.N. Ram, K. Dinesh and S. Jacob, *"CFD analysis and experimental investigations towards optimizing the parameters of Ranque–Hilsch vortex tube"*, International Journal of Heat and Mass Transfer, Vol. 48, pp. 1961-1973, 2005.

62. Kassner, R. and E. Knoernschild, *"Friction laws and energy transfer in circular flow"*, Technical Report F-TR-2198-ND, Wright-Patterson Air Force Base, 1948.

63. Kurosaka, M. *"Acoustic streaming in swirling flow"*, Journal of Fluid Mechanics, page p. 139ff, November 1982.

64. Deissler, R. and M. Perlmutter, *"Analysis of the flow and energy separation in a turbulent vortex"*, International Journal of Heat and Mass Transfer, Vol. 1, pp. 173–191, 1960.

65. Van Deemter, J. J., *"On the theory of the Ranque–Hilsch cooling effect"*, Applied Scientific Research (Series A), Vol. 3, pp. 174–196, 1952.

66. Hinze, O., *"Turbulence"*, McGraw-Hill Series in Mechanical Engineering. McGraw-Hill, second edition, pp. 473ff deal explicity with the Ranque-Hilsch Vortex Tube, 1975.

67. Sibulkin, M., *"Unsteady, viscous, circular flow. Part 3: Application to the Ranque–Hilsch vortex tube"*, Journal of Fluid Mechanics, Vol. 12, pp. 269–293, 1962.

68. Sibulkin, M., *"Unsteady, viscous, circular flow. Part 1: The line impulse of angular momentum"*, Journal of Fluid Mechanics, Vol. 11, pp. 291–308, 1961.

69. Sibulkin, M., *"Unsteady, viscous, circular flow. Part 2: The cylinder of finite radius"*, Journal of Fluid Mechanics, Vol. 12, pp. 148–158, 1961.

70. Linderstrom-Lang, C. U., *"The three-dimensional distributions of tangential velocity and total-temperature in vortex tubes"*, Journal of Fluid Mechanics, Vol. 45(1), pp. 161–187, 1971.

71. Lewellen, W. S., *"A solution for three dimensional vortex flows with strong circulation"* Journal of Fluid Mechanics, Vol. 14(1), pp. 420ff, 1962.

72. Scheper, G. W., *"Flow patterns and a heat transfer theory for the vortex heating and refrigerating tube"*, Master's thesis, Union College, Schenectady, USA

73. Cohen, K., *"The Theory of Isotope Separation"*, McGraw-Hill, New York, 1951.

74. Gulyaev, A. I., *"Vortex tubes and the vortex effect"*, Soviet Physics: Technical Physics, Vol. 10(10), pp. 1441ff, April 1966.

75. Lay, J. E., *"An experimental and analytical study of vortex-flow temperature separation by superposition of spiral and axial flows part 1"*, Transactions of the ASME, pp. 202–212, August 1959.

76. Lay, J. E., *"An experimental and analytical study of vortex-flow temperature separation by superposition of spiral and axial flows part 2"*, Transactions of the ASME, pp. 213–222, August 1959.

77. Cockerill, T. T.*"Thermodynamics and fluid mechanics of a Ranque-Hilsch vortex tube"*, Ph.D. Thesis, University of Cambridge, 1998.

78. Sonin, Ain A., *"Equation of motion for viscous fluids"*, Department of Mechanical Engineering Massachusetts Institute of Technology Cambridge, Massachusetts 02139, 8th edition, 2001.

79. Moran, M. J., *"Availability Analysis"*, ASME Press, 1989.

80. Vonnegut, B., *"Vortex thermometer for measuring true air temperature and true air speeds in flight"*, Review of Scientific Instruments, Vol. 121, pp. 136–141, 1950.

81. Vortec Corporation catalogue. Company Catalogue, 10125 Carver Road, Cincinnati, Ohio 45242-9976, USA, UK Distributor: MEECH VORTEC, Burford House, 15 Thorney Leys Business Park, Witney, Oxford, OX8 7GE, 1992.

82. T. J. Bruno, *"Laboratory applications of the vortex tube"*, Canadian Journal of Chemical Education, Vol. 64, pp. 987–988, 1987.

83. Landecker, K., *"A two stage refrigeration and power producing arrangement consisting of a vortex cooling tube and a thermoelectric stage"*, Energy Conservation, Vol. 17, pp. 119–122.

84. Baz, A. and D. Uhler, *"A compressed gas powered heating system for underwater divers"*, Ocean Engineering, Vol. 13(3), pp. 273–290, 1986.

85. ITW Vortec Companiy. Online. Available at http://www.vortexitalia.net.

86. Baz, A., J. Gilheany and A. Kalvitas, *"Feasibility of vortex tube assisted environmental control of an underwater research habitat"*, Ocean Engineering, Vol. 15(1), pp. 34–54, 1987.

87. Baz, A., R. Johnston and D. Uhler, *"Dynamics of vortex tube assisted hyperbaric chambers"*, Ocean Engineering, Vol. 13(4), pp. 387–408, 1986.

88. Fin'ko, V. E., *"Cooling and condensation of gas in a vortex flow"*, Soviet Physics: Technical Physics, Vol. 28(9), pp. 1089ff, September 1983.

89. Johnson, A. F., *"Quantitative study of the Hilsch heat separator"*, Can. J. Res., Vol. 25, Sect. F, 299, 1947.

90. Wenig, H. G., *"The Ranque-Hilsch effect in a vortex tube"*, Ph.D. Thesis, New York University, 1952.

91. Elser, K. and M. Hoch, *"Das verhaltn verschiedener gase und die trennung von gasgemischen in einem wirbelrohr"*, Z. Naturf, 6a (25), 1951.

92. Raterman, K. T., M. McKellar, A. Podgorney, D. Stacey and T. A. Turner, *"A vortex contactor for carbon dioxide separations"*, Idaho National Engineering and Environmental Laboratory, INEEL/CON-01-00258, 2001.

93. Kulkarni, M. R. and C. R. Sardesai, *"Enrichment of methane concentration via separation of gases using vortex tubes"*, J. Energy Engrg, Vol. 128(1), pp. 1–12, 2002.

94. Khodorkov, I. L., N. V. Poshernev and M. A. Zhidkov, *"The vortex tube - A universal device for heating, cooling, cleaning, and drying gases and separating gas mixtures"*, Chemical and Petroleum Engineering, Vol. 39(7-8), pp. 409–15, 2003.

95. Keller, J. U. M. U., Göbel, R. Staudt, Inst. Fluid- & Thermodynamik, Universität Siegen, 57068 Siegen

APPENDIX A: EXPERIMENTAL DATA AND CALCULATIONS OF SECTION 5.4.1 "Effect of the Number of Inlet Nozzles in Vortex Generators"

G=1, L = 20 D ,D=16mm, Cone Angle =40^0, P=6 Bar (g)

$Q_{read,h}$ (l/min)	$Q_{read,c}$ (l/min)	$Q_{act,h}$ (l/min)	$Q_{act,c}$ (l/min)	$\rho_{air,c}$ (kg/m^3)	$\rho_{air,h}$ (kg/m^3)	m_c (kg/min)	m_h (kg/min)	m_t (kg/min)	T_i (C^0)	T_h (C^0)	T_c (C^0)	μ_c	T_h-T_i (C^0)	T_i-T_c (C^0)	ΔT_{isen} (C^0)	μ_{isen} (%)
500	0	515.644	0.000	1.294	1.243	0.000	0.641	0.641	17	21.2	9.6	0.00	4.2	-7.4	121.180	6.107
470	30	484.459	31.730	1.307	1.241	0.041	0.601	0.643	17	21.5	6.7	0.06	4.5	-10.3	121.180	8.500
450	50	463.450	53.246	1.325	1.239	0.071	0.574	0.645	17	22	2.9	0.11	5	-14.1	121.180	11.636
420	80	431.459	85.834	1.345	1.233	0.115	0.532	0.647	17	23.5	-1.2	0.18	6.5	-18.2	121.180	15.019
400	100	410.222	107.709	1.356	1.229	0.146	0.504	0.650	17	24.5	-3.3	0.22	7.5	-20.3	121.180	16.752
350	150	356.912	162.530	1.372	1.215	0.223	0.434	0.657	17	27.9	-6.5	0.34	10.9	-23.5	121.180	19.393
320	180	324.919	195.476	1.378	1.205	0.269	0.391	0.661	17	30.5	-7.7	0.41	13.5	-24.7	121.180	20.383
290	200	293.014	217.441	1.381	1.193	0.300	0.350	0.650	17	33.5	-8.3	0.46	16.5	-25.3	121.180	20.878
200	300	199.082	326.039	1.380	1.158	0.450	0.230	0.680	17	42.8	-8.1	0.66	25.8	-25.1	121.180	20.713
150	350	148.795	378.881	1.369	1.150	0.519	0.171	0.690	17	45	-6	0.75	28	-23	121.180	18.980
120	380	118.478	409.066	1.354	1.139	0.554	0.135	0.689	17	48	-3	0.80	31	-20	121.180	16.504
100	400	98.579	427.443	1.334	1.135	0.570	0.112	0.682	17	49	1	0.84	32	-16	121.180	13.203
50	450	49.251	479.129	1.325	1.134	0.635	0.056	0.690	17	49.5	3	0.92	32.5	-14	121.180	11.553
0	500	0.000	525.743	1.292	1.170	0.679	0.000	0.679	17	39.5	10	1.00	22.5	-7	121.180	5.777
						Av. Mass Flow Rate		**0.011**	**kg/s**						$\mu_{isenmax}$ =	**20.878**

G=2, L = 20D ,D=16 mm, Cone Angle =40^0, P=6 Bar (g)

$Q_{read,h}$ (l/min)	$Q_{read,c}$ (l/min)	$Q_{act,h}$ (l/min)	$Q_{act,c}$ (l/min)	$\rho_{air,c}$ (kg/m^3)	$\rho_{air,h}$ (kg/m^3)	m_c (kg/min)	m_h (kg/min)	m_t (kg/min)	T_i (C^0)	T_h (C^0)	T_c (C^0)	μ_c	T_h-T_i (C^0)	T_i-T_c (C^0)	ΔT_{isen} (C^0)	μ_{isen} (%)
850	0	885.208	0.000	1.294	1.267	0.000	1.122	1.122	15	15.5	9.5	0.00	0.5	-5.5	120.345	4.570
800	50	829.980	53.636	1.345	1.258	0.072	1.044	1.116	15	17.7	-1.1	0.06	2.7	-16.1	120.345	13.378
750	100	773.335	109.030	1.389	1.242	0.151	0.961	1.112	16	21.3	-9.8	0.14	5.3	-25.8	120.763	21.364
700	150	717.287	165.120	1.416	1.227	0.234	0.880	1.114	16	25.0	-14.8	0.21	9.0	-30.8	120.763	25.505
660	200	670.036	221.536	1.434	1.204	0.318	0.807	1.124	16	30.6	-18.0	0.28	14.6	-34.0	120.763	28.154
630	250	637.068	276.379	1.428	1.195	0.395	0.761	1.156	16	33.0	-17.0	0.34	17.0	-33.0	120.763	27.326
570	300	569.916	330.881	1.421	1.168	0.470	0.666	1.136	17	40.0	-15.8	0.41	23.0	-32.8	121.180	27.067
530	350	528.238	383.944	1.406	1.161	0.540	0.613	1.153	17	42.0	-13.0	0.47	25.0	-30.0	121.180	24.756
450	400	444.988	438.288	1.403	1.143	0.615	0.508	1.123	17	47.0	-12.4	0.55	30.0	-29.4	121.180	24.261
400	450	394.009	491.288	1.393	1.134	0.684	0.447	1.131	17	49.5	-10.5	0.61	32.5	-27.5	121.180	22.693
350	500	342.379	542.784	1.377	1.118	0.747	0.383	1.130	18	54.0	-7.5	0.66	36.0	-25.5	121.598	20.971
300	550	291.031	595.384	1.369	1.100	0.815	0.320	1.135	18	59.5	-6.0	0.72	41.5	-24.0	121.598	19.737
240	600	231.610	646.852	1.358	1.088	0.878	0.252	1.130	18	63.0	-3.8	0.78	45.0	-21.8	121.598	17.928
200	650	192.181	698.426	1.349	1.079	0.942	0.207	1.150	19	65.9	-2.0	0.82	46.9	-21.0	122.016	17.211
150	700	143.272	747.616	1.333	1.066	0.996	0.153	1.149	19	70.0	1.3	0.87	51.0	-17.7	122.016	14.506
100	750	95.238	796.388	1.317	1.060	1.049	0.101	1.150	19	72.0	4.5	0.91	53.0	-14.5	122.016	11.884
40	800	38.150	845.681	1.306	1.063	1.104	0.041	1.145	19	71.0	7.0	0.96	52.0	-12.0	122.016	9.835
0	850	0.000	892.190	1.287	1.098	1.149	0.000	1.149	19	60.0	11.0	1.00	41.0	-8.0	122.016	6.557
						Av. Mass Flow Rate		**0.019**	**kg/s**						$\mu_{isenmax}$ = (%)	**28.154**

G=4, L = 20D ,D=16 mm, Cone Angle =40^0, P=6 Bar (g)

$Q_{read,h}$ (l/min)	$Q_{read,c}$ (l/min)	$Q_{act,h}$ (l/min)	$Q_{act,c}$ (l/min)	$\rho_{air,c}$ (kg/m^3)	$\rho_{air,h}$ (kg/m^3)	m_c (kg/min)	m_h (kg/min)	m_t (kg/min)	T_i (C^0)	T_h (C^0)	T_c (C^0)	μ_c	T_h-T_i (C^0)	T_i-T_c (C^0)	ΔT_{isen}	μ_{isen}
1500	0	1542.22	0.00	1.27	1.24	0.000	1.905	1.905	21	23.0	14.0	0.00	2.0	-7.0	122.851	5.698
1450	100	1487.06	106.47	1.32	1.23	0.141	1.827	1.969	22	24.5	3.0	0.07	2.5	-19.0	123.269	15.413
1400	200	1434.57	215.30	1.35	1.23	0.292	1.760	2.052	22	25.0	-3.0	0.14	3.0	-25.0	123.269	20.281
1350	250	1381.02	270.12	1.36	1.22	0.368	1.689	2.057	22	26.0	-5.0	0.18	4.0	-27.0	123.269	21.903
1300	350	1326.55	379.59	1.37	1.22	0.522	1.614	2.136	22	27.5	-7.0	0.24	5.5	-29.0	123.269	23.526
1250	400	1273.84	435.05	1.38	1.21	0.601	1.546	2.147	22	28.3	-8.5	0.28	6.3	-30.5	123.269	24.743
1200	450	1218.45	490.36	1.39	1.20	0.680	1.468	2.148	22	30.5	-9.5	0.32	8.5	-31.5	123.269	25.554
1150	450	1165.76	491.29	1.39	1.20	0.684	1.400	2.084	22	31.5	-10.5	0.33	9.5	-32.5	123.269	26.365
1100	500	1103.37	546.92	1.40	1.18	0.765	1.297	2.062	22	38.0	-11.5	0.37	16.0	-33.5	123.269	27.176
1050	600	1048.17	657.56	1.40	1.16	0.923	1.220	2.143	23	41.0	-12.5	0.43	18.0	-35.5	123.686	28.702
1000	650	996.67	709.91	1.39	1.16	0.989	1.157	2.146	23	42.0	-10.7	0.46	19.0	-33.7	123.686	27.246
900	750	889.98	816.48	1.38	1.14	1.131	1.017	2.148	23	47.0	-9.0	0.53	24.0	-32.0	123.686	25.872
850	800	832.76	869.60	1.38	1.12	1.201	0.934	2.135	23	53.0	-8.2	0.56	30.0	-31.2	123.686	25.225
800	850	770.89	921.87	1.37	1.08	1.267	0.836	2.103	23	64.0	-7.0	0.60	41.0	-30.0	123.686	24.255
750	880	720.57	952.61	1.37	1.08	1.304	0.777	2.082	23	66.0	-6.0	0.63	43.0	-29.0	123.686	23.446

700	950	668.60	1026.47	1.36	1.07	1.400	0.713	2.113	23	70.0	-5.0	0.66	47.0	-28.0	123.686	22.638
650	1000	616.81	1078.89	1.36	1.05	1.467	0.649	2.116	23	74.5	-4.2	0.69	51.5	-27.2	123.686	21.991
600	1040	568.96	1115.02	1.34	1.05	1.498	0.598	2.095	23	75.0	-0.8	0.71	52.0	-23.8	123.686	19.242
550	1070	521.17	1140.50	1.33	1.05	1.514	0.547	2.061	23	75.5	2.4	0.73	52.5	-20.6	123.686	16.655
500	1120	472.44	1188.63	1.32	1.04	1.564	0.493	2.057	23	77.5	4.8	0.76	54.5	-18.2	123.686	14.715
450	1150	424.29	1218.50	1.31	1.04	1.598	0.441	2.039	23	79.0	5.7	0.78	56.0	-17.3	123.686	13.987
400	1200	375.81	1268.52	1.31	1.03	1.656	0.388	2.044	23	81.5	7.0	0.81	58.5	-16.0	123.686	12.936
300	1270	282.26	1337.75	1.30	1.03	1.734	0.292	2.026	23	80.5	9.0	0.86	57.5	-14.0	123.686	11.319
250	1300	235.38	1364.29	1.29	1.04	1.756	0.244	1.999	23	80.0	11.1	0.88	57.0	-11.9	123.686	9.621
200	1320	189.11	1381.88	1.28	1.04	1.770	0.198	1.967	23	77.0	12.5	0.90	54.0	-10.5	123.686	8.489
160	1380	152.38	1440.91	1.27	1.06	1.836	0.161	1.997	23	72.0	14.0	0.92	49.0	-9.0	123.686	7.276
100	1400	97.52	1453.46	1.26	1.11	1.830	0.108	1.939	23	56.0	17.3	0.94	33.0	-5.7	123.686	4.608
0	1450	0.00	1504.86	1.26	1.15	1.894	0.000	1.894	23	45.0	17.5	1.00	22.0	-5.5	123.686	4.447
						Av. Mass Flow Rate		**0.034**	**kg/s**					$\mu_{isenmax}$= (%)		**28.702**

APPENDIX B: EXPERIMENTAL DATA AND CALCULATIONS OF SECTION 5.4.2 "Effect of the Length of the Hot Tube"

L = 15D, G=1, D=16 mm, Cone Angle =40^0, P=6 Bar (g)

$Q_{read,h}$ (l/min)	$Q_{read,c}$ (l/min)	$Q_{act,h}$ (l/min)	$Q_{act,c}$ (l/min)	$\rho_{air,c}$ (kg/m^3)	$\rho_{air,h}$ (kg/m^3)	m_c (kg/min)	m_h (kg/min)	m_t (kg/min)	T_i (C^0)	T_h (C^0)	T_c (C^0)	μ_c	T_h-T_i (C^0)	T_i-T_c (C^0)	ΔT_{isen}	μ_{isen}
500	0	515.382	0.000	1.292	1.241	0.000	0.640	0.640	18	21.5	10.0	0.00	3.5	-8.0	121.598	6.579
450	50	462.667	53.237	1.325	1.235	0.071	0.571	0.642	18	23.0	3.0	0.11	5.0	-15.0	121.598	12.336
420	80	431.095	85.723	1.342	1.231	0.115	0.531	0.646	18	24.0	-0.5	0.18	6.0	-18.5	121.598	15.214
400	100	409.878	107.272	1.345	1.227	0.144	0.503	0.647	18	25.0	-1.1	0.22	7.0	-19.1	121.598	15.707
350	150	358.043	160.437	1.337	1.223	0.214	0.438	0.652	18	26.0	0.5	0.33	8.0	-17.5	121.598	14.392
320	180	326.808	191.999	1.329	1.219	0.255	0.398	0.654	18	27.0	2.0	0.39	9.0	-16.0	121.598	13.158
250	240	254.472	255.906	1.328	1.211	0.340	0.308	0.648	18	29.0	2.2	0.52	11.0	-15.8	121.598	12.994
200	300	202.575	319.709	1.327	1.199	0.424	0.243	0.667	18	32.0	2.5	0.64	14.0	-15.5	121.598	12.747
160	340	161.795	362.008	1.325	1.195	0.480	0.193	0.673	18	33.0	3.0	0.71	15.0	-15.0	121.598	12.336
120	400	121.089	424.740	1.317	1.190	0.560	0.144	0.704	18	34.3	4.5	0.80	16.3	-13.5	121.598	11.102
50	450	50.356	475.272	1.303	1.185	0.619	0.060	0.679	18	35.5	7.5	0.91	17.5	-10.5	121.598	8.635
0	500	0.000	524.817	1.287	1.199	0.676	0.000	0.676	18	32.0	11.0	1.00	14.0	-7.0	121.598	5.757
						Av. Mass Flow Rate		**0.011**	**kg/s**						$\mu_{isenmax}$ = (%)	**15.707**

L = 20D, G=1, D=16 mm, Cone Angle =40^0, P=6 Bar (g)

$Q_{read,h}$ (l/min)	$Q_{read,c}$ (l/min)	$Q_{act,h}$ (l/min)	$Q_{act,c}$ (l/min)	$\rho_{air,c}$ (kg/m^3)	$\rho_{air,h}$ (kg/m^3)	m_c (kg/min)	m_h (kg/min)	m_t (kg/min)	T_i (C^0)	T_h (C^0)	T_c (C^0)	μ_c	T_h-T_i (C^0)	T_i-T_c (C^0)	Δt_{isen} (C^0)	μ_{isen} (%)
500	0	514.945	0.000	1.288	1.239	0.000	0.638	0.638	18	22.0	10.8	0.00	4.0	-7.2	121.598	5.921
450	50	463.058	53.045	1.315	1.237	0.070	0.573	0.643	18	22.5	5.0	0.11	4.5	-13.0	121.598	10.691
420	80	431.459	85.489	1.334	1.233	0.114	0.532	0.646	18	23.5	1.0	0.18	5.5	-17.0	121.598	13.980
400	100	410.429	107.371	1.347	1.230	0.145	0.505	0.650	18	24.2	-1.6	0.22	6.2	-19.6	121.598	16.119
380	120	389.188	129.322	1.357	1.226	0.175	0.477	0.652	18	25.3	-3.6	0.27	7.3	-21.6	121.598	17.763
340	180	347.118	193.732	1.354	1.218	0.262	0.423	0.685	18	27.2	-2.9	0.38	9.2	-20.9	121.598	17.188
180	300	181.723	321.581	1.343	1.191	0.432	0.216	0.648	18	34.0	-0.7	0.67	16.0	-18.7	121.598	15.379
150	350	150.945	374.696	1.339	1.183	0.502	0.179	0.680	18	36.0	0.0	0.74	18.0	-18.0	121.598	14.803
130	370	130.398	395.529	1.335	1.176	0.528	0.153	0.681	18	38.0	0.8	0.78	20.0	-17.2	121.598	14.145
100	400	100.226	426.665	1.329	1.174	0.567	0.118	0.685	18	38.5	2.0	0.83	20.5	-16.0	121.598	13.158
50	450	50.438	475.696	1.306	1.189	0.621	0.060	0.681	18	34.5	7.0	0.91	16.5	-11.0	121.598	9.046
						Av. Mass Flow Rate		**0.010**	**kg/s**						$\mu_{isenmax}$ = (%)	**17.763**

L = 25D, G=1, D=16 mm, Cone Angle =40^0, P=6 Bar (g)

$Q_{read,h}$ (l/min)	$Q_{read,c}$ (l/min)	$Q_{act,h}$ (l/min)	$Q_{act,c}$ (l/min)	$\rho_{air,c}$ (kg/m^3)	$\rho_{air,h}$ (kg/m^3)	m_c (kg/min)	m_h (kg/min)	m_t (kg/min)	T_i (C^0)	T_h (C^0)	T_c (C^0)	μ_c	T_h-T_i (C^0)	T_i-T_c (C^0)	Δt_{isen} (C^0)	μ_{isen} (%)
500	0	514.509	0.000	1.287	1.237	0.000	0.637	0.637	18	22.5	11.0	0.00	4.5	-7.0	121.598	5.757
460	40	472.949	42.474	1.317	1.235	0.056	0.584	0.640	18	23.0	4.5	0.09	5.0	-13.5	121.598	11.102
430	75	441.360	80.146	1.334	1.231	0.107	0.543	0.650	18	24.0	1.0	0.16	6.0	-17.0	121.598	13.980
400	100	410.153	107.253	1.344	1.229	0.144	0.504	0.648	18	24.6	-1.0	0.22	6.6	-19.0	121.598	15.625
380	120	389.058	128.893	1.348	1.225	0.174	0.477	0.650	18	25.5	-1.8	0.27	7.5	-19.8	121.598	16.283
350	150	357.446	161.175	1.349	1.219	0.217	0.436	0.653	18	27.0	-2.0	0.33	9.0	-20.0	121.598	16.448
320	180	326.265	193.589	1.352	1.215	0.262	0.396	0.658	18	28.0	-2.5	0.40	10.0	-20.5	121.598	16.859
300	200	305.367	215.378	1.355	1.211	0.292	0.370	0.662	18	29.0	-3.2	0.44	11.0	-21.2	121.598	17.434
250	250	253.634	269.322	1.356	1.203	0.365	0.305	0.670	18	31.0	-3.4	0.54	13.0	-21.4	121.598	17.599
200	300	201.586	323.246	1.357	1.187	0.438	0.239	0.678	18	35.0	-3.5	0.65	17.0	-21.5	121.598	17.681
160	350	160.619	376.076	1.349	1.177	0.507	0.189	0.696	18	37.5	-2.0	0.73	19.5	-20.0	121.598	16.448
120	380	120.174	407.186	1.342	1.172	0.546	0.141	0.687	18	39.0	-0.5	0.80	21.0	-18.5	121.598	15.214
100	400	99.826	426.665	1.329	1.164	0.567	0.116	0.683	18	41.0	2.0	0.83	23.0	-16.0	121.598	13.158
50	450	49.834	476.547	1.310	1.161	0.624	0.058	0.682	18	42.0	6.0	0.92	24.0	-12.0	121.598	9.869
0	500	0.000	527.610	1.301	1.183	0.686	0.000	0.686	18	36.0	8.0	1.00	18.0	-10.0	121.598	8.224
						Av. Mass Flow Rate		**0.011**	**kg/s**						$\mu_{isenmax}$ = (%)	**17.681**

L = 30D, G=1, D=16 mm, Cone Angle =40^0, P=6 Bar (g)

$Q_{read,h}$ (l/min)	$Q_{read,c}$ (l/min)	$Q_{act,h}$ (l/min)	$Q_{act,c}$ (l/min)	$\rho_{air,c}$ (kg/m^3)	$\rho_{air,h}$ (kg/m^3)	m_c (kg/min)	m_h (kg/min)	m_t (kg/min)	T_i (C^0)	T_h (C^0)	T_c (C^0)	μ_c	T_h-T_i (C^0)	T_i-T_c (C^0)	Δt_{isen} (C^0)	μ_{isen} (%)
500	0	514.075	0.000	1.292	1.235	0.000	0.635	0.635	18	23.0	10.0	0.00	5.0	-8.0	121.598	6.579
460	40	472.152	42.574	1.324	1.231	0.056	0.581	0.638	18	24.0	3.2	0.09	6.0	-14.8	121.598	12.171
430	70	441.137	74.939	1.339	1.230	0.100	0.542	0.643	18	24.3	0.0	0.16	6.3	-18.0	121.598	14.803
400	100	409.878	107.450	1.349	1.227	0.145	0.503	0.648	18	25.0	-2.0	0.22	7.0	-20.0	121.598	16.448
340	160	346.657	172.430	1.357	1.215	0.234	0.421	0.655	18	28.0	-3.6	0.36	10.0	-21.6	121.598	17.763
310	190	315.285	205.027	1.361	1.209	0.279	0.381	0.660	18	29.5	-4.3	0.42	11.5	-22.3	121.598	18.339
280	220	284.071	237.444	1.361	1.203	0.323	0.342	0.665	18	31.0	-4.4	0.49	13.0	-22.4	121.598	18.421
260	240	263.347	259.078	1.362	1.199	0.353	0.316	0.668	18	32.0	-4.5	0.53	14.0	-22.5	121.598	18.504
200	300	201.423	323.366	1.358	1.185	0.439	0.239	0.678	18	35.5	-3.7	0.65	17.5	-21.7	121.598	17.846
170	320	170.657	344.476	1.354	1.177	0.466	0.201	0.667	18	37.5	-3.0	0.70	19.5	-21.0	121.598	17.270
150	350	150.218	376.076	1.349	1.172	0.507	0.176	0.683	18	39.0	-2.0	0.74	21.0	-20.0	121.598	16.448
120	380	119.982	406.071	1.334	1.168	0.542	0.140	0.682	18	40.0	1.0	0.79	22.0	-17.0	121.598	13.980
100	400	99.747	425.892	1.325	1.163	0.564	0.116	0.680	18	41.5	3.0	0.83	23.5	-15.0	121.598	12.336
50	450	49.993	475.696	1.306	1.168	0.621	0.058	0.680	18	40.0	7.0	0.91	22.0	-11.0	121.598	9.046
0	500	0.000	521.162	1.269	1.183	0.662	0.000	0.662	18	36.0	15.0	1.00	18.0	-3.0	121.598	2.467
						Av. Mass Flow Rate		**0.011**	**kg/s**						$\mu_{isenmax}$ = (%)	**18.504**

L = 35D, G=1, D=16 mm, Cone Angle =40^0, P=6 Bar (g)

$Q_{read,h}$ (l/min)	$Q_{read,c}$ (l/min)	$Q_{act,h}$ (l/min)	$Q_{act,c}$ (l/min)	$\rho_{air,c}$ (kg/m^3)	$\rho_{air,h}$ (kg/m^3)	m_c (kg/min)	m_h (kg/min)	m_t (kg/min)	T_i (C^0)	T_h (C^0)	T_c (C^0)	μ_c	T_h-T_i (C^0)	T_i-T_c (C^0)	Δt_{isen} (C^0)	μ_{isen} (%)
500	0	514.075	0.000	1.276	1.235	0.000	0.635	0.635	18	23.0	13.5	0.00	5.0	-4.5	121.598	3.701
460	40	472.152	42.360	1.310	1.231	0.056	0.581	0.637	18	24.0	6.0	0.09	6.0	-12.0	121.598	9.869
440	60	451.472	64.058	1.332	1.230	0.085	0.555	0.641	18	24.2	1.5	0.13	6.2	-16.5	121.598	13.569
400	100	409.741	107.056	1.339	1.226	0.143	0.502	0.646	18	25.2	0.0	0.22	7.2	-18.0	121.598	14.803
370	130	378.187	139.326	1.342	1.221	0.187	0.462	0.649	18	26.5	-0.6	0.29	8.5	-18.6	121.598	15.296
340	160	346.945	171.730	1.346	1.217	0.231	0.422	0.653	18	27.5	-1.4	0.35	9.5	-19.4	121.598	15.954
320	180	325.833	193.339	1.348	1.211	0.261	0.395	0.655	18	28.8	-1.8	0.40	10.8	-19.8	121.598	16.283
300	200	304.863	214.940	1.350	1.207	0.290	0.368	0.658	18	30.0	-2.1	0.44	12.0	-20.1	121.598	16.530
270	230	273.566	247.272	1.351	1.200	0.334	0.328	0.662	18	31.8	-2.3	0.50	13.8	-20.3	121.598	16.694
240	270	242.692	290.223	1.350	1.195	0.392	0.290	0.682	18	33.0	-2.2	0.57	15.0	-20.2	121.598	16.612
200	300	201.914	322.232	1.348	1.191	0.434	0.240	0.675	18	34.0	-1.8	0.64	16.0	-19.8	121.598	16.283
180	320	181.428	343.335	1.345	1.187	0.462	0.215	0.677	18	35.0	-1.2	0.68	17.0	-19.2	121.598	15.790
150	350	150.945	374.696	1.339	1.183	0.502	0.179	0.680	18	36.0	0.0	0.74	18.0	-18.0	121.598	14.803
130	370	130.650	395.385	1.334	1.180	0.528	0.154	0.682	18	36.8	1.0	0.77	18.8	-17.0	121.598	13.980
100	400	100.387	425.892	1.325	1.177	0.564	0.118	0.682	18	37.5	3.0	0.83	19.5	-15.0	121.598	12.336
50	450	50.274	476.974	1.313	1.181	0.626	0.059	0.686	18	36.5	5.5	0.91	18.5	-12.5	121.598	10.280
0	500	0.000	520.710	1.267	1.195	0.660	0.000	0.660	18	33.0	15.5	1.00	15.0	-2.5	121.598	2.056
						Av. Mass Flow Rate		**0.011**	**kg/s**						$\mu_{isenmax}$ = (%)	**16.694**

L = 40D, G=1, D=16 mm, Cone Angle =40^0, P=6 Bar (g)

$Q_{read,h}$ (l/min)	$Q_{read,c}$ (l/min)	$Q_{act,h}$ (l/min)	$Q_{act,c}$ (l/min)	$\rho_{air,c}$ (kg/m^3)	$\rho_{air,h}$ (kg/m^3)	m_c (kg/min)	m_h (kg/min)	m_t (kg/min)	T_i (C^0)	T_h (C^0)	T_c (C^0)	μ_c	T_h-T_i (C^0)	T_i-T_c (C^0)	Δt_{isen} (C^0)	μ_{isen} (%)
500	0	514.248	0.000	1.288	1.236	0.000	0.636	0.636	18	22.8	10.8	0.00	4.8	-7.2	121.598	5.921
460	40	472.949	42.246	1.303	1.235	0.055	0.584	0.639	18	23.0	7.5	0.09	5.0	-10.5	121.598	8.635
450	50	462.511	53.140	1.320	1.234	0.070	0.571	0.641	18	23.2	4.0	0.11	5.2	-14.0	121.598	11.513
420	80	431.459	85.489	1.334	1.233	0.114	0.532	0.646	18	23.5	1.0	0.18	5.5	-17.0	121.598	13.980
400	100	410.222	107.351	1.347	1.229	0.145	0.504	0.649	18	24.5	-1.5	0.22	6.5	-19.5	121.598	16.036
380	120	389.384	128.988	1.350	1.227	0.174	0.478	0.652	18	25.0	-2.2	0.27	7.0	-20.2	121.598	16.612
360	140	368.273	150.625	1.353	1.223	0.204	0.450	0.654	18	26.0	-2.7	0.31	8.0	-20.7	121.598	17.023
340	160	347.234	172.302	1.355	1.219	0.233	0.423	0.657	18	27.0	-3.2	0.36	9.0	-21.2	121.598	17.434
300	200	305.772	215.617	1.358	1.214	0.293	0.371	0.664	18	28.2	-3.8	0.44	10.2	-21.8	121.598	17.928
280	220	284.774	237.179	1.358	1.209	0.322	0.344	0.666	18	29.5	-3.8	0.48	11.5	-21.8	121.598	17.928
240	250	243.090	269.622	1.359	1.199	0.366	0.291	0.658	18	32.0	-4.0	0.56	14.0	-22.0	121.598	18.092
200	300	202.079	323.126	1.356	1.193	0.438	0.241	0.679	18	33.5	-3.3	0.65	15.5	-21.3	121.598	17.517
180	320	181.428	344.285	1.353	1.187	0.466	0.215	0.681	18	35.0	-2.7	0.68	17.0	-20.7	121.598	17.023
160	340	161.138	365.129	1.348	1.185	0.492	0.191	0.683	18	35.5	-1.7	0.72	17.5	-19.7	121.598	16.201
140	360	140.768	385.968	1.343	1.181	0.518	0.166	0.685	18	36.5	-0.8	0.76	18.5	-18.8	121.598	15.461
120	380	120.561	406.813	1.339	1.179	0.545	0.142	0.687	18	37.0	0.0	0.79	19.0	-18.0	121.598	14.803
100	390	100.354	416.377	1.332	1.177	0.555	0.118	0.673	18	37.7	1.5	0.82	19.7	-16.5	121.598	13.569
50	450	50.413	476.974	1.313	1.188	0.626	0.060	0.686	18	34.8	5.5	0.91	16.8	-12.5	121.598	10.280
0	500	0.000	520.260	1.265	1.203	0.658	0.000	0.658	18	31.0	16.0	1.00	13.0	-2.0	121.598	1.645
						Av. Mass Flow Rate		**0.011**	**kg/s**						$\mu_{isenmax}$ = (%)	**18.092**

L = 45D, G=1, D=16 mm, Cone Angle =40^0, P=6 Bar (g)

$Q_{read,h}$ (l/min)	$Q_{read,c}$ (l/min)	$Q_{act,h}$ (l/min)	$Q_{act,c}$ (l/min)	$\rho_{air,c}$ (kg/m^3)	$\rho_{air,h}$ (kg/m^3)	m_c (kg/min)	m_h (kg/min)	m_t (kg/min)	T_i (C^0)	T_h (C^0)	T_c (C^0)	μ_c	T_h-T_i (C^0)	T_i-T_c (C^0)	Δt_{isen} (C^0)	μ_{isen} (%)
500	0	514.075	0.000	1.283	1.235	0.000	0.635	0.635	18	23.0	12.0	0.00	5.0	-6.0	121.598	4.934
450	50	462.511	53.045	1.315	1.234	0.070	0.571	0.641	18	23.2	5.0	0.11	5.2	-13.0	121.598	10.691
420	80	431.459	85.645	1.339	1.233	0.115	0.532	0.647	18	23.5	0.0	0.18	5.5	-18.0	121.598	14.803
400	100	410.567	107.253	1.344	1.231	0.144	0.505	0.650	18	24.0	-1.0	0.22	6.0	-19.0	121.598	15.625
380	120	389.711	128.822	1.347	1.229	0.173	0.479	0.652	18	24.5	-1.5	0.27	6.5	-19.5	121.598	16.036
350	150	358.343	161.265	1.351	1.225	0.218	0.439	0.657	18	25.5	-2.3	0.33	7.5	-20.3	121.598	16.694
320	180	327.081	193.768	1.354	1.221	0.262	0.399	0.662	18	26.5	-3.0	0.40	8.5	-21.0	121.598	17.270
280	220	285.957	237.047	1.357	1.219	0.322	0.348	0.670	18	27.0	-3.5	0.48	9.0	-21.5	121.598	17.681
250	250	254.683	269.422	1.357	1.213	0.366	0.309	0.674	18	28.5	-3.6	0.54	10.5	-21.6	121.598	17.763
200	300	203.075	323.006	1.355	1.205	0.438	0.245	0.682	18	30.5	-3.1	0.64	12.5	-21.1	121.598	17.352
160	340	162.193	365.331	1.349	1.201	0.493	0.195	0.688	18	31.5	-2.0	0.72	13.5	-20.0	121.598	16.448
140	370	141.686	396.835	1.344	1.197	0.533	0.170	0.703	18	32.5	-1.0	0.76	14.5	-19.0	121.598	15.625
120	390	121.346	417.519	1.339	1.195	0.559	0.145	0.704	18	33.0	0.0	0.79	15.0	-18.0	121.598	14.803
100	410	101.039	437.730	1.332	1.193	0.583	0.121	0.704	18	33.5	1.5	0.83	15.5	-16.5	121.598	13.569
50	450	50.644	477.833	1.317	1.199	0.630	0.061	0.690	18	32.0	4.5	0.91	14.0	-13.5	121.598	11.102
0	500	0.000	521.162	1.269	1.211	0.662	0.000	0.662	18	29.0	15.0	1.00	11.0	-3.0	121.598	2.467
						Av. Mass Flow Rate		**0.011**	**kg/s**					$\mu_{isenmax}$ = (%)		**17.763**

L = 50D, G=1, D=16 mm, Cone Angle =40^0, P=6 Bar (g)

$Q_{read,h}$ (l/min)	$Q_{read,c}$ (l/min)	$Q_{act,\ h}$ (l/min)	$Q_{act,\ c}$ (l/min)	$\rho_{air,\ c}$ (kg/m^3)	$\rho_{air,\ h}$ (kg/m^3)	m_c (kg/min)	m_h (kg/min)	m_t (kg/min)	T_i (C^0)	T_h (C^0)	T_c (C^0)	μ_c	T_h-T_i (C^0)	T_i-T_c (C^0)	Δt_{isen} (C^0)	μ_{isen} (%)
500	0	515.819	0.000	1.295	1.244	0.000	0.641	0.641	18	21.0	9.3	0.00	3.0	-8.7	121.598	7.155
470	30	484.048	31.798	1.313	1.239	0.042	0.600	0.642	18	22.0	5.5	0.07	4.0	-12.5	121.598	10.280
420	80	432.042	85.802	1.344	1.236	0.115	0.534	0.650	18	22.7	-1.0	0.18	4.7	-19.0	121.598	15.625
400	100	410.982	107.490	1.350	1.233	0.145	0.507	0.652	18	23.4	-2.2	0.22	5.4	-20.2	121.598	16.612
380	120	390.039	129.107	1.353	1.231	0.175	0.480	0.655	18	24.0	-2.7	0.27	6.0	-20.7	121.598	17.023
350	150	358.643	161.593	1.356	1.227	0.219	0.440	0.659	18	25.0	-3.4	0.33	7.0	-21.4	121.598	17.599
340	160	347.407	172.558	1.359	1.220	0.235	0.424	0.658	18	26.7	-4.0	0.36	8.7	-22.0	121.598	18.092
320	190	326.536	205.027	1.361	1.217	0.279	0.397	0.676	18	27.5	-4.3	0.41	9.5	-22.3	121.598	18.339
280	240	285.245	259.126	1.362	1.213	0.353	0.346	0.699	18	28.5	-4.6	0.51	10.5	-22.6	121.598	18.586
200	300	202.575	323.426	1.358	1.199	0.439	0.243	0.682	18	32.0	-3.8	0.64	14.0	-21.8	121.598	17.928
180	330	182.019	355.044	1.353	1.195	0.480	0.217	0.698	18	33.0	-2.7	0.69	15.0	-20.7	121.598	17.023
150	370	151.559	397.127	1.346	1.193	0.535	0.181	0.715	18	33.5	-1.4	0.75	15.5	-19.4	121.598	15.954
130	400	131.138	428.460	1.341	1.189	0.574	0.156	0.730	18	34.5	-0.3	0.79	16.5	-18.3	121.598	15.050
100	430	100.924	458.665	1.329	1.190	0.610	0.120	0.730	18	34.2	2.0	0.84	16.2	-16.0	121.598	13.158
40	460	40.449	487.574	1.313	1.195	0.640	0.048	0.688	18	33.0	5.5	0.93	15.0	-12.5	121.598	10.280
0	500	0.000	521.162	1.269	1.207	0.662	0.000	0.662	18	30.0	15.0	1.00	12.0	-3.0	121.598	2.467

Av. Mass Flow Rate **0.011** **kg/s**

$\mu_{isenmax}$ (%) = **18.586**

APPENDIX C: EXPERIMENTAL DATA AND CALCULATIONS OF SECTION 5.4.3 "Effect of the Vortex Cone Angles"

Cone Angle =40^0, L = 20D, G=1, D=16 mm, P=6 Bar (g)

$Q_{read,h}$ (l/min)	$Q_{read,c}$ (l/min)	$Q_{act,h}$ (l/min)	$Q_{act,c}$ (l/min)	$\rho_{air,c}$ (kg/m^3)	$\rho_{air,h}$ (kg/m^3)	m_c (kg/min)	m_h (kg/min)	m_t (kg/min)	T_i (C^0)	T_h (C^0)	T_c (C^0)	μ_c	T_h-T_i (C^0)	T_i-T_c (C^0)	Δt_{isen} (C^0)	μ_{isen} (%)
500	0	515.64	0.00	1.29	1.24	0.000	0.641	0.641	17	21.2	9.6	0.00	4.2	-7.4	121.180	6.107
470	30	484.46	31.73	1.31	1.24	0.041	0.601	0.643	17	21.5	6.7	0.06	4.5	-10.3	121.180	8.500
450	50	463.45	53.25	1.33	1.24	0.071	0.574	0.645	17	22.0	2.9	0.11	5.0	-14.1	121.180	11.636
420	80	431.46	85.83	1.35	1.23	0.115	0.532	0.647	17	23.5	-1.2	0.18	6.5	-18.2	121.180	15.019
400	100	410.22	107.71	1.36	1.23	0.146	0.504	0.650	17	24.5	-3.3	0.22	7.5	-20.3	121.180	16.752
370	130	378.50	140.54	1.37	1.22	0.192	0.463	0.655	17	26.0	-5.3	0.29	9.0	-22.3	121.180	18.402
350	150	356.91	162.53	1.37	1.22	0.223	0.434	0.657	17	27.9	-6.5	0.34	10.9	-23.5	121.180	19.393
320	180	324.92	195.48	1.38	1.20	0.269	0.391	0.661	17	30.5	-7.7	0.41	13.5	-24.7	121.180	20.383
290	200	293.01	217.44	1.38	1.19	0.300	0.350	0.650	17	33.5	-8.3	0.46	16.5	-25.3	121.180	20.878
200	300	199.08	325.98	1.38	1.16	0.450	0.230	0.680	17	42.8	-8.0	0.66	25.8	-25.0	121.180	20.630
150	350	148.79	378.88	1.37	1.15	0.519	0.171	0.690	17	45.0	-6.0	0.75	28.0	-23.0	121.180	18.980
120	380	118.48	409.07	1.35	1.14	0.554	0.135	0.689	17	48.0	-3.0	0.80	31.0	-20.0	121.180	16.504
100	400	98.58	427.44	1.33	1.14	0.570	0.112	0.682	17	49.0	1.0	0.84	32.0	-16.0	121.180	13.203
50	450	49.25	479.13	1.32	1.13	0.635	0.056	0.690	17	49.5	3.0	0.92	32.5	-14.0	121.180	11.553
0	500	0.00	525.74	1.29	1.17	0.679	0.000	0.679	17	39.5	10.0	1.00	22.5	-7.0	121.180	5.777
						Av. Mass Flow Rate		**0.011**	**kg/s**						**$\mu_{isenmax}$ = (%)**	**20.878**

Cone Angle =45^0, L = 20D, G=1, D=16 mm, P=6 Bar (g)

$Q_{read,h}$ (l/min)	$Q_{read,c}$ (l/min)	$Q_{act,h}$ (l/min)	$Q_{act,c}$ (l/min)	$\rho_{air,c}$ (kg/m^3)	$\rho_{air,h}$ (kg/m^3)	m_c (kg/min)	m_h (kg/min)	m_t (kg/min)	T_i (C^0)	T_h (C^0)	T_c (C^0)	μ_c	T_h-T_i (C^0)	T_i-T_c (C^0)	Δt_{isen} (C^0)	μ_{isen} (%)
500	0	515.91	0.00	1.28	1.24	0.000	0.642	0.642	16	20.9	11.6	0.00	4.9	-4.4	120.763	3.644
470	30	484.54	31.73	1.31	1.24	0.041	0.602	0.643	16	21.4	6.7	0.06	5.4	-9.3	120.763	7.701
450	50	463.53	53.28	1.33	1.24	0.071	0.575	0.645	16	21.9	2.5	0.11	5.9	-13.5	120.763	11.179
420	70	432.04	74.91	1.34	1.24	0.100	0.534	0.634	16	22.7	0.2	0.16	6.7	-15.8	120.763	13.084
400	100	410.57	107.57	1.35	1.23	0.145	0.505	0.651	16	24.0	-2.6	0.22	8.0	-18.6	120.763	15.402
360	130	367.97	140.73	1.37	1.22	0.193	0.449	0.642	16	26.5	-6.0	0.30	10.5	-22.0	120.763	18.218
330	160	335.96	173.69	1.38	1.21	0.239	0.407	0.646	16	28.9	-7.5	0.37	12.9	-23.5	120.763	19.460
280	200	283.14	217.32	1.38	1.19	0.300	0.338	0.638	16	33.0	-8.0	0.47	17.0	-24.0	120.763	19.874
220	270	220.00	293.93	1.38	1.17	0.407	0.257	0.664	17	39.9	-9.0	0.61	22.9	-26.0	121.180	21.456
200	300	198.86	326.29	1.38	1.16	0.451	0.230	0.681	17	43.5	-8.5	0.66	26.5	-25.5	121.180	21.043
170	320	167.19	346.66	1.37	1.13	0.475	0.189	0.664	17	50.5	-6.4	0.72	33.5	-23.4	121.180	19.310
150	350	146.85	377.47	1.36	1.12	0.513	0.164	0.677	17	53.5	-4.0	0.76	36.5	-21.0	121.180	17.330
120	390	116.19	418.90	1.35	1.10	0.565	0.127	0.692	17	60.8	-1.8	0.82	43.8	-18.8	121.180	15.514
100	410	96.53	438.93	1.34	1.09	0.588	0.105	0.693	17	62.8	0.0	0.85	45.8	-17.0	121.180	14.029
50	450	48.19	478.61	1.32	1.09	0.633	0.052	0.685	17	63.8	3.6	0.92	46.8	-13.4	121.180	11.058
0	500	0.00	524.82	1.29	1.12	0.676	0.000	0.676	17	53.0	**11.0**	1.00	36.0	-6.0	121.180	4.951
						Av. Mass Flow Rate		**0.011**	**kg/s**						$\mu_{isenmax}$ = (%)	**21.456**

Cone Angle =60^0, L = 20D, G=1, D=16 mm, P=6 Bar (g)

$Q_{read,h}$ (l/min)	$Q_{read,c}$ (l/min)	$Q_{act,h}$ (l/min)	$Q_{act,c}$ (l/min)	$\rho_{air,c}$ (kg/m^3)	$\rho_{air,h}$ (kg/m^3)	m_c (kg/min)	m_h (kg/min)	m_t (kg/min)	T_i (C^0)	T_h (C^0)	T_c (C^0)	μ_c	T_h-T_i (C^0)	T_i-T_c (C^0)	Δt_{isen} (C^0)	μ_{isen} (%)
480	0	498.16	0.00	1.27	1.26	0.000	0.627	0.627	16	17.5	14.7	0.00	1.5	-1.3	120.763	1.076
460	20	477.24	21.09	1.30	1.26	0.027	0.600	0.628	16	17.7	8.4	0.04	1.7	-7.6	120.763	6.293
430	40	445.73	42.50	1.32	1.26	0.056	0.560	0.616	16	18.2	4.2	0.09	2.2	-11.8	120.763	9.771
400	80	412.94	86.04	1.35	1.25	0.116	0.514	0.630	16	20.6	-2.5	0.18	4.6	-18.5	120.763	15.319
380	100	391.36	108.15	1.37	1.24	0.148	0.485	0.633	15	22.0	-5.5	0.23	7.0	-20.5	120.345	17.034
350	140	358.52	151.98	1.38	1.23	0.209	0.440	0.649	15	25.2	-7.5	0.32	10.2	-22.5	120.345	18.696
320	160	325.46	173.89	1.38	1.21	0.240	0.393	0.633	15	29.5	-8.1	0.38	14.5	-23.1	120.345	19.195
270	200	273.70	217.52	1.38	1.20	0.301	0.329	0.629	15	31.5	-8.5	0.48	16.5	-23.5	120.345	19.527
250	230	252.47	250.25	1.38	1.19	0.346	0.301	0.647	15	33.8	-8.7	0.53	18.8	-23.7	120.345	19.693
220	270	220.67	293.88	1.38	1.18	0.407	0.259	0.666	15	38.0	-8.9	0.61	23.0	-23.9	120.345	19.860
200	290	199.97	315.35	1.38	1.17	0.436	0.234	0.669	15	40.0	-8.4	0.65	25.0	-23.4	120.345	19.444
170	310	168.90	336.59	1.38	1.15	0.464	0.195	0.658	15	44.0	-7.6	0.70	29.0	-22.6	120.345	18.779
150	340	147.75	368.68	1.37	1.13	0.507	0.168	0.674	15	49.5	-6.9	0.75	34.5	-21.9	120.345	18.198
120	380	117.48	410.28	1.36	1.12	0.559	0.132	0.690	15	53.5	-4.6	0.81	38.5	-19.6	120.345	16.286
100	400	97.24	429.80	1.35	1.10	0.580	0.107	0.687	15	57.9	-2.0	0.84	42.9	-17.0	120.345	14.126
30	450	29.13	480.26	1.33	1.10	0.639	0.032	0.671	15	58.9	**1.7**	0.95	43.9	-13.3	120.345	11.052
0	500	0.00	525.74	1.29	1.13	0.679	0.000	0.679	15	49.5	**10.0**	1.00	34.5	-5.0	120.345	4.155
						Av. Mass Flow Rate		**0.011**	**kg/s**						$\mu_{isenmax}$ = (%)	**19.860**

Cone Angle =75^0, L = 20D, G=1, D=16 mm, P=6 Bar (g)

$Q_{read,h}$ (l/min)	$Q_{read,c}$ (l/min)	$Q_{act,h}$ (l/min)	$Q_{act,c}$ (l/min)	$\rho_{air,c}$ (kg/m^3)	$\rho_{air,h}$ (kg/m^3)	m_c (kg/min)	m_h (kg/min)	m_t (kg/min)	T_i (C^0)	T_h (C^0)	T_c (C^0)	μ_c	T_h-T_i (C^0)	T_i-T_c (C^0)	Δt_{isen} (C^0)	μ_{isen} (%)
500	0	513.21	0.00	1.29	1.23	0.000	0.632	0.632	17	24.0	9.4	0.00	7.0	-7.6	121.180	6.272
470	30	482.17	31.84	1.32	1.23	0.042	0.593	0.635	17	24.3	4.7	0.07	7.3	-12.3	121.180	10.150
430	70	440.99	75.41	1.36	1.23	0.102	0.542	0.644	17	24.5	-3.4	0.16	7.5	-20.4	121.180	16.834
400	110	410.02	118.77	1.36	1.23	0.162	0.503	0.665	17	24.8	-4.6	0.24	7.8	-21.6	121.180	17.825
370	140	378.19	151.61	1.37	1.22	0.208	0.462	0.669	17	26.5	-6.2	0.31	9.5	-23.2	121.180	19.145
350	170	356.44	184.17	1.37	1.21	0.253	0.432	0.684	17	28.7	-6.4	0.37	11.7	-23.4	121.180	19.310
270	210	272.81	227.71	1.37	1.19	0.313	0.325	0.638	17	33.5	-6.9	0.49	16.5	-23.9	121.180	19.723
250	250	249.60	271.14	1.37	1.16	0.373	0.291	0.663	17	40.9	-7.0	0.56	23.9	-24.0	121.180	19.805
200	300	197.62	324.75	1.37	1.14	0.445	0.225	0.670	17	47.5	-6.0	0.66	30.5	-23.0	121.180	18.980
170	320	167.35	346.08	1.37	1.13	0.473	0.189	0.662	17	49.9	-5.5	0.71	32.9	-22.5	121.180	18.567
140	370	137.06	398.67	1.36	1.12	0.541	0.153	0.694	17	53.5	-3.5	0.78	36.5	-20.5	121.180	16.917
120	400	116.94	429.56	1.35	1.11	0.579	0.130	0.709	17	56.5	-1.7	0.82	39.5	-18.7	121.180	15.432
100	420	97.01	449.55	1.34	1.10	0.602	0.107	0.708	17	59.5	0.1	0.85	42.5	-16.9	121.180	13.946
50	440	48.43	469.50	1.33	1.10	0.625	0.053	0.678	17	60.5	1.8	0.92	43.5	-15.2	121.180	12.543
0	500	0.00	525.19	1.29	1.14	0.677	0.000	0.677	17	48.8	10.6	1.00	31.8	-6.4	121.180	5.281
						Av. Mass Flow Rate		**0.011**	**kg/s**						$\mu_{isenmax}$ = (%)	**19.805**

APPENDIX D: EXPERIMENTAL DATA AND CALCULATIONS OF SECTION 5.4.4 "Insulation Effect"

D=16mm, L=15D , Cone Angle=40^0, G=1, P=6 Bar(g)

$Q_{read,h}$ (l/min)	$Q_{read,c}$ (l/min)	$Q_{act,\ h}$ (l/min)	$Q_{act,\ c}$ (l/min)	$\rho_{air,\ c}$ (kg/m^3)	$\rho_{air,\ h}$ (kg/m^3)	m_c (kg/min)	m_h (kg/min)	m_t (kg/min)	T_i (C^0)	T_h (C^0)	T_c (C^0)	μ_c	T_h-T_i (C^0)	T_i-T_c (C^0)	Δt_{isen} (C^0)	μ_{isen} (%)
460	0	478.639	0.000	1.289	1.265	0.000	0.606	0.606	15	16.0	10.6	0.00	1.0	-4.4	120.345	3.656
430	30	445.655	31.827	1.315	1.255	0.042	0.559	0.601	15	18.3	5.0	0.07	3.3	-10.0	120.345	8.309
390	60	403.025	64.046	1.331	1.248	0.085	0.503	0.588	15	20.0	1.6	0.14	5.0	-13.4	120.345	11.135
360	100	370.259	107.490	1.350	1.236	0.145	0.458	0.603	15	22.8	-2.2	0.24	7.8	-17.2	120.345	14.292
300	150	306.894	161.803	1.360	1.223	0.220	0.375	0.595	16	26.0	-4.1	0.37	10.0	-20.1	120.763	16.644
250	220	254.094	237.709	1.364	1.207	0.324	0.307	0.631	16	29.9	-5.0	0.51	13.9	-21.0	120.763	17.389
220	260	222.468	280.772	1.363	1.195	0.383	0.266	0.648	17	33.0	-4.7	0.59	16.0	-21.7	121.180	17.907
190	300	191.507	323.666	1.360	1.187	0.440	0.227	0.668	17	35.0	-4.2	0.66	18.0	-21.2	121.180	17.495
160	320	160.748	344.540	1.355	1.179	0.467	0.190	0.656	17	37.0	-3.1	0.71	20.0	-20.1	121.180	16.587
120	350	120.367	375.660	1.346	1.176	0.506	0.142	0.647	17	38.0	-1.4	0.78	21.0	-18.4	121.180	15.184
100	370	100.145	396.035	1.339	1.172	0.530	0.117	0.648	18	39.0	0.1	0.82	21.0	-17.9	121.598	14.721
50	400	49.953	426.510	1.328	1.166	0.567	0.058	0.625	18	40.5	2.2	0.91	22.5	-15.8	121.598	12.994
0	460	0.000	483.257	1.290	1.211	0.623	0.000	0.623	18	29.0	10.5	1.00	11.0	-7.5	121.598	6.168
						Av. Mass Flow Rate		**0.010**	**kg/s**						$\mu_{isenmax}$ = (%)	**17.907**

Insulated D=16mm, L=15D , Cone Angle=40^0, G=1, P=6 Bar(g)

$Q_{read,h}$ (l/min)	$Q_{read,c}$ (l/min)	$Q_{act,h}$ (l/min)	$Q_{act,c}$ (l/min)	$\rho_{air,c}$ (kg/m^3)	$\rho_{air,h}$ (kg/m^3)	m_c (kg/min)	m_h (kg/min)	m_t (kg/min)	T_i (C^0)	T_h (C^0)	T_c (C^0)	μ_c	T_h-T_i (C^0)	T_i-T_c (C^0)	Δt_{isen} (C^0)	μ_{isen} (%)
460	0	472.152	0.000	1.296	1.231	0.000	0.581	0.581	19	24.0	9.0	0.00	5.0	-10.0	122.016	8.196
430	30	440.545	31.741	1.308	1.226	0.042	0.540	0.582	19	25.1	6.5	0.07	6.1	-12.5	122.016	10.245
400	60	409.192	63.884	1.325	1.223	0.085	0.500	0.585	19	26.0	3.0	0.14	7.0	-16.0	122.016	13.113
360	100	367.353	107.056	1.339	1.217	0.143	0.447	0.590	19	27.5	0.0	0.24	8.5	-19.0	122.016	15.572
340	120	345.911	128.940	1.349	1.209	0.174	0.418	0.592	19	29.3	-2.0	0.29	10.3	-21.0	122.016	17.211
300	160	304.361	172.366	1.356	1.203	0.234	0.366	0.600	19	31.0	-3.4	0.39	12.0	-22.4	122.016	18.358
250	200	252.024	215.898	1.362	1.187	0.294	0.299	0.593	19	34.9	-4.5	0.50	15.9	-23.5	122.016	19.260
200	260	200.612	280.720	1.362	1.176	0.382	0.236	0.618	19	38.0	-4.6	0.62	19.0	-23.6	122.016	19.342
170	290	169.704	312.587	1.358	1.164	0.424	0.198	0.622	19	41.0	-3.7	0.68	22.0	-22.7	122.016	18.604
140	310	139.314	333.588	1.353	1.157	0.451	0.161	0.613	19	43.0	-2.8	0.74	24.0	-21.8	122.016	17.867
120	330	119.036	353.934	1.344	1.150	0.476	0.137	0.613	19	45.0	-1.0	0.78	26.0	-20.0	122.016	16.391
100	360	99.041	385.402	1.339	1.146	0.516	0.114	0.630	19	46.0	0.0	0.82	27.0	-19.0	122.016	15.572
80	380	79.109	405.849	1.333	1.143	0.541	0.090	0.631	19	47.0	1.3	0.86	28.0	-17.7	122.016	14.506
40	410	39.598	436.145	1.322	1.145	0.577	0.045	0.622	19	46.3	3.5	0.93	27.3	-15.5	122.016	12.703
0	470	0.000	493.763	1.290	1.179	0.637	0.000	0.637	19	37.0	10.5	1.00	18.0	-8.5	122.016	6.966
						Av. Mass Flow Rate		**0.010**	**kg/s**						$\mu_{isenmax}$ = (%)	**19.342**

APPENDIX E: EXPERIMENTAL DATA AND CALCULATIONS OF SECTION 5.4.5 "Material of the Hot Tube"

ALUMINUM PIPE D=19 mm, L = 15D , Cone Angle=40^0, G=1, P=6 Bar (g)

$Q_{read,h}$ (l/min)	$Q_{read,c}$ (l/min)	$Q_{act,h}$ (l/min)	$Q_{act,c}$ (l/min)	$\rho_{air,c}$ (kg/m^3)	$\rho_{air,h}$ (kg/m^3)	m_c (kg/min)	m_h (kg/min)	m_t (kg/min)	T_i (C^0)	T_h (C^0)	T_c (C^0)	μ_c	T_h-T_i (C^0)	T_i-T_c (C^0)	Δt_{isen} (C^0)	μ_{isen} (%)
500	0	515.382	0.000	1.292	1.241	0.000	0.640	0.640	18	21.5	10.0	0.00	3.5	-8.0	121.598	6.579
450	50	462.667	53.237	1.325	1.235	0.071	0.571	0.642	18	23.0	3.0	0.11	5.0	-15.0	121.598	12.336
420	80	431.095	85.723	1.342	1.231	0.115	0.531	0.646	18	24.0	-0.5	0.18	6.0	-18.5	121.598	15.214
400	100	409.878	107.272	1.345	1.227	0.144	0.503	0.647	18	25.0	-1.1	0.22	7.0	-19.1	121.598	15.707
350	150	358.043	160.437	1.337	1.223	0.214	0.438	0.652	18	26.0	0.5	0.33	8.0	-17.5	121.598	14.392
320	180	326.808	191.999	1.329	1.219	0.255	0.398	0.654	18	27.0	2.0	0.39	9.0	-16.0	121.598	13.158
250	250	254.472	266.569	1.328	1.211	0.354	0.308	0.662	18	29.0	2.2	0.53	11.0	-15.8	121.598	12.994
200	300	202.575	319.709	1.327	1.199	0.424	0.243	0.667	18	32.0	2.5	0.64	14.0	-15.5	121.598	12.747
160	340	161.795	362.008	1.325	1.195	0.480	0.193	0.673	18	33.0	3.0	0.71	15.0	-15.0	121.598	12.336
120	380	121.089	403.503	1.317	1.190	0.532	0.144	0.676	18	34.3	4.5	0.79	16.3	-13.5	121.598	11.102
50	450	50.356	475.272	1.303	1.185	0.619	0.060	0.679	18	35.5	7.5	0.91	17.5	-10.5	121.598	8.635
0	500	0.000	524.817	1.287	1.199	0.676	0.000	0.676	18	32.0	11.0	1.00	14.0	-7.0	121.598	5.757
						Av. Mass Flow Rate		**0.011**	**kg/s**						$\mu_{isenmax}$ = (%)	**15.707**

STEEL PIPE D=19 mm, L = 15D , Cone Angle=40^0, G=1, P=6 Bar (g)

$Q_{read,h}$ (l/min)	$Q_{read,c}$ (l/min)	$Q_{act,h}$ (l/min)	$Q_{act,c}$ (l/min)	$\rho_{air,c}$ (kg/m^3)	$\rho_{air,h}$ (kg/m^3)	m_c (kg/min)	m_h (kg/min)	m_t (kg/min)	T_i (C^0)	T_h (C^0)	T_c (C^0)	μ_c	T_h-T_i (C^0)	T_i-T_c (C^0)	Δt_{isen} (C^0)	μ_{isen} (%)
500	0	514.335	0.000	1.296	1.236	0.000	0.636	0.636	18	22.7	9.0	0.00	4.7	-9.0	121.598	7.401
450	50	462.511	52.997	1.313	1.234	0.070	0.571	0.640	18	23.2	5.5	0.11	5.2	-12.5	121.598	10.280
420	80	431.095	85.567	1.337	1.231	0.114	0.531	0.645	18	24.0	0.5	0.18	6.0	-17.5	121.598	14.392
400	100	409.878	107.213	1.343	1.227	0.144	0.503	0.647	18	25.0	-0.8	0.22	7.0	-18.8	121.598	15.461
370	130	378.756	139.557	1.347	1.224	0.188	0.464	0.652	18	25.6	-1.5	0.29	7.6	-19.5	121.598	16.036
350	150	357.506	161.324	1.352	1.219	0.218	0.436	0.654	18	26.9	-2.5	0.33	8.9	-20.5	121.598	16.859
320	180	326.536	192.807	1.341	1.217	0.258	0.397	0.656	18	27.5	-0.3	0.39	9.5	-18.3	121.598	15.050
300	200	305.367	214.112	1.339	1.211	0.287	0.370	0.656	18	29.0	0.0	0.44	11.0	-18.0	121.598	14.803
250	240	253.843	256.232	1.332	1.205	0.341	0.306	0.647	18	30.5	1.5	0.53	12.5	-16.5	121.598	13.569
200	280	202.575	298.829	1.331	1.199	0.398	0.243	0.641	18	32.0	1.7	0.62	14.0	-16.3	121.598	13.405
150	350	150.823	372.656	1.325	1.181	0.494	0.178	0.672	18	36.5	3.0	0.73	18.5	-15.0	121.598	12.336
120	390	120.464	414.645	1.321	1.177	0.548	0.142	0.690	18	37.5	3.8	0.79	19.5	-14.2	121.598	11.678
100	410	100.065	434.577	1.313	1.170	0.570	0.117	0.688	18	39.5	5.5	0.83	21.5	-12.5	121.598	10.280
0	500	0.000	526.674	1.296	1.199	0.683	0.000	0.683	18	32.0	9.0	1.00	14.0	-9.0	121.598	7.401
						Av. Mass Flow Rate		**0.011**	**kg/s**						$\mu_{isenmax}$ = (%)	**16.859**

APPENDIX F: EXPERIMENTAL DATA AND CALCULATIONS OF SECTION 5.4.6 "Cold Orifice Ratio"

D=19 mm (d/D=0.418), L = 20D, Cone Angle=40^0, G=1, P=6 Bar (g)

$Q_{read,h}$ (l/min)	$Q_{read,c}$ (l/min)	$Q_{act,h}$ (l/min)	$Q_{act,c}$ (l/min)	$\rho_{air,c}$ (kg/m^3)	$\rho_{air,h}$ (kg/m^3)	m_c (kg/min)	m_h (kg/min)	m_t (kg/min)	T_i (C^0)	T_h (C^0)	T_c (C^0)	μ_c	T_h-T_i (C^0)	T_i-T_c (C^0)	Δt_{isen} (C^0)	μ_{isen} (%)
500	0	514.945	0.000	1.288	1.239	0.000	0.638	0.638	18	22.0	10.8	0.000	4.0	-7.2	121.598	5.921
450	50	463.058	53.045	1.315	1.237	0.070	0.573	0.643	18	22.5	5.0	0.109	4.5	-13.0	121.598	10.691
420	80	431.459	85.489	1.334	1.233	0.114	0.532	0.646	18	23.5	1.0	0.177	5.5	-17.0	121.598	13.980
400	100	410.429	107.371	1.347	1.230	0.145	0.505	0.650	18	24.2	-1.6	0.223	6.2	-19.6	121.598	16.119
380	120	389.188	129.322	1.357	1.226	0.175	0.477	0.652	18	25.3	-3.6	0.269	7.3	-21.6	121.598	17.763
340	180	347.118	193.732	1.354	1.218	0.262	0.423	0.685	18	27.2	-2.9	0.383	9.2	-20.9	121.598	17.188
180	300	181.723	321.581	1.343	1.191	0.432	0.216	0.648	18	34.0	-0.7	0.666	16.0	-18.7	121.598	15.379
150	350	150.945	374.696	1.339	1.183	0.502	0.179	0.680	18	36.0	0.0	0.737	18.0	-18.0	121.598	14.803
130	370	130.398	395.529	1.335	1.176	0.528	0.153	0.681	18	38.0	0.8	0.775	20.0	-17.2	121.598	14.145
100	400	100.226	426.665	1.329	1.174	0.567	0.118	0.685	18	38.5	2.0	0.828	20.5	-16.0	121.598	13.158
50	450	50.438	475.696	1.306	1.189	0.621	0.060	0.681	18	34.5	7.0	0.912	16.5	-11.0	121.598	9.046
						Av. Mass Flow Rate		**0.011**	**kg/s**						$\mu_{isenmax}$ = (%)	**17.763**

***D=16 mm (d/D=0.496)*, L = 20D, Cone Angle=40^0, G=1, P=6 Bar (g)**

$Q_{read,h}$ (l/min)	$Q_{read,c}$ (l/min)	$Q_{act,h}$ (l/min)	$Q_{act,c}$ (l/min)	$\rho_{air,c}$ (kg/m^3)	$\rho_{air,h}$ (kg/m^3)	m_c (kg/min)	m_h (kg/min)	m_t (kg/min)	T_i (C^0)	T_h (C^0)	T_c (C^0)	μ_c	T_h-T_i (C^0)	T_i-T_c (C^0)	Δt_{isen} (C^0)	μ_{isen} (%)
500	0	514.945	0.000	1.307	1.239	0.000	0.638	0.638	17	22.0	6.8	0.000	5.0	-10.2	121.180	8.417
460	30	473.589	31.925	1.323	1.238	0.042	0.587	0.629	17	22.2	3.3	0.067	5.2	-13.7	121.180	11.305
450	50	462.823	53.518	1.339	1.236	0.072	0.572	0.644	18	22.8	0.1	0.111	4.8	-17.9	121.598	14.721
410	80	420.478	85.992	1.350	1.229	0.116	0.517	0.633	18	24.5	-2.2	0.183	6.5	-20.2	121.598	16.612
370	120	378.187	129.611	1.363	1.221	0.177	0.462	0.638	18	26.5	-4.8	0.277	8.5	-22.8	121.598	18.750
350	140	356.734	151.496	1.368	1.214	0.207	0.433	0.640	18	28.2	-5.8	0.324	10.2	-23.8	121.598	19.573
320	170	324.919	184.097	1.370	1.205	0.252	0.391	0.644	18	30.5	-6.2	0.392	12.5	-24.2	121.598	19.902
270	200	272.673	216.463	1.369	1.192	0.296	0.325	0.621	18	33.8	-5.9	0.477	15.8	-23.9	121.598	19.655
220	240	221.207	259.319	1.364	1.181	0.354	0.261	0.615	18	36.5	-5.0	0.575	18.5	-23.0	121.598	18.915
170	300	170.029	323.907	1.362	1.169	0.441	0.199	0.640	18	39.8	-4.6	0.689	21.8	-22.6	121.598	18.586
150	320	149.620	344.349	1.353	1.163	0.466	0.174	0.640	18	41.5	-2.8	0.728	23.5	-20.8	121.598	17.106
120	340	119.317	364.726	1.345	1.155	0.490	0.138	0.628	18	43.5	-1.1	0.781	25.5	-19.1	121.598	15.707
100	360	99.056	385.614	1.341	1.146	0.517	0.114	0.631	18	45.9	-0.3	0.820	27.9	-18.3	121.598	15.050
50	400	49.637	426.278	1.327	1.152	0.566	0.057	0.623	18	44.5	2.5	0.908	26.5	-15.5	121.598	12.747
0	440	0.000	462.246	1.290	1.187	0.596	0.000	0.596	18	35.0	10.5	1.000	17.0	-7.5	121.598	6.168
						Av. Mass Flow Rate		**0.011**	**kg/s**						$\mu_{isenmax}$ = (%)	**19.902**

***D=12 mm (d/D=0.661)*, L = 20D, Cone Angle=40^0, G=1, P=6 Bar (g)**

$Q_{read,h}$ (l/min)	$Q_{read,c}$ (l/min)	$Q_{act,h}$ (l/min)	$Q_{act,c}$ (l/min)	$\rho_{air,c}$ (kg/m^3)	$\rho_{air,h}$ (kg/m^3)	m_c (kg/min)	m_h (kg/min)	m_t (kg/min)	T_i (C^0)	T_h (C^0)	T_c (C^0)	μ_c	T_h-T_i (C^0)	T_i-T_c (C^0)	Δt_{isen} (C^0)	μ_{isen} (%)
430	0	444.361	0.000	1.296	1.248	0.000	0.554	0.554	17	20.0	9.2	0.000	3.0	-7.8	121.180	6.437
400	30	413.007	31.600	1.296	1.246	0.041	0.514	0.555	17	20.5	9.0	0.074	3.5	-8.0	121.180	6.602
360	70	370.886	74.236	1.314	1.240	0.098	0.460	0.558	17	21.8	5.2	0.175	4.8	-11.8	121.180	9.738
330	100	338.946	106.570	1.327	1.233	0.141	0.418	0.559	17	23.6	2.5	0.253	6.6	-14.5	121.180	11.966
300	130	307.409	138.919	1.334	1.227	0.185	0.377	0.563	17	25.0	1.0	0.330	8.0	-16.0	121.180	13.203
270	160	275.974	171.321	1.340	1.221	0.230	0.337	0.566	17	26.5	-0.1	0.405	9.5	-17.1	121.180	14.111
250	180	254.472	193.055	1.344	1.211	0.259	0.308	0.568	17	29.0	-1.0	0.457	12.0	-18.0	121.180	14.854
190	230	192.289	246.908	1.347	1.197	0.332	0.230	0.563	17	32.5	-1.5	0.591	15.5	-18.5	121.180	15.266
160	250	161.531	268.230	1.345	1.191	0.361	0.192	0.553	17	34.0	-1.2	0.652	17.0	-18.2	121.180	15.019
140	280	140.996	300.142	1.343	1.185	0.403	0.167	0.570	17	35.5	-0.7	0.707	18.5	-17.7	121.180	14.606
120	310	120.658	331.935	1.340	1.181	0.445	0.143	0.587	17	36.5	-0.1	0.757	19.5	-17.1	121.180	14.111
100	330	100.387	352.640	1.334	1.177	0.471	0.118	0.589	17	37.5	1.0	0.799	20.5	-16.0	121.180	13.203
50	370	50.169	394.307	1.327	1.176	0.523	0.059	0.582	17	37.8	2.5	0.899	20.8	-14.5	121.180	11.966
0	420	0.000	443.350	1.302	1.197	0.577	0.000	0.577	17	32.5	7.8	1.000	15.5	-9.2	121.180	7.592
						Av. Mass Flow Rate		**0.009**	**kg/s**						$\mu_{isenmax}$ = (%)	**15.266**

APPENDIX G: EXPERIMENTAL DATA AND CALCULATIONS OF SECTION 5.4.7 "Inlet Pressure"

***P=2 Bar(g)*, L=20D , Cone Angle=40^0, D=19mm, G=1**

$Q_{read,h}$ (l/min)	$Q_{read,c}$ (l/min)	$Q_{act,h}$ (l/min)	$Q_{act,c}$ (l/min)	$\rho_{air,c}$ (kg/m^3)	$\rho_{air,h}$ (kg/m^3)	m_c (kg/min)	m_h (kg/min)	m_t (kg/min)	T_i (C^0)	T_h (C^0)	T_c (C^0)	μ_c	T_h-T_i (C^0)	T_i-T_c (C^0)	Δt_{isen} (C^0)	μ_{isen} (%)
200	0	206.22	0.00	1.291	1.242	0.000	0.256	0.256	17	21.3	10.1	0.00	4.3	-6.9	75.029	9.196
180	20	185.54	21.03	1.292	1.241	0.027	0.230	0.258	17	21.5	10.0	0.11	4.5	-7.0	75.029	9.330
160	40	164.87	42.13	1.296	1.241	0.055	0.205	0.259	17	21.7	9.0	0.21	4.7	-8.0	75.029	10.662
140	60	144.14	63.31	1.301	1.238	0.082	0.179	0.261	17	22.2	8.0	0.32	5.2	-9.0	75.029	11.995
120	80	123.42	84.43	1.302	1.236	0.110	0.153	0.262	17	22.8	7.9	0.42	5.8	-9.1	75.029	12.129
100	100	102.78	105.58	1.302	1.234	0.138	0.127	0.264	17	23.2	7.7	0.52	6.2	-9.3	75.029	12.395
50	150	51.36	158.31	1.302	1.233	0.206	0.063	0.269	17	23.6	7.9	0.76	6.6	-9.1	75.029	12.129
0	200	0.00	210.48	1.294	1.235	0.272	0.000	0.272	17	23.0	9.5	1.00	6.0	-7.5	75.029	9.996
						Av. Mass Flow Rate		**0.004**	**kg/s**						$\mu_{isenmax}$ = (%)	**12.395**

***P=3 Bar(g)*, L=20D , Cone Angle=40^0, D=19mm, G=1**

$Q_{read,h}$ (l/min)	$Q_{read,c}$ (l/min)	$Q_{act,h}$ (l/min)	$Q_{act,c}$ (l/min)	$\rho_{air,c}$ (kg/m^3)	$\rho_{air,h}$ (kg/m^3)	m_c (kg/min)	m_h (kg/min)	m_t (kg/min)	T_i (C^0)	T_h (C^0)	T_c (C^0)	μ_c	T_h-T_i (C^0)	T_i-T_c (C^0)	Δt_{isen} (C^0)	μ_{isen} (%)
300	0	309.75	0.00	1.290	1.246	0.000	0.386	0.386	17	20.5	10.5	0.00	3.5	-6.5	91.963	7.068
280	20	289.06	21.03	1.291	1.245	0.027	0.360	0.387	17	20.6	10.1	0.07	3.6	-6.9	91.963	7.503
260	40	268.23	42.22	1.302	1.244	0.055	0.334	0.389	17	21.0	7.8	0.14	4.0	-9.2	91.963	10.004
240	60	247.34	63.46	1.307	1.241	0.083	0.307	0.390	17	21.6	6.7	0.21	4.6	-10.3	91.963	11.200
220	80	226.50	84.87	1.315	1.238	0.112	0.281	0.392	17	22.2	5.0	0.28	5.2	-12.0	91.963	13.049
180	120	184.82	127.54	1.320	1.232	0.168	0.228	0.396	17	23.8	4.0	0.43	6.8	-13.0	91.963	14.136
160	140	164.01	148.82	1.320	1.228	0.196	0.201	0.398	17	24.8	3.9	0.49	7.8	-13.1	91.963	14.245
140	160	143.34	170.14	1.321	1.225	0.225	0.176	0.400	17	25.5	3.7	0.56	8.5	-13.3	91.963	14.462
120	180	122.57	191.44	1.322	1.219	0.253	0.149	0.402	17	26.9	3.6	0.63	9.9	-13.4	91.963	14.571
100	200	101.96	212.48	1.319	1.215	0.280	0.124	0.404	17	28.0	4.2	0.69	11.0	-12.8	91.963	13.919
30	230	30.62	243.79	1.313	1.217	0.320	0.037	0.357	17	27.3	5.5	0.90	10.3	-11.5	91.963	12.505
0	260	0.00	273.63	1.294	1.231	0.354	0.000	0.354	17	24.0	9.5	1.00	7.0	-7.5	91.963	8.155
						Av. Mass Flow Rate		**0.006**	**kg/s**						$\mu_{isenmax}$ = (%)	**14.571**

***P=4 Bar(g)*, L=20D , Cone Angle=40^0, D=19mm, G=1**

$Q_{read,h}$ (l/min)	$Q_{read,c}$ (l/min)	$Q_{act,h}$ (l/min)	$Q_{act,c}$ (l/min)	$\rho_{air,c}$ (kg/m^3)	$\rho_{air,h}$ (kg/m^3)	m_c (kg/min)	m_h (kg/min)	m_t (kg/min)	T_i (C^0)	T_h (C^0)	T_c (C^0)	μ_c	T_h-T_i (C^0)	T_i-T_c (C^0)	Δt_{isen} (C^0)	μ_{isen} (%)
350	0	359.85	0.00	1.297	1.235	0.000	0.444	0.444	17	23.0	8.9	0.00	6.0	-8.1	104.175	7.775
320	30	328.67	31.81	1.314	1.233	0.042	0.405	0.447	17	23.6	5.3	0.09	6.6	-11.7	104.175	11.231
300	50	307.82	53.20	1.323	1.230	0.070	0.379	0.449	17	24.2	3.4	0.16	7.2	-13.6	104.175	13.055
270	80	276.53	85.43	1.332	1.226	0.114	0.339	0.453	17	25.3	1.4	0.25	8.3	-15.6	104.175	14.975
250	100	255.66	106.94	1.336	1.222	0.143	0.312	0.455	17	26.2	0.6	0.31	9.2	-16.4	104.175	15.743
220	130	224.38	139.10	1.338	1.215	0.186	0.273	0.459	17	27.8	0.3	0.41	10.8	-16.7	104.175	16.031
200	150	203.58	160.58	1.339	1.211	0.215	0.246	0.462	17	29.0	0.0	0.47	12.0	-17.0	104.175	16.319
180	180	182.95	192.70	1.339	1.207	0.258	0.221	0.479	17	29.9	0.0	0.54	12.9	-17.0	104.175	16.319
150	200	151.98	214.35	1.342	1.200	0.288	0.182	0.470	17	31.8	-0.6	0.61	14.8	-17.6	104.175	16.895
100	250	101.12	267.35	1.336	1.195	0.357	0.121	0.478	17	33.0	0.6	0.75	16.0	-16.4	104.175	15.743
40	300	40.53	319.13	1.322	1.200	0.422	0.049	0.471	17	31.8	3.5	0.90	14.8	-13.5	104.175	12.959
0	330	0.00	347.60	1.296	1.215	0.451	0.000	0.451	17	28.0	9.0	1.00	11.0	-8.0	104.175	7.679
						Av. Mass Flow Rate		**0.008**	**kg/s**						$\mu_{isenmax}$ = (%)	**16.895**

***P=5 Bar(g)*, L=20D , Cone Angle=40^0, D=19mm, G=1**

$Q_{read,h}$ (l/min)	$Q_{read,c}$ (l/min)	$Q_{act,h}$ (l/min)	$Q_{act,c}$ (l/min)	$\rho_{air,c}$ (kg/m^3)	$\rho_{air,h}$ (kg/m^3)	m_c (kg/min)	m_h (kg/min)	m_t (kg/min)	T_i (C^0)	T_h (C^0)	T_c (C^0)	μ_c	T_h-T_i (C^0)	T_i-T_c (C^0)	Δt_{isen} (C^0)	μ_{isen} (%)
420	0	432.55	0.00	1.304	1.239	0.000	0.536	0.536	17	22.0	7.3	0.00	5.0	-9.7	113.592	8.539
380	30	390.76	31.90	1.321	1.236	0.042	0.483	0.525	17	22.9	3.8	0.08	5.9	-13.2	113.592	11.621
350	60	359.25	64.20	1.338	1.231	0.086	0.442	0.528	17	24.0	0.3	0.16	7.0	-16.7	113.592	14.702
320	90	327.74	96.60	1.346	1.226	0.130	0.402	0.532	17	25.3	-1.4	0.24	8.3	-18.4	113.592	16.198
300	120	306.64	129.08	1.352	1.221	0.175	0.374	0.549	17	26.5	-2.6	0.32	9.5	-19.6	113.592	17.255
260	150	265.09	161.50	1.355	1.215	0.219	0.322	0.541	17	28.0	-3.1	0.40	11.0	-20.1	113.592	17.695
220	190	223.35	204.53	1.354	1.204	0.277	0.269	0.546	17	30.6	-3.0	0.51	13.6	-20.0	113.592	17.607
160	230	161.93	247.50	1.353	1.197	0.335	0.194	0.529	17	32.5	-2.8	0.63	15.5	-19.8	113.592	17.431
140	250	141.39	268.58	1.349	1.192	0.362	0.168	0.531	17	33.8	-1.9	0.68	16.8	-18.9	113.592	16.639
120	280	120.89	300.36	1.345	1.186	0.404	0.143	0.547	17	35.3	-1.1	0.74	18.3	-18.1	113.592	15.934
100	300	100.50	321.34	1.341	1.180	0.431	0.119	0.549	17	36.8	-0.3	0.78	19.8	-17.3	113.592	15.230
40	330	40.03	351.81	1.328	1.170	0.467	0.047	0.514	17	39.5	2.3	0.91	22.5	-14.7	113.592	12.941
0	390	0.00	410.30	1.293	1.205	0.531	0.000	0.531	17	30.5	9.7	1.00	13.5	-7.3	113.592	6.427
						Av. Mass Flow Rate		**0.009**	**kg/s**						$\mu_{isenmax}$ = (%)	**17.695**

***P=6 Bar(g)*, L=20D , Cone Angle=40^0, D=19mm, G=1**

$Q_{read,h}$ (l/min)	$Q_{read,c}$ (l/min)	$Q_{act,h}$ (l/min)	$Q_{act,c}$ (l/min)	$\rho_{air,c}$ (kg/m^3)	$\rho_{air,h}$ (kg/m^3)	m_c (kg/min)	m_h (kg/min)	m_t (kg/min)	T_i (C^0)	T_h (C^0)	T_c (C^0)	μ_c	T_h-T_i (C^0)	T_i-T_c (C^0)	Δt_{isen} (C^0)	μ_{isen} (%)
500	0	514.94	0.00	1.307	1.239	0.000	0.638	0.638	17	22.0	6.8	0.00	5.0	-10.2	121.180	8.417
460	30	473.59	31.92	1.323	1.238	0.042	0.587	0.629	17	22.2	3.3	0.07	5.2	-13.7	121.180	11.305
450	50	462.82	53.52	1.339	1.236	0.072	0.572	0.644	18	22.8	0.1	0.11	4.8	-17.9	121.598	14.721
410	80	420.48	85.99	1.350	1.229	0.116	0.517	0.633	18	24.5	-2.2	0.18	6.5	-20.2	121.598	16.612
370	120	378.19	129.61	1.363	1.221	0.177	0.462	0.638	18	26.5	-4.8	0.28	8.5	-22.8	121.598	18.750
350	140	356.73	151.50	1.368	1.214	0.207	0.433	0.640	18	28.2	-5.8	0.32	10.2	-23.8	121.598	19.573
320	170	324.92	184.10	1.370	1.205	0.252	0.391	0.644	18	30.5	-6.2	0.39	12.5	-24.2	121.598	19.902
270	200	272.67	216.46	1.369	1.192	0.296	0.325	0.621	18	33.8	-5.9	0.48	15.8	-23.9	121.598	19.655
220	240	221.21	259.32	1.364	1.181	0.354	0.261	0.615	18	36.5	-5.0	0.58	18.5	-23.0	121.598	18.915
170	300	170.03	323.91	1.362	1.169	0.441	0.199	0.640	18	39.8	-4.6	0.69	21.8	-22.6	121.598	18.586
150	320	149.62	344.35	1.353	1.163	0.466	0.174	0.640	18	41.5	-2.8	0.73	23.5	-20.8	121.598	17.106
120	340	119.32	364.73	1.345	1.155	0.490	0.138	0.628	18	43.5	-1.1	0.78	25.5	-19.1	121.598	15.707
100	360	99.06	385.61	1.341	1.146	0.517	0.114	0.631	18	45.9	-0.3	0.82	27.9	-18.3	121.598	15.050
50	400	49.64	426.28	1.327	1.152	0.566	0.057	0.623	18	44.5	2.5	0.91	26.5	-15.5	121.598	12.747
0	440	0.00	462.25	1.290	1.187	0.596	0.000	0.596	18	35.0	10.5	1.00	17.0	-7.5	121.598	6.168
						Av. Mass Flow Rate		**0.011**	**kg/s**						$\mu_{isenmax}$ = (%)	**19.902**

***P=7 Bar(g)*, L=20D , Cone Angle=40^0, D=19mm, G=1**

$Q_{read,h}$ (l/min)	$Q_{read,c}$ (l/min)	$Q_{act,h}$ (l/min)	$Q_{act,c}$ (l/min)	$\rho_{air,c}$ (kg/m^3)	$\rho_{air,h}$ (kg/m^3)	m_c (kg/min)	m_h (kg/min)	m_t (kg/min)	T_i (C^0)	T_h (C^0)	T_c (C^0)	μ_c	T_h-T_i (C^0)	T_i-T_c (C^0)	Δt_{isen} (C^0)	μ_{isen} (%)
560	0	577.23	0.00	1.309	1.241	0.000	0.717	0.717	18	21.5	6.3	0.00	3.5	-11.7	127.929	9.146
530	30	545.47	31.90	1.321	1.238	0.042	0.675	0.717	18	22.4	3.8	0.06	4.4	-14.2	127.929	11.100
500	50	513.81	53.53	1.339	1.234	0.072	0.634	0.706	18	23.3	0.0	0.10	5.3	-18.0	127.929	14.070
470	70	480.80	75.56	1.362	1.223	0.103	0.588	0.691	18	26.0	-4.5	0.15	8.0	-22.5	127.929	17.588
430	100	438.06	108.60	1.378	1.213	0.150	0.531	0.681	18	28.5	-7.7	0.22	10.5	-25.7	127.929	20.089
380	160	385.84	174.02	1.382	1.205	0.241	0.465	0.705	18	30.5	-8.5	0.34	12.5	-26.5	127.929	20.715
350	190	353.64	206.53	1.381	1.193	0.285	0.422	0.707	18	33.5	-8.2	0.40	15.5	-26.2	127.929	20.480
300	260	298.15	281.93	1.374	1.154	0.387	0.344	0.731	18	43.8	-6.9	0.53	25.8	-24.9	127.929	19.464
200	350	196.28	379.38	1.373	1.125	0.521	0.221	0.742	19	51.9	-6.7	0.70	32.9	-25.7	128.369	20.020
160	400	156.88	430.36	1.353	1.123	0.582	0.176	0.758	19	52.5	-2.7	0.77	33.5	-21.7	128.369	16.904
120	430	117.33	461.19	1.344	1.117	0.620	0.131	0.751	19	54.3	-1.0	0.83	35.3	-20.0	128.369	15.580
100	450	97.38	481.49	1.338	1.108	0.644	0.108	0.752	19	57.0	0.3	0.86	38.0	-18.7	128.369	14.567
50	510	48.87	543.50	1.327	1.116	0.721	0.055	0.776	19	54.5	2.5	0.93	35.5	-16.5	128.369	12.854
0	560	0.00	587.80	1.287	1.153	0.757	0.000	0.757	19	44.0	11.0	1.00	25.0	-8.0	128.369	6.232
						Av. Mass Flow Rate		**0.012**	**kg/s**						$\mu_{isenmax}$ = (%)	**20.715**

***P=8 Bar(g)*, L=20D , Cone Angle=40^0, D=19mm, G=1**

$Q_{read,h}$ (l/min)	$Q_{read,c}$ (l/min)	$Q_{act,h}$ (l/min)	$Q_{act,c}$ (l/min)	$\rho_{air,c}$ (kg/m^3)	$\rho_{air,h}$ (kg/m^3)	m_c (kg/min)	m_h (kg/min)	m_t (kg/min)	T_i (C^0)	T_h (C^0)	T_c (C^0)	μ_c	T_h-T_i (C^0)	T_i-T_c (C^0)	Δt_{isen} (C^0)	μ_{isen} (%)
620	0	638.21	0.00	1.302	1.238	0.000	0.790	0.790	19	22.3	7.8	0.00	3.3	-11.2	133.775	8.372
580	35	595.62	37.23	1.322	1.232	0.049	0.734	0.783	19	23.7	3.5	0.06	4.7	-15.5	133.775	11.587
540	70	553.24	75.26	1.351	1.226	0.102	0.679	0.780	19	25.1	-2.3	0.13	6.1	-21.3	133.775	15.922
500	110	510.72	119.01	1.368	1.219	0.163	0.623	0.785	19	26.9	-5.7	0.21	7.9	-24.7	133.775	18.464
470	150	478.25	163.24	1.384	1.210	0.226	0.579	0.804	19	29.2	-8.8	0.28	10.2	-27.8	133.775	20.781
420	190	425.06	207.04	1.387	1.197	0.287	0.509	0.796	19	32.5	-9.5	0.36	13.5	-28.5	133.775	21.304
380	240	383.01	261.52	1.387	1.187	0.363	0.455	0.817	19	35.0	-9.5	0.44	16.0	-28.5	133.775	21.304
360	280	361.10	305.05	1.387	1.176	0.423	0.425	0.848	19	38.0	-9.4	0.50	19.0	-28.4	133.775	21.230
330	300	329.95	326.41	1.383	1.168	0.451	0.385	0.837	19	40.0	-8.7	0.54	21.0	-27.7	133.775	20.706
300	320	299.00	347.32	1.376	1.161	0.478	0.347	0.825	19	42.0	-7.4	0.58	23.0	-26.4	133.775	19.735
250	370	247.60	401.13	1.373	1.146	0.551	0.284	0.835	19	46.0	-6.8	0.66	27.0	-25.8	133.775	19.286
220	400	216.94	432.84	1.368	1.136	0.592	0.246	0.839	19	48.8	-5.8	0.71	29.8	-24.8	133.775	18.539
180	440	176.78	473.92	1.356	1.127	0.642	0.199	0.842	19	51.4	-3.3	0.76	32.4	-22.3	133.775	16.670
140	480	137.06	514.81	1.344	1.120	0.692	0.153	0.845	19	53.5	-1.0	0.82	34.5	-20.0	133.775	14.950
100	520	97.60	556.69	1.339	1.113	0.745	0.109	0.854	19	55.5	0.0	0.87	36.5	-19.0	133.775	14.203
50	570	48.69	606.90	1.325	1.108	0.804	0.054	0.858	20	57.0	3.0	0.94	37.0	-17.0	134.233	12.665
0	620	0.00	651.92	1.292	1.141	0.842	0.000	0.842	20	47.5	10.0	1.00	27.5	-10.0	134.233	7.450
						Av. Mass Flow Rate		**0.014**	**kg/s**						**$\mu_{isenmax}$ = (%)**	**21.304**

***P=9 Bar(g)*, L=20D , Cone Angle=40^0, D=19mm, G=1**

$Q_{read,h}$ (l/min)	$Q_{read,c}$ (l/min)	$Q_{act,h}$ (l/min)	$Q_{act,c}$ (l/min)	$\rho_{air,c}$ (kg/m^3)	$\rho_{air,h}$ (kg/m^3)	m_c (kg/min)	m_h (kg/min)	m_t (kg/min)	T_i (C^0)	T_h (C^0)	T_c (C^0)	μ_c	T_h-T_i (C^0)	T_i-T_c (C^0)	Δt_{isen} (C^0)	μ_{isen} (%)
650	0	674.59	0.00	1.284	1.259	0.000	0.849	0.849	17	17.5	11.8	0.00	0.5	-5.2	137.512	3.781
620	30	639.83	31.71	1.306	1.244	0.041	0.796	0.838	18	20.8	7.0	0.05	2.8	-11.0	137.986	7.972
560	70	573.83	75.10	1.345	1.227	0.101	0.704	0.805	19	25.0	-1.2	0.13	6.0	-20.2	138.460	14.589
500	130	507.27	140.78	1.370	1.203	0.193	0.610	0.803	20	31.0	-6.2	0.24	11.0	-26.2	138.934	18.858
450	220	452.47	238.96	1.379	1.181	0.329	0.535	0.864	23	36.5	-7.8	0.38	13.5	-30.8	140.356	21.944
400	300	398.04	324.94	1.371	1.157	0.445	0.461	0.906	23	43.0	-6.3	0.49	20.0	-29.3	140.356	20.875
350	400	346.92	430.12	1.351	1.148	0.581	0.398	0.979	24	45.5	-2.4	0.59	21.5	-26.4	140.830	18.746
280	450	275.59	481.66	1.339	1.132	0.645	0.312	0.957	24	50.0	0.1	0.67	26.0	-23.9	140.830	16.971
220	500	215.87	534.50	1.335	1.125	0.714	0.243	0.957	24	52.0	0.8	0.75	28.0	-23.2	140.830	16.474
160	550	156.76	586.13	1.327	1.122	0.778	0.176	0.954	24	53.0	2.5	0.82	29.0	-21.5	140.830	15.267
120	600	117.30	637.34	1.318	1.116	0.840	0.131	0.971	24	54.5	4.3	0.87	30.5	-19.7	140.830	13.989
100	620	97.60	657.16	1.313	1.113	0.863	0.109	0.971	24	55.5	5.5	0.89	31.5	-18.5	140.830	13.136
0	700	0.00	729.63	1.269	1.153	0.926	0.000	0.926	24	44.0	15.0	1.00	20.0	-9.0	140.830	6.391
						Av. Mass Flow Rate		**0.015**	**kg/s**						$\mu_{isenmax}$ = (%)	**21.944**

P=12 Bar(g), L=20D , Cone Angle=40^0, D=19mm, G=1

$Q_{read,h}$ (l/min)	$Q_{read,c}$ (l/min)	$Q_{act,h}$ (l/min)	$Q_{act,c}$ (l/min)	$\rho_{air,c}$ (kg/m^3)	$\rho_{air,h}$ (kg/m^3)	m_c (kg/min)	m_h (kg/min)	m_t (kg/min)	T_i (C^0)	T_h (C^0)	T_c (C^0)	μ_c	T_h-T_i (C^0)	T_i-T_c (C^0)	Δt_{isen} (C^0)	μ_{isen} (%)
800	0	828.13	0.00	1.318	1.252	0.000	1.037	1.037	16	19.0	4.3	0.00	3.0	-11.7	147.998	7.906
750	50	775.05	53.78	1.352	1.248	0.073	0.967	1.040	16	20.0	-2.6	0.07	4.0	-18.6	147.998	12.568
700	100	721.90	108.80	1.383	1.243	0.150	0.897	1.048	16	21.2	-8.7	0.14	5.2	-24.7	147.998	16.689
650	150	667.17	165.41	1.421	1.231	0.235	0.821	1.056	16	24.0	-15.7	0.22	8.0	-31.7	147.998	21.419
620	200	634.25	221.75	1.436	1.223	0.319	0.776	1.094	16	26.0	-18.5	0.29	10.0	-34.5	147.998	23.311
580	270	590.87	300.43	1.447	1.213	0.435	0.717	1.151	15	28.5	-20.3	0.38	13.5	-35.3	147.486	23.935
550	300	558.18	333.61	1.445	1.203	0.482	0.672	1.154	15	30.8	-20.0	0.42	15.8	-35.0	147.486	23.731
500	370	505.20	411.05	1.442	1.193	0.593	0.603	1.195	15	33.5	-19.5	0.50	18.5	-34.5	147.486	23.392
430	450	432.01	498.46	1.434	1.179	0.715	0.510	1.224	15	37.0	-18.0	0.58	22.0	-33.0	147.486	22.375
380	500	380.55	551.68	1.422	1.172	0.785	0.446	1.231	15	39.0	-16.0	0.64	24.0	-31.0	147.486	21.019
300	550	298.53	604.50	1.411	1.157	0.853	0.345	1.199	15	43.0	-14.0	0.71	28.0	-29.0	147.486	19.663
240	580	238.07	634.42	1.398	1.150	0.887	0.274	1.161	14	45.0	-11.5	0.76	31.0	-25.5	146.974	17.350
160	600	158.22	652.94	1.384	1.143	0.903	0.181	1.084	14	47.0	-8.8	0.83	33.0	-22.8	146.974	15.513
100	690	98.27	746.94	1.369	1.128	1.023	0.111	1.134	14	51.0	-6.0	0.90	37.0	-20.0	146.974	13.608
50	750	49.29	807.37	1.354	1.135	1.093	0.056	1.149	14	49.0	-3.0	0.95	35.0	-17.0	146.974	11.567
0	810	0.00	857.78	1.310	1.174	1.124	0.000	1.124	14	38.5	6.0	1.00	24.5	-8.0	146.974	5.443
						Av. Mass Flow Rate		**0.019**	**kg/s**						$\mu_{isenmax}$ = (%)	**23.935**

***P=14 Bar(g)*, L=20D , Cone Angle=40^0, D=19mm, G=1**

$Q_{read,h}$ (l/min)	$Q_{read,c}$ (l/min)	$Q_{act,h}$ (l/min)	$Q_{act,c}$ (l/min)	$\rho_{air,c}$ (kg/m^3)	$\rho_{air,h}$ (kg/m^3)	m_c (kg/min)	m_h (kg/min)	m_t (kg/min)	T_i (C^0)	T_h (C^0)	T_c (C^0)	μ_c	T_h-T_i (C^0)	T_i-T_c (C^0)	Δt_{isen} (C^0)	μ_{isen} (%)
860	0	886.46	0.00	1.320	1.241	0.000	1.100	1.100	18	21.5	4.0	0.00	3.5	-14.0	154.701	9.050
800	50	820.44	54.18	1.372	1.229	0.074	1.008	1.083	18	24.5	-6.5	0.07	6.5	-24.5	154.701	15.837
750	100	764.05	109.80	1.409	1.213	0.155	0.927	1.081	19	28.5	-13.5	0.14	9.5	-32.5	155.233	20.936
680	200	687.07	220.46	1.420	1.193	0.313	0.820	1.133	19	33.5	-15.5	0.28	14.5	-34.5	155.233	22.225
650	300	654.62	332.17	1.433	1.185	0.476	0.776	1.252	20	35.5	-17.8	0.38	15.5	-37.8	155.764	24.267
620	320	621.90	353.63	1.427	1.176	0.505	0.731	1.236	20	38.0	-16.8	0.41	18.0	-36.8	155.764	23.626
560	400	558.14	438.62	1.405	1.161	0.616	0.648	1.264	20	42.0	-12.8	0.49	22.0	-32.8	155.764	21.058
500	500	495.20	545.88	1.393	1.146	0.760	0.568	1.328	20	46.0	-10.5	0.57	26.0	-30.5	155.764	19.581
400	600	393.10	649.75	1.370	1.128	0.890	0.444	1.334	20	51.0	-6.2	0.67	31.0	-26.2	155.764	16.820
350	680	341.86	735.15	1.366	1.115	1.004	0.381	1.385	20	55.0	-5.3	0.72	35.0	-25.3	155.764	16.243
300	720	292.13	775.50	1.356	1.108	1.051	0.324	1.375	20	57.0	-3.3	0.76	37.0	-23.3	155.764	14.959
250	780	242.71	836.11	1.343	1.101	1.123	0.267	1.390	21	59.0	-0.7	0.81	38.0	-21.7	156.295	13.884
180	800	174.49	854.11	1.332	1.098	1.138	0.192	1.329	21	60.0	1.5	0.86	39.0	-19.5	156.295	12.476
150	840	145.19	892.76	1.320	1.095	1.178	0.159	1.337	21	61.0	4.0	0.88	40.0	-17.0	156.295	10.877
100	880	96.94	931.08	1.308	1.098	1.218	0.106	1.324	21	60.0	6.5	0.92	39.0	-14.5	156.295	9.277
0	940	0.00	984.93	1.283	1.125	1.263	0.000	1.263	21	52.0	12.0	1.00	31.0	-9.0	156.295	5.758
						Av. Mass Flow Rate		**0.021**	**kg/s**						**$\mu_{isenmax}$ = (%)**	**24.267**

P=15.5 Bar(g), L=20D , Cone Angle=40^0, D=19mm, G=1

$Q_{read,h}$ (l/min)	$Q_{read,c}$ (l/min)	$Q_{act,h}$ (l/min)	$Q_{act,c}$ (l/min)	$\rho_{air,c}$ (kg/m^3)	$\rho_{air,h}$ (kg/m^3)	m_c (kg/min)	m_h (kg/min)	m_t (kg/min)	T_i (C^0)	T_h (C^0)	T_c (C^0)	μ_c	T_h-T_i (C^0)	T_i-T_c (C^0)	Δt_{isen} (C^0)	μ_{isen} (%)
920	0	935.68	0.00	1.299	1.209	0.000	1.131	1.131	26	29.5	8.5	0.00	3.5	-17.5	162.709	10.755
860	70	870.79	74.82	1.335	1.198	0.100	1.043	1.143	27	32.2	0.9	0.09	5.2	-26.1	163.253	15.987
820	120	826.50	129.78	1.367	1.187	0.177	0.981	1.158	28	35.0	-5.5	0.15	7.0	-33.5	163.797	20.452
780	220	782.39	239.96	1.390	1.176	0.334	0.920	1.253	28	38.0	-10.0	0.27	10.0	-38.0	163.797	23.199
720	300	717.61	328.53	1.401	1.161	0.460	0.833	1.293	28	42.0	-12.1	0.36	14.0	-40.1	163.797	24.482
660	400	652.65	438.71	1.406	1.143	0.617	0.746	1.362	29	47.0	-12.9	0.45	18.0	-41.9	164.341	25.496
610	480	599.47	523.44	1.390	1.128	0.727	0.676	1.404	29	51.0	-9.9	0.52	22.0	-38.9	164.341	23.670
560	550	547.81	598.08	1.382	1.118	0.826	0.613	1.439	29	54.0	-8.4	0.57	25.0	-37.4	164.341	22.758
520	600	506.36	650.73	1.374	1.108	0.894	0.561	1.455	29	57.0	-7.0	0.61	28.0	-36.0	164.341	21.906
460	680	445.51	734.05	1.362	1.096	0.999	0.488	1.488	29	60.6	-4.5	0.67	31.6	-33.5	164.341	20.384
340	780	326.66	839.66	1.354	1.079	1.137	0.352	1.489	29	66.0	-3.0	0.76	37.0	-32.0	164.341	19.472
280	820	268.22	878.99	1.343	1.072	1.180	0.288	1.468	28	68.0	-0.7	0.80	40.0	-28.7	163.797	17.522
200	880	191.03	939.00	1.330	1.066	1.249	0.204	1.453	28	70.0	1.8	0.86	42.0	-26.2	163.797	15.995
160	940	152.60	1000.85	1.325	1.063	1.326	0.162	1.488	28	71.0	3.0	0.89	43.0	-25.0	163.797	15.263
110	980	105.07	1038.74	1.313	1.066	1.364	0.112	1.476	27	70.0	5.5	0.92	43.0	-21.5	163.253	13.170
0	1050	0.00	1104.06	1.292	1.090	1.426	0.000	1.426	26	62.5	10.0	1.00	36.5	-16.0	162.709	9.834
						Av. Mass Flow Rate		**0.023**	**kg/s**						**$\mu_{isenmax}$ = (%)**	**25.496**